GENERAL INSTABILITY OF ORTHOTROPICALLY STIFFENED CYLINDERS,

PART I ;

AXIAL COMPRESSION, TORSION AND HYDROSTATIC PRESSURE LOADINGS .

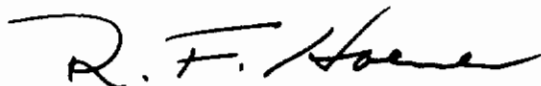ROGER MILLIGAN
GEORGE GERARD
C. LAKSHMIKANTHAM
HERBERT BECKER

FOREWORD

This report was prepared by Allied Research Associates, Inc. under USAF Contract No. AF 33(615)-1228. The contract was initiated under Project No. 1467, Task No. 146703; BPSN 4 (6199-146703-62405334). The work was administered under the direction of the Air Force Flight Dynamics Laboratory, Research and Technology Division, Messrs. Adel Abdessalam, and Royce Forman project engineers.

This report covers work conducted on this phase from November 1963 to June 1965.

The work was performed in the ARA Division of Allied Research Associates, Inc. and the Allied report number is ARA Technical Report No. 258-2.

This technical report has been reviewed and is approved.

RICHARD F. HOENER
Acting Chief
Structures Division

ABSTRACT

The general applicability of orthotropic stability theory to aerospace shell structures was examined experimentally. For this purpose a series of careful experiments were performed on orthotropically stiffened cylinders designed to fail in the elastic general instability mode under three separate loading conditions: axial compression, torsion and hydrostatic pressure. Experimental results obtained during the program verified that for all loading conditions considered linear orthotropic theory results in accurate predictions of cylinder strength.

As a result of observed discrepancies between experiment and previously existing theory for longitudinally stiffened cylinders under axial compression, theoretical studies were initiated which resulted in the discovery of a new asymmetric failure mode for this cylinder configuration. Based on this new failure mode, good correlation between experiment and theory was obtained except when the longitudinal stiffened cylinder configurations approached that corresponding to an isotropic cylinder. Other theoretical investigations performed during the program established that cylinder boundary conditions have a pronounced effect on the buckling strength of orthotropic cylinders under hydrostatic pressure loading.

iii

TABLE OF CONTENTS

ILLUSTRATIONS

Illustrations (Continued)

Illustrations (Continued)

TABLES

SYMBOLS

A		cross sectional area of test specimen enclosed by the cylinder radius, in^2
B_1		membrane axial rigidity in longitudinal direction, ppi
B_2		membrane axial rigidity in circumferential direction, ppi
B_3		membrane shear rigidity (average), ppi
$\overline{B}/B_3$	$=$	$4\,B_2/B_3$ ($\nu = 0$)
C		test machine calibration factor, lbs/psi
D_1		bending rigidity in longitudinal direction, in. lbs.
D_2		bending rigidity in circumferential direction, in. lbs.
D_3		twisting rigidity (average), in. lbs.
$\overline{D}/D_1$	$=$	D_3/D_1 ($\nu = 0$)
E		Young's modulus, psi
F		torsional rigidity coefficient
F_t		Equation (5.5)
F_x		Equation (4.3)
F_y		Equation (6.2)
G		Shear modulus, psi
I		area moment of inertia of skin per unit width, in^3
I_s		area moment of inertia of skin and stiffener per unit width in a plane perpendicular to the longitudinal direction, in^3
I_f		area moment of inertia of skin and stiffener per unit width in a plane perpendicular to circumferential direction, in^3
J		torsional moment of inertia per unit width, in^3
J_o		torsional moment of inertia per unit width associated with grid stiffened design, in^3
ΔJ_o		incremental torsional moment of inertia per unit width associated with grid stiffened design, in^3
K		torsional moment of inertia coefficient
L		cylinder length, in.

$\overline{L}$ length of short side of long flat plate, distance between cylinder stiffeners, in.

N_x axial load per unit width, ppi

N_y circumferential load per unit width, ppi

N_{xy} shear load per unit width, ppi

P_x total axial compressive load, lbs.

$P_{x_{exp}}$ experimental value for total axial compressive load, lbs.

R cylinder radius, in

T total torsion loading, in. lbs

T_{exp} experimental value for total torsion loading, in. lbs

U asymmetric axial compression buckling coefficient

Z curvature parameter

Z_t curvature parameter associated with cylinders under torsion loading

Z_x curvature parameter associated with cylinders under axial compressive loading

Z_y curvature parameter associated with cylinders under hydrostatic pressure loading

GSC   grid stiffened cylinder

IC   isotropic cylinder

LSC   longitudinally stiffened cylinder

RSC   ring stiffened cylinder

b   stiffener height, in.

d   stiffener spacing, in.

d_f stiffener spacing in longitudinal direction, in.

d_s stiffener spacing in circumferential direction, in.

h   height of skin plus stiffener, in.

k_t cylinder buckling coefficient under torsion loading

$k_{t_{exp}}$ experimental value for cylinder buckling coefficient under torsion loading

k_x	cylinder buckling coefficient under axial compressive loading
$k_{x_{exp}}$	experimental value for cylinder buckling coefficient under axial compressive loading
$k_{x_{m=1}}$	axial compressive buckling coefficient for cylinder buckling in the asymmetric mode associated with one buckle half wave length along the longitudinal cylinder axis
$k_{x_{m=cont}}$	axial compressive buckling coefficient for cylinder buckling in the asymmetric mode associated with several buckle wave lengths along the longitudinal cylinder axis
k_y	cylinder buckling coefficient under hydrostatic pressure loading
$k_{y_{exp}}$	experimental value for cylinder buckling coefficient under hydrostatic pressure loading
p_{exp}	test machine pressure loading at specimen failure, psi
p_y	hydrostatic pressure loading at buckling, psi
$p_{y_{exp}}$	experimental value for hydrostatic pressure loading at buckling, psi
q	unit loading in shear, ppi
$\bar{t}$	effective shear thickness
t	cylinder wall thickness, in.
t_f	area of sheet and stiffener per unit width in a plane perpendicular to the circumferential direction, in.
t_s	area of sheet and stiffener per unit width in a plane perpendicular to the longitudinal direction, in.
t_{av}	average cylinder wall thickness, in.
t_{min}	minimum cylinder wall thickness, in.
Δt_s	increment in effective wall thickness provided by longerons, in.
Δt_f	increment in effective wall thickness provided by frames, in.
u_s, u_f	experimental coefficients for determination of effective thickness of orthotropic cylinder
w	stiffener width, in.
w_f	stiffener width in longitudinal direction, in.
w_s	stiffener width in circumferential direction, in.

α $\quad = \quad$ $B_1 D_2 / B_2 D_1$

β $\qquad$ wavelength parameter

$\overline{\beta}$ $\qquad$ see equation Appendix A

γ $\quad = \quad$ $B_3 \overline{D} / \overline{B} D_1$

ϵ $\qquad$ axial strain, in/in.

ν $\qquad$ Poisson's ratio

σ $\qquad$ axial compressive stress, psi

σ_x $\qquad$ buckling stress in axial compression, psi

$\sigma_{x_{exp}}$ $\qquad$ experimental value of axial compressive buckling stress, psi

$\sigma_{x_{m=1}}$ $\qquad$ axial compressive buckling stress in the asymmetric mode associated with one buckle half wave length along the longitudinal cylinder axis, psi

τ $\qquad$ shear stress, psi

τ_{exp} $\qquad$ experimental value for critical buckling stress in torsion, psi

$d\theta/dx$ $\qquad$ twist per unit length, in.$^{-1}$

GENERAL INSTABILITY OF ORTHOTROPICALLY
STIFFENED CYLINDERS

1. INTRODUCTION

The major objective of the program described herein is to conduct a series of careful experiments on elastic general instability of orthotropically stiffened cylinders under axial compression, torsion and hydrostatic pressure and correlate the experimental data with available theory (Refs. 1, 2, 3). The test data on orthotropic cylinders available prior to this program were reviewed in Ref. 1 and together with the more recent data of Ref. 4 constituted an inadequate set of data from which to judge the general applicability of orthotropic stability theory to aerospace shell structures. The present program was designed to fill this important gap in our present knowledge for cylinders designed specifically to test the validity of orthotropic stability theory.

This report contains a description of the test specimens, procedures and results obtained under a variety of loading conditions for ring, longitudinal and grid stiffening systems. In Section 2, the correlation of theory and experimental results is presented and it was found that excellent correlation between linear stability theory and experiment exists for all cases. It is to be noted that it was necessary in this program to extend the theory contained in Refs. 1 - 3 in two cases because of significant aspects of orthotropic cylinder behavior revealed by the experimental data. For longitudinally stiffened cylinders under compression, a previously unsuspected linear buckling mode has been obtained which accurately preducts the behavior of such cylinders (Appendix A). Stiffened cylinders under external hydrostatic pressure were found to be extremely sensitive to boundary conditions necessitating the development of the theory for clamped edges (Appendix B).

In Section 3, calculations of the extensional and flexural rigidities of the stiffened cylinders are presented and correlated with experimental results. This is an important aspect of the problem since application of orthotropic theory requires an accurate knowledge of these properties. Section 4, 5 and 6 contain a complete description of the experimental details for each of the loading conditions.

1

2.   CORRELATION OF THEORY AND EXPERIMENTAL RESULTS

All cylinders tested in this program were designed to fail in the elastic general instability mode.   They were very carefully machined of 6061-T6 aluminum alloy with closely spaced integral longitudinal, ring, or grid (longitudinal and ring) stiffening systems to form nominally 8 inch diameter orthotropic cylinders of various lengths.   They were carefully tested with particular attention to boundary conditions in specially designed testing machines which utilized pneumatic loading systems in all cases.

Axial Compression

The theory presented in Ref. 3 and extended in Appendix A indicates that buckling can occur in the axisymmetric or asymmetric mode depending upon the relation between the two geometric parameters α and γ as illustrated in Figure 2.1. The cylinder design points of this program are shown in Figure 2.1.   Although it was desired to test longitudinally stiffened cylinders with $\gamma < \alpha$, it was not possible to design such cylinders of monolithic construction.   Consequently $\gamma > \alpha$ for all longitudinally stiffened cylinders tested in this program.

Ring Stiffened Cylinders

The correlation of general instability theory with test data on failure of ring stiffened cylinders is shown in Figures 2.2, 2.3 and 2.4.   The test data are primarily for externally ring stiffened cylinders but also include several internally ring stiffened and grid stiffened cylinders.   The latter are considered to be in the ring stiffened category because of their relative α values.

Manufacturing variations can affect the interpretation of the test results significantly for ring stiffened cylinders because the thin sheet is the load carrying member.   Consequently, the correlation is presented in Figure 2.2 based upon the average properties of the minimum circumferential section whereas Figure 2.3 is based upon the minimum properties at this section.   (See Section 4 for discussion of this procedure).   A comparison of the data presented in these two figures indicates that the correlation for most test points is essentially unaffected thereby indicating the high quality of the cylinders.

The correlation between linear theory and experiment for moderate length cylinders is excellent in both figures.   In fact, the test points in Figure 2.3 based

2
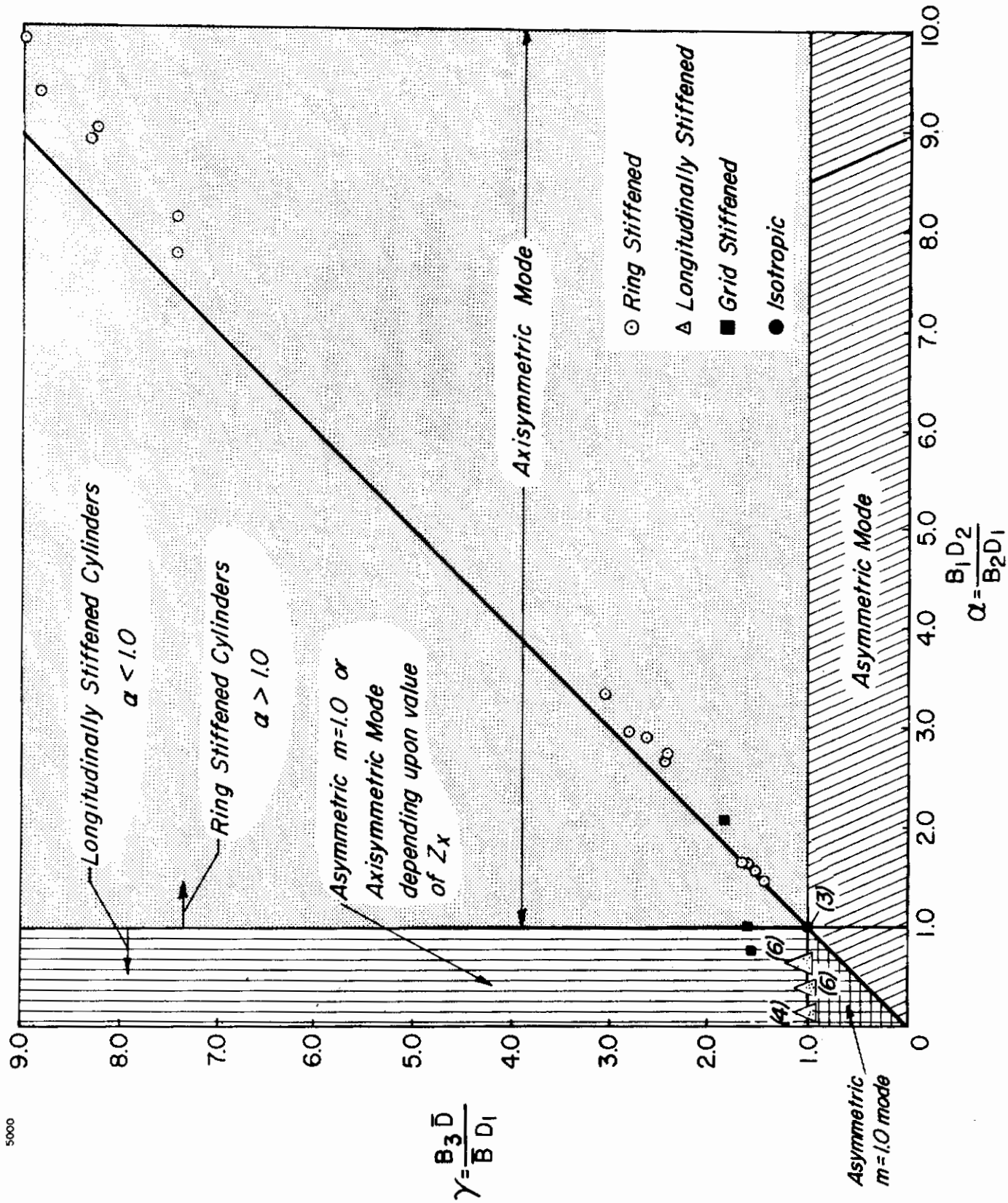
Fig. 2.1 Cylinder Design Points for Compressive Instability Tests

3
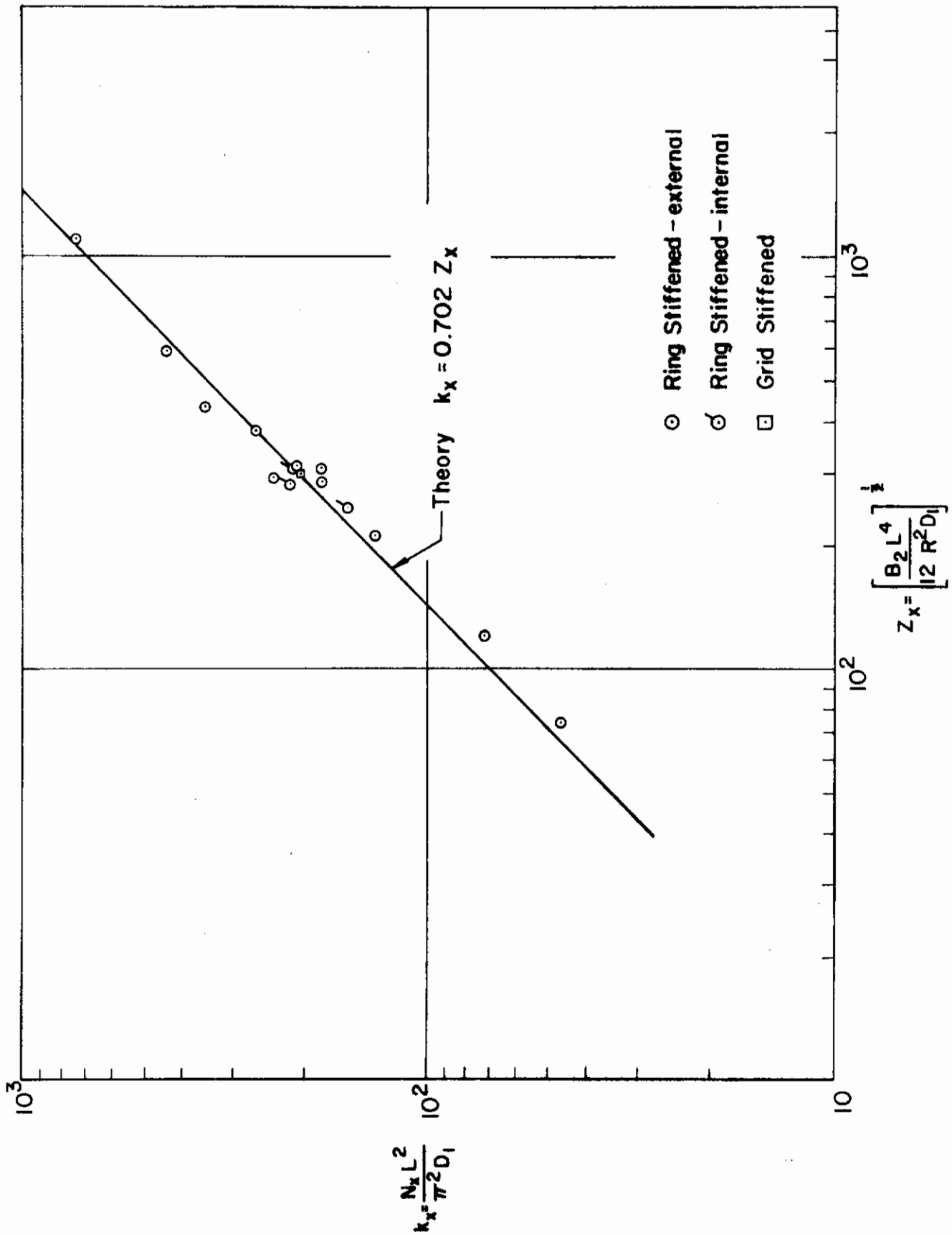
Fig. 2.2   Correlation of Theory and Experiments for Ring Stiffened
Cylinders in Compression Based on Average Properties

4
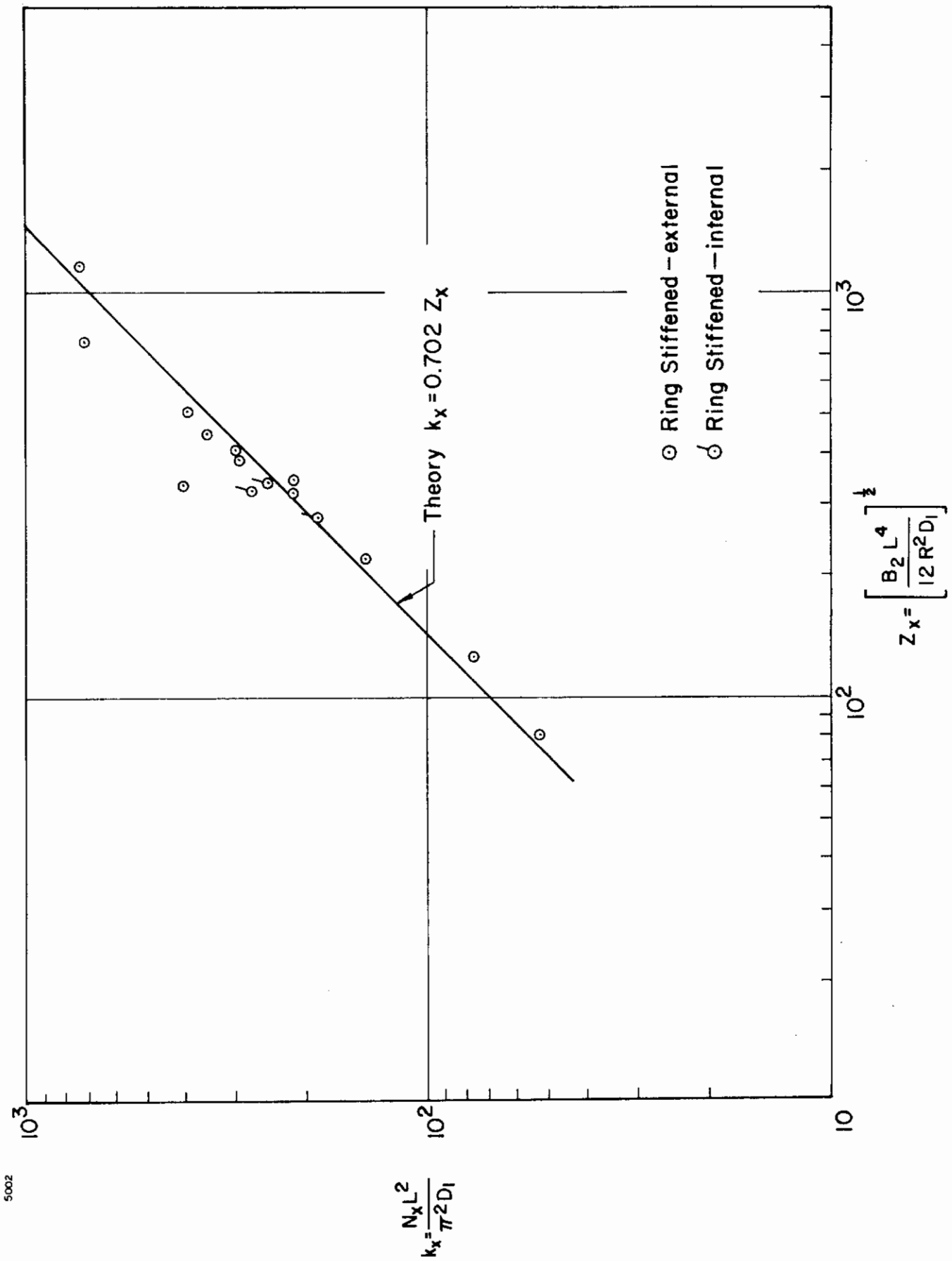
Fig. 2.3   Correlation of Theory and Experiments for Ring Stiffened Cylinders Under Compression Based on Minimum Properties

The figure plots $k_x = \dfrac{N_x L^2}{\pi^2 D_1}$ versus $Z_x = \left[\dfrac{B_2 L^4}{12 R^2 D_1}\right]^{\frac{1}{2}}$

Theory $k_x = 0.702\, Z_x$

⊙ Ring Stiffened — external
⊘ Ring Stiffened — internal

5002

5
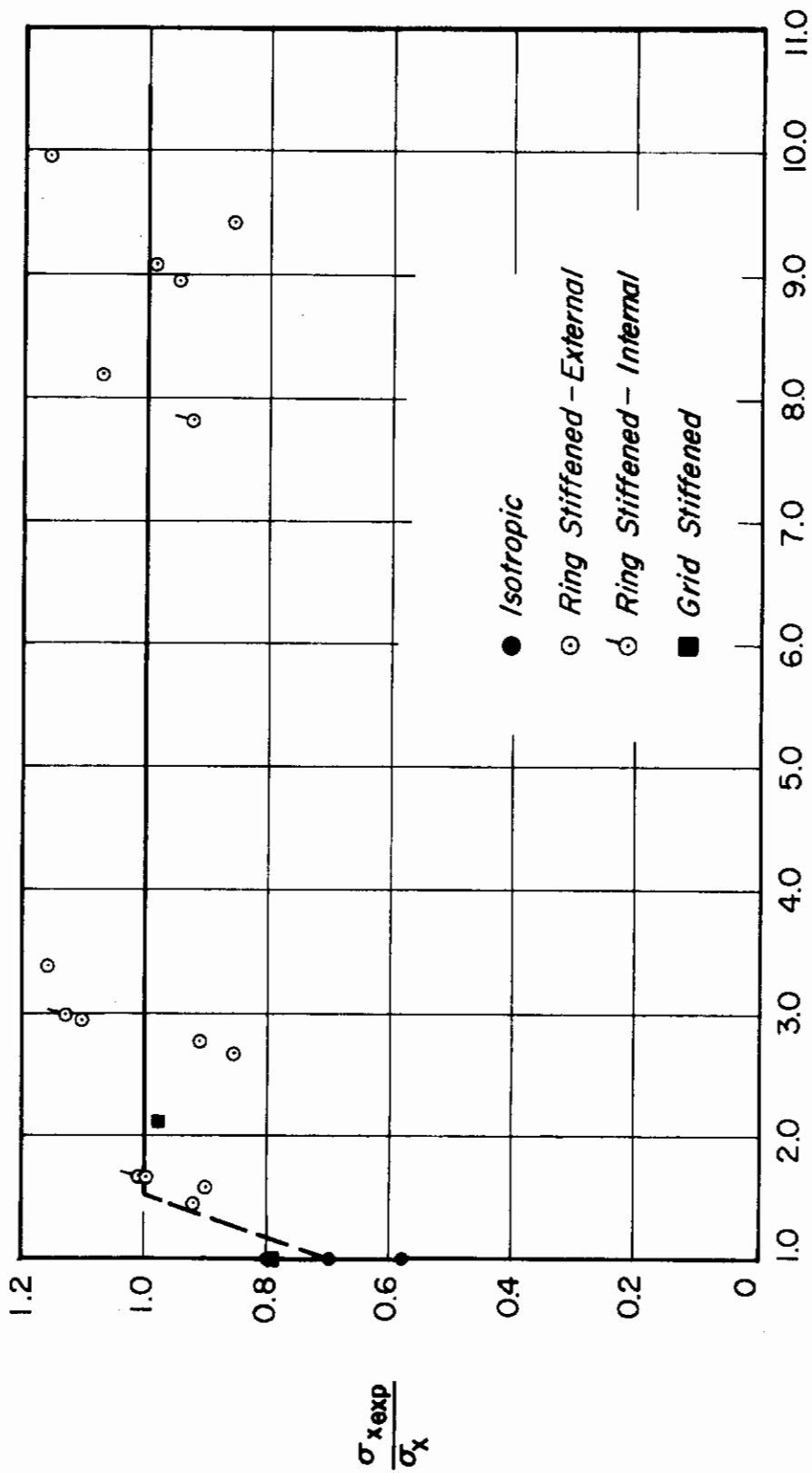
$$\alpha = \frac{B_1 D_2}{B_2 D_1}$$

Fig. 2.4   Stress Ratio for Ring Stiffened Cylinders Under Compression
Based on Average Properties

upon the minimum properties tend to be above rather than below the theoretical predictions. A comparison of the test points for internally ring stiffened cylinders with corresponding externally ring stiffened cylinders indicates no effect of stiffener location in these tests. Finally, the test data on grid stiffened cylinders are almost in perfect agreement with theory, thereby indicating that their characterization in terms of the α and γ parameters is valid. In this case there is no ambiguity in the area of the load carrying material since the longitudinal stiffeners participate in addition to the skin.

Figure 2.4 presents these data in a somewhat different form for the purpose of comparison with 3 machined isotropic cylinder tests conducted as part of this program. Here the experimental/theoretical stress ratio is plotted as a function of the governing parameter, α. It can be observed that even at as low a value of α as 1.5, the ring cylinder test data check linear orthotropic theory. The isotropic cylinder data at $\alpha = 1$ fall consistently below the theory as may be expected although the test data on these cylinders are considerably higher than normally obtained. The singificant point here is that cylinders with even a small degree of ring stiffening behave according to linear orthotropic theory.

Longitudinally Stiffened Cylinders

As indicated in Figure 2.1, the longitudinally stiffened cylinders were all designed with $\gamma > \alpha$ and consequently it was believed that these cylinders should buckle in the axisymmetric mode according to linear orthotropic theory. The test data are shown in Figure 2.5 and although they exhibit relatively small scatter, they consistently fail at roughly 0.7 of the buckling stress predicted by the axisymmetric mode of linear orthotropic theory. Note there is no significant effect of the stiffener location upon the failure strength.

Also shown in Figure 2.5, is the minimum post buckling to classical stress ratio based on the nonlinear orthotropic theoretical results of Almroth, Ref. 5. The cylinders tested in this program appeared to be of moderate length since several longitudinal wavelengths were observed. Furthermore, their α and γ values were such that the minimum post buckling stress ratio corresponded essentially to that of an isotropic cylinder. It can be observed that the test data lie far above the minimum post buckling stress ratio and consequently the latter has little, if any, value for design purposes.

7
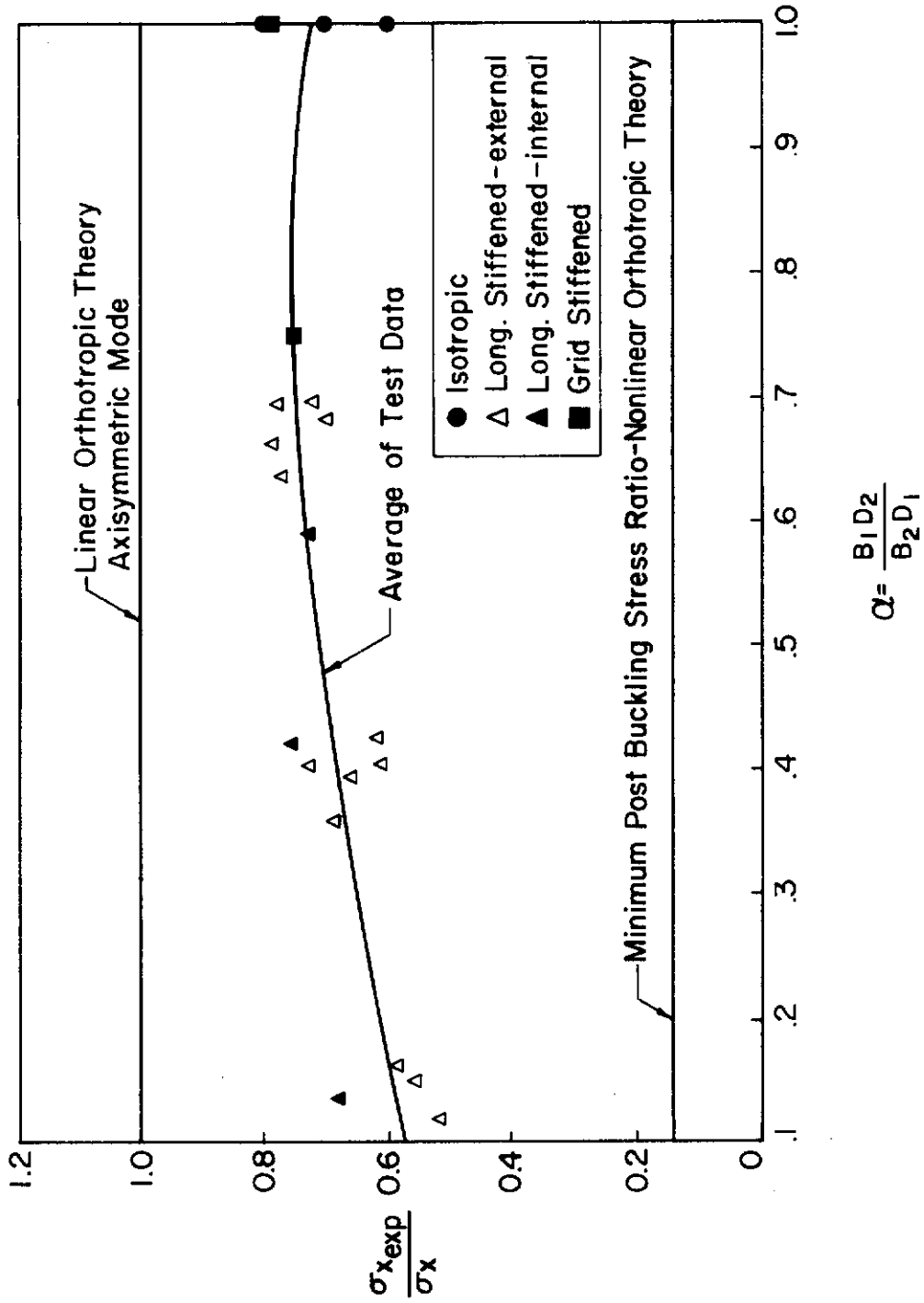
Fig. 2.5   Stress Ratio for Longitudinally Stiffened Cylinders Under Compression

5004

8

As a result of the poor correlation observed in Figure 2.5, the linear orthotropic stability theory of Ref. 3 was reexamined and it was discovered that an m = 1 asymmetric mode gave lower results than that of the axisymmetric mode primarily thought to govern in the $\gamma > \alpha < 1$ regions of Figure 2.1. This theoretical development is completely described in Appendix A. The calculated results for this new theoretical mode are shown in Figures 2.6, 2.7 and 2.8 for the average values of α, γ and δ of the grouped test data on longitudinal stiffened cylinders under compression. It can be observed that the test data and theory are in substantially good agreement from these figures as well as Figure 2.9 which presents all of the test data on longitudinal and grid stiffened ($\alpha \leq 1$) cylinders in a unified form.

It is of some interest to conjecture upon the physical significance of the newly discovered m = 1 asymmetric mode. One possible hypothesis is associated with the concept that the longitudinal stiffeners by themselves tend to buckle as Euler columns in the m = 1 mode. The cylinder formed by the continuous curved skin thus acts to support the unstable longitudinals above the flat stiffened panel buckling stress. The longitudinals, being unstable contribute only load carrying ability to the cylinder but essentially no bending stiffness. Consequently, for reasonably long cylinders, failure occurs approximately at the buckling stress of the skin cylinder. It is to be noted that calculations based upon this hypothesis for the physical significance of the m = 1 asymmetric mode give results significantly close to those obtained in Figure 2.9.

Post Buckling Behavior Under Compression

While the results prescribed in Figure 2.9 represent substantial agreement with the m = 1 asymmetric mode of linear orthotropic theory, we shall now examine these data somewhat more critically in terms of the presentation of Figure 2.10. Here we can observe that although theory and test data are in good agreement at low values of α, there is a distinct departure from theory as the isotropic cylinder data at $\alpha = 1$ is approached.

In effect, the unusual sensitivity of isotropic cylinders to imperfections establishes a singularity at $\alpha = 1$ when the data of Figures 2.4 and 2.10 are considered together. Although the test data of Figure 2.4 are insufficient to indicate how far beyond $\alpha = 1$ a sensitivity to imperfections exists, the data of Figure 2.10 do indicate an important effect in the range as $0.5 < \alpha < 1$.

9

$$a = .14, \quad \gamma = .97, \quad \delta = 1.0$$

Axisymmetric Theory
.702Z

m = 1.0 Asymmetric Theory

△ Longitudinally Stiffened – External

▲ Longitudinally Stiffened – Internal

$$k_x = N_x L^2 / \pi^2 D_1$$

$$Z_x = \left[B_2 L^4 / 12 R^2 D_1 \right]^{\frac{1}{2}}$$
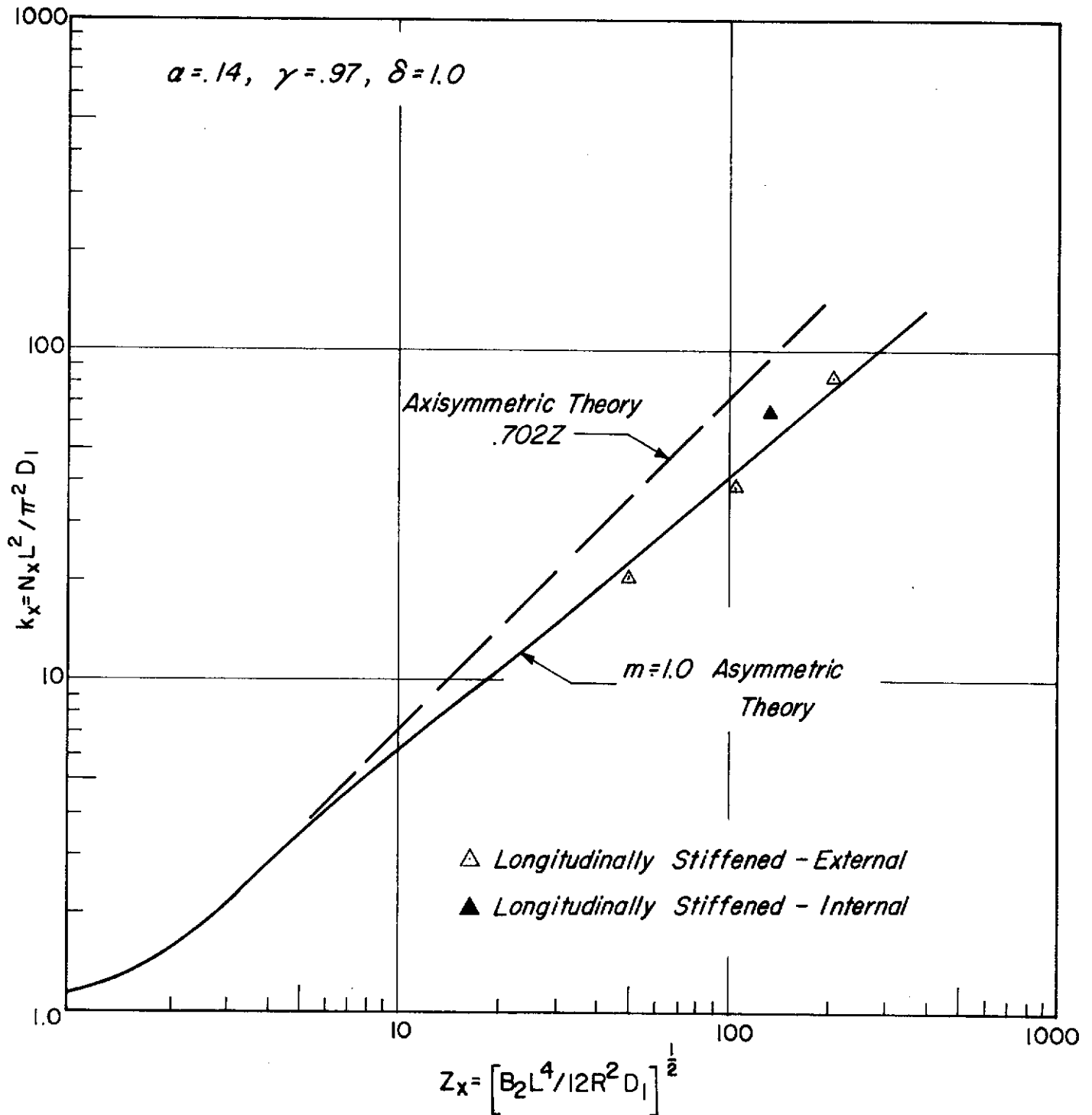
Fig. 2.6   Correlation of m = 1 Asymmetric Theory and Experiments for Longitudinally Stiffened Cylinders Under Compression

5005

10

$$a = .40, \quad \gamma = .95 \quad \delta = 1.0$$

$$k_x = \frac{N_x L^2}{\pi^2 D_1}$$

Axisymmetric Theory
.702 Z

m = 1.0 Asymmetric Theory

△   Longitudinally Stiffened – External

▲   Longitudinally Stiffened – Internal

$$Z_x = \left[B_2 L^4 / 12 R^2 D_1 \right]^{\frac{1}{2}}$$
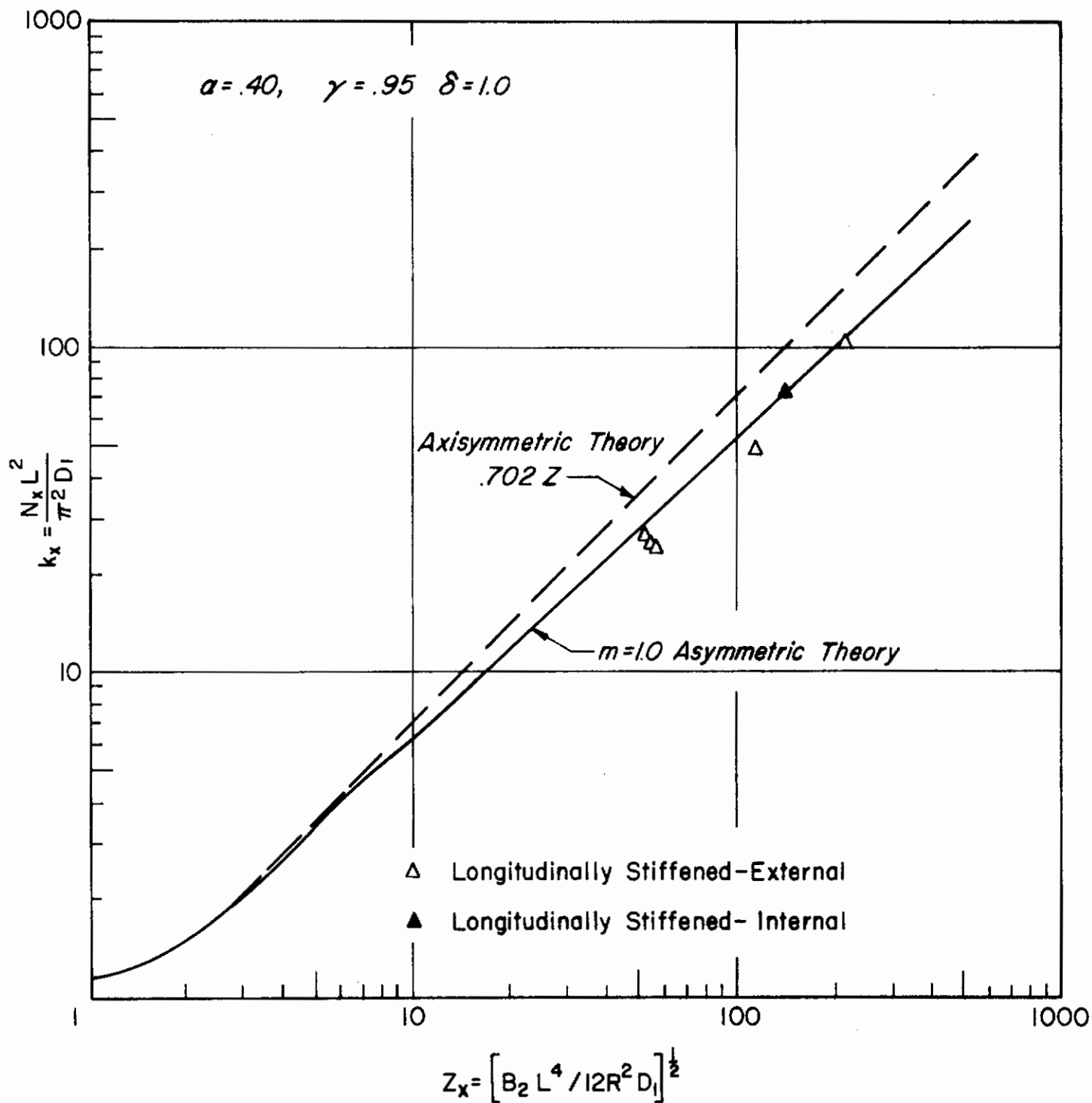
Fig. 2.7   Correlation of m = 1 Asymmetric Theory and Experiments for Longitudinally Stiffened Cylinders Under Compression

5006
5024

11

$$\alpha = .66, \quad \gamma = 1.0, \quad \delta = 1.0$$

Axisymmetric Theory .702Z

$$k_x = \frac{N_x L^2}{\pi^2 D_1}$$

$$Z_x = \left[B_2 L^4 / 12 R^2 D_1 \right]^{\frac{1}{2}}$$

$m = 1.0$ Asymmetric Theory

△ Longitudinally Stiffened – External

▲ Longitudinally Stiffened – Internal
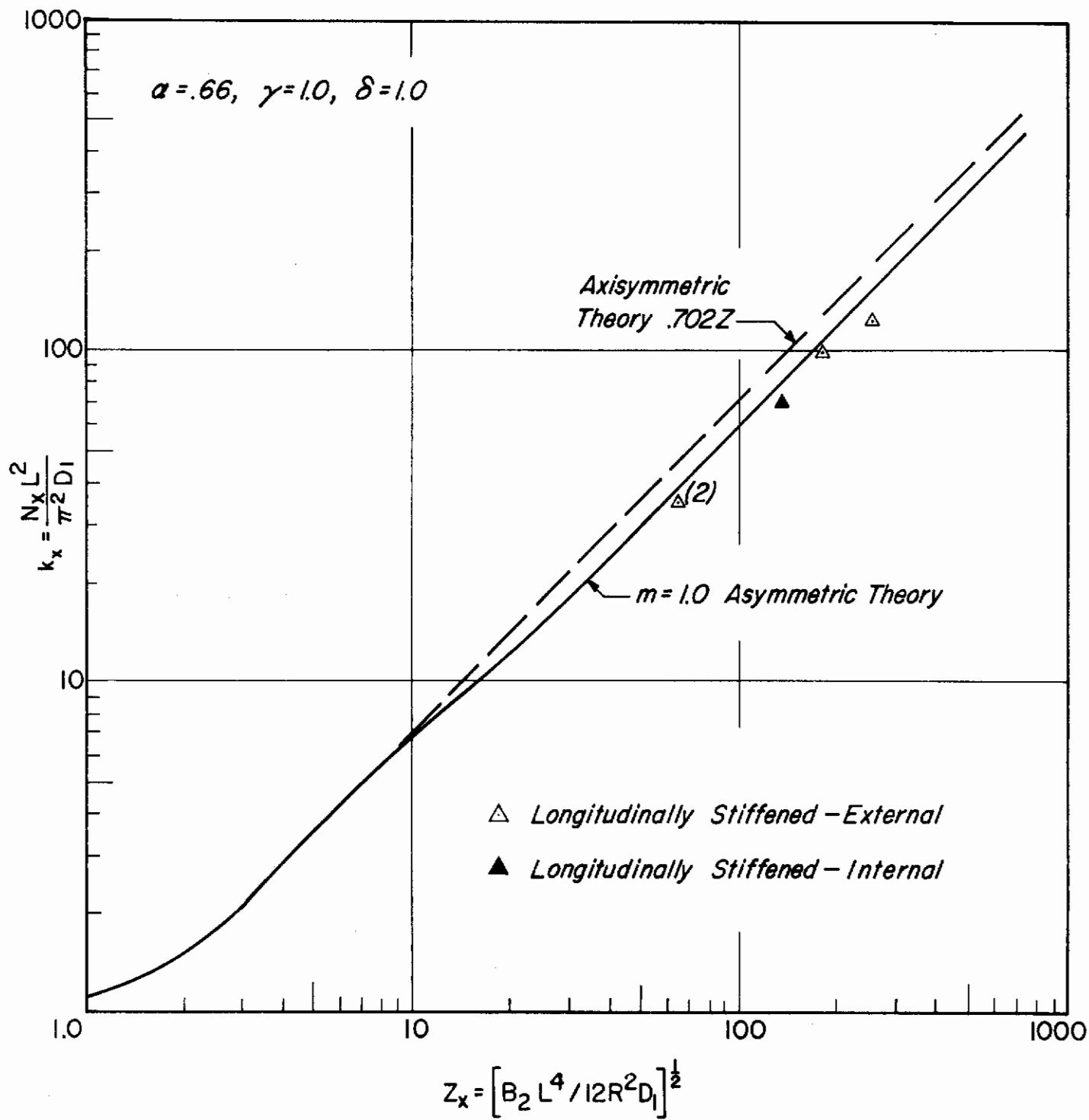
Fig. 2.8 Correlation of m = 1 Asymmetric Theory and Experiments for Longitudinally Stiffened Cylinders Under Compression

12
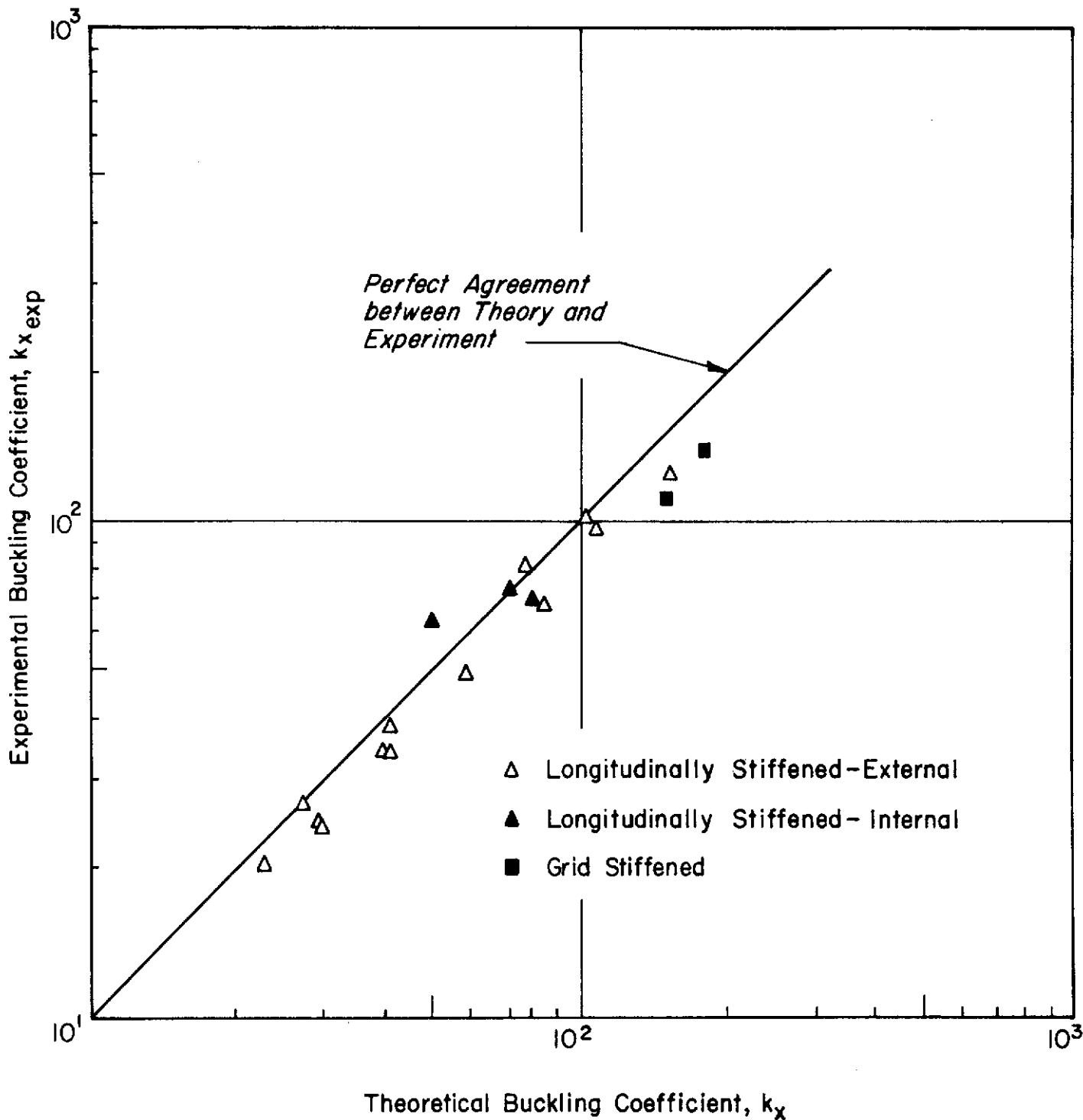
Fig. 2.9   Correlation of Theory and Experiments for Grid and Longitudinally
Stiffened Cylinders Under Compression

5008

13
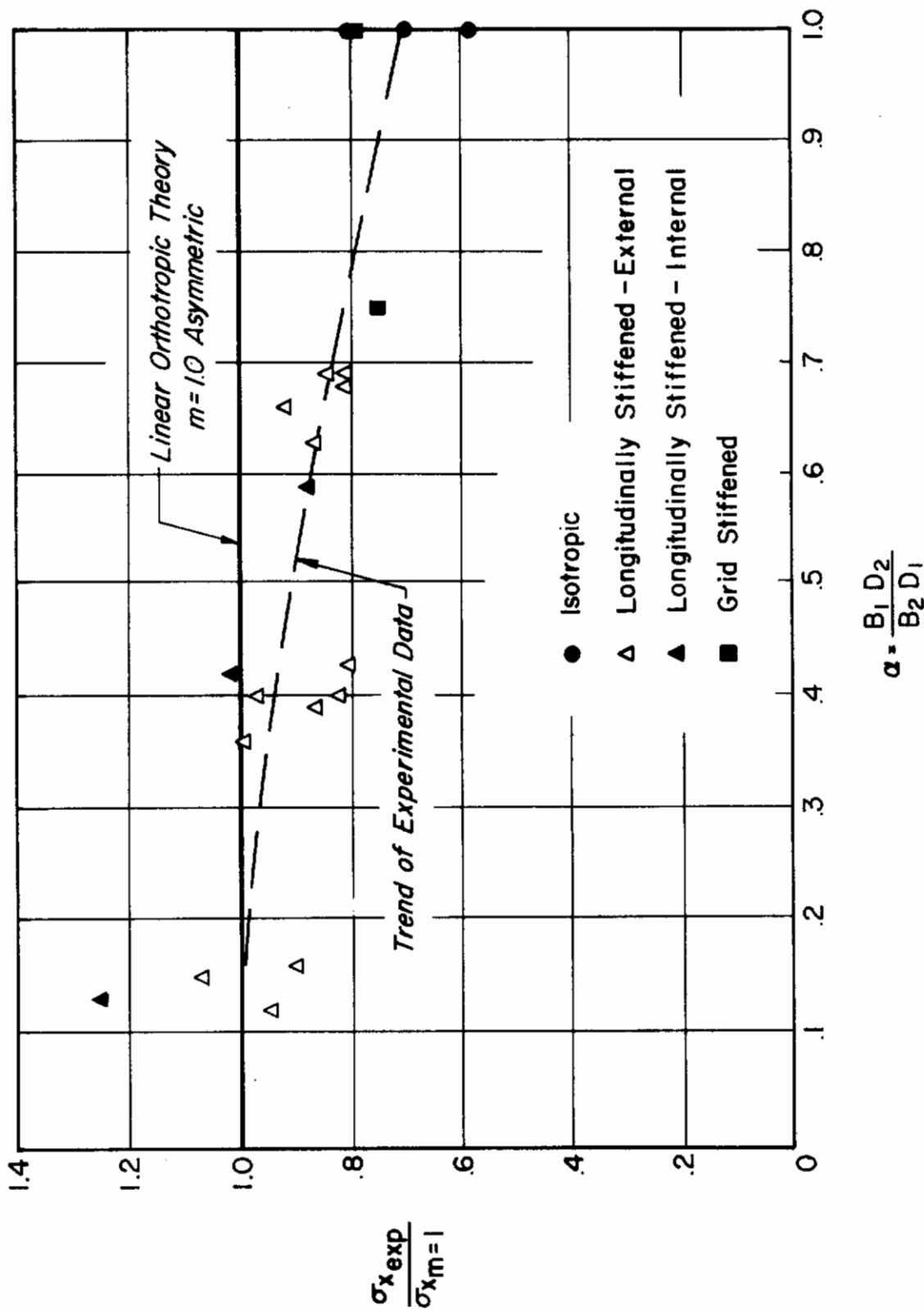
Fig. 2.10   Stress Ratio for Grid and Longitudinally Stiffened Cylinders Under Compression

In order to gain a better insight into the reasons for the behavior of the stiffened cylinders in compression, it is profitable to consider their post buckling behavior. The major value of nonlinear theory is that by examination of the post buckling behavior, it can provide an explanation of the conditions under which linear theory may be applicable (Ref. 3). For this purpose we shall examine the post buckling behavior of ring and longitudinally stiffened cylinders based to some extent on the results of Refs. 5 and 6.

The post buckling behavior of a ring stiffened cylinder is illustrated in Figure 2.11a. It can be observed that the axisymmetric buckling mode is the only one possible. In the post buckling region, both axisymmetric and asymmetric modes are possible with the location of the asymmetric branch depending upon the relative values of α and γ. If we suppose that the ring stiffened cylinder possesses some small imperfection, then it would tend to follow the dashed curve upon loading. When it intersects the asymmetric branch, this should approximate failure since with continued end shortening it would follow down the asymmetric branch. However, since this intersection is removed from the buckling region, we can expect the failure load to be closely approximated by the theoretical linear buckling stress.

For longitudinally stiffened cylinders, the relative roles of the axisymmetric and possible m = 1 asymmetric modes are illustrated in Figure 2.11b. The axisymmetric buckling stress is always greater than or equal to that for asymmetric buckling in this case. Again if we assume that a cylinder with small imperfections tends to follow the dashed line upon loading, then the intersection with the asymmetric post buckling branch occurs in the buckling region for the $\alpha = 0.7$ and $\alpha = 1$ cases. Thus, failure can occur at a fraction of the asymmetric buckling load for these cases as observed in Figure 2.10. As a consequence, the sharp decline of the post buckling asymmetric branch appears to be responsible for the lack of agreement with linear theory observed in Figure 2.10 for the $\alpha > 0.5$ data. On the other hand, the rise of the asymmetric post buckling branch for $\alpha = 0.1$ would account for the good correlation with linear theory observed for these data.

Torsion

The correlation of general instability theory with test data on failure of stiffened cylinders under torsion is shown in Figures 2.12, 2.13 and 2.14. The ring stiffened cylinder data were all within the moderate length region and excellent correlation with theory is indicated in Figure 2.12.

15

Buckling   Failure

Axisymmetric

Asymmetric

Imperfection

$\dfrac{\sigma}{\sigma_{axi}}$

a) Ring Stiffened Cylinders
$\alpha > 1.0, \quad 1.0 < \gamma < \alpha$

End Shortening

Buckling

Axisymmetric

Imperfection

Failure

$\alpha = 0.1$ Asymmetric m=1

$\alpha = 0.7$ Asymmetric m=1

$\alpha = 1.0$ Asymmetric m=1

$\dfrac{\sigma}{\sigma_{axi}}$

b) Longitudinally Stiffened Cylinders
$\alpha < 1.0, \quad \alpha < \gamma < 1.0$

End Shortening
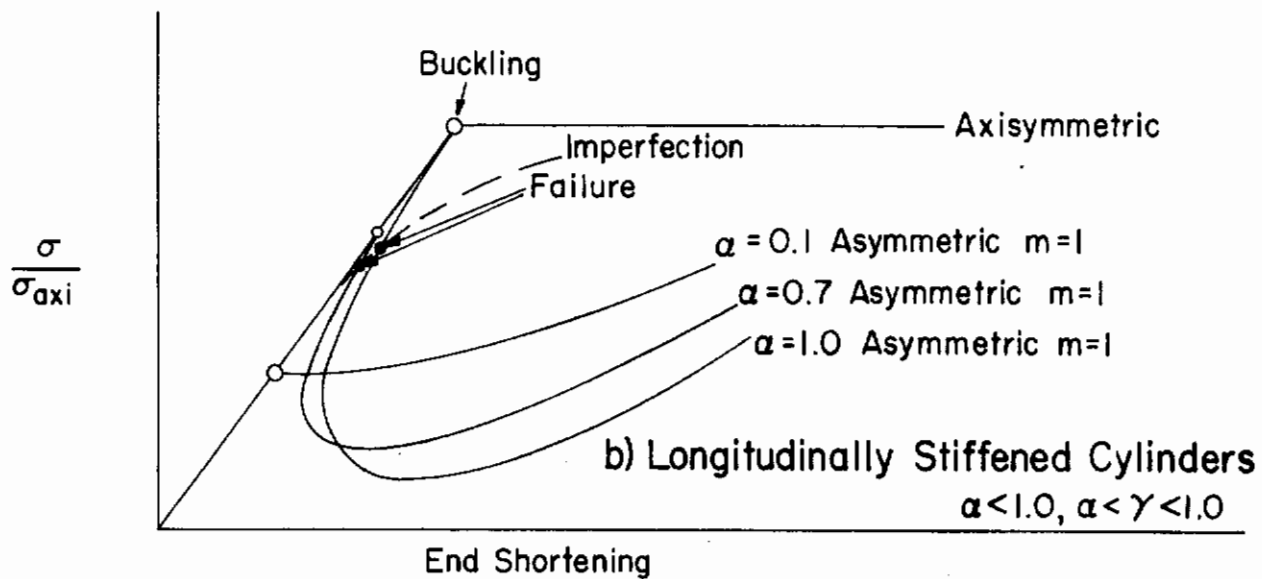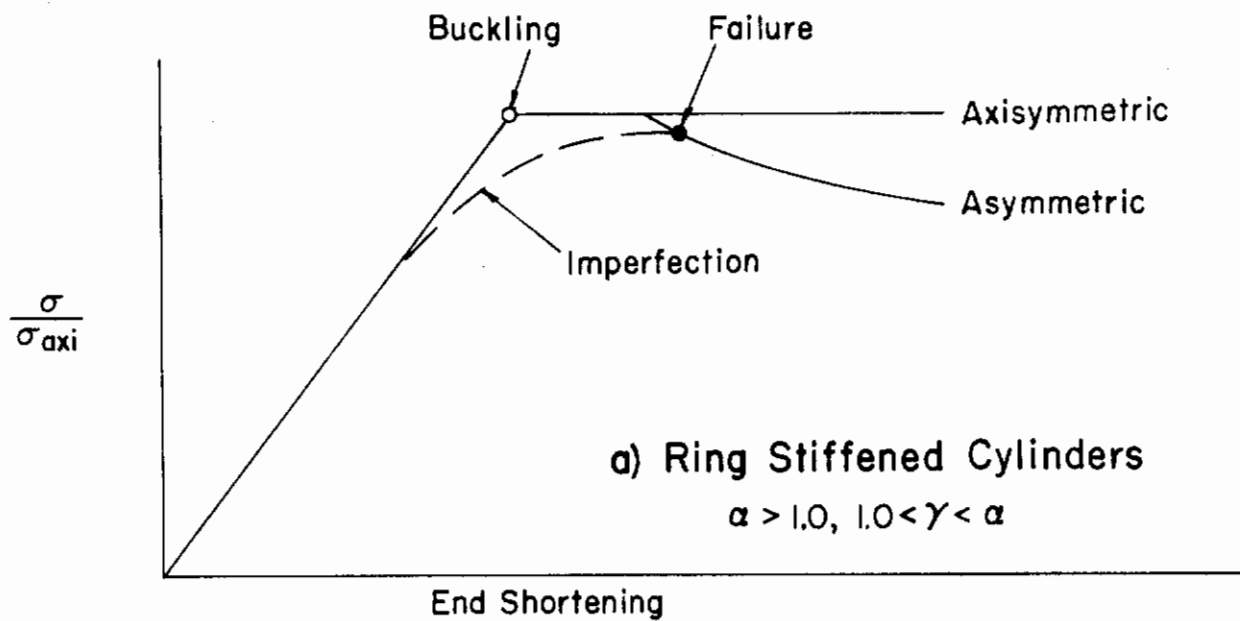
Fig. 2.11 Probable Post Buckling Behavior of Cylinders Under Compression
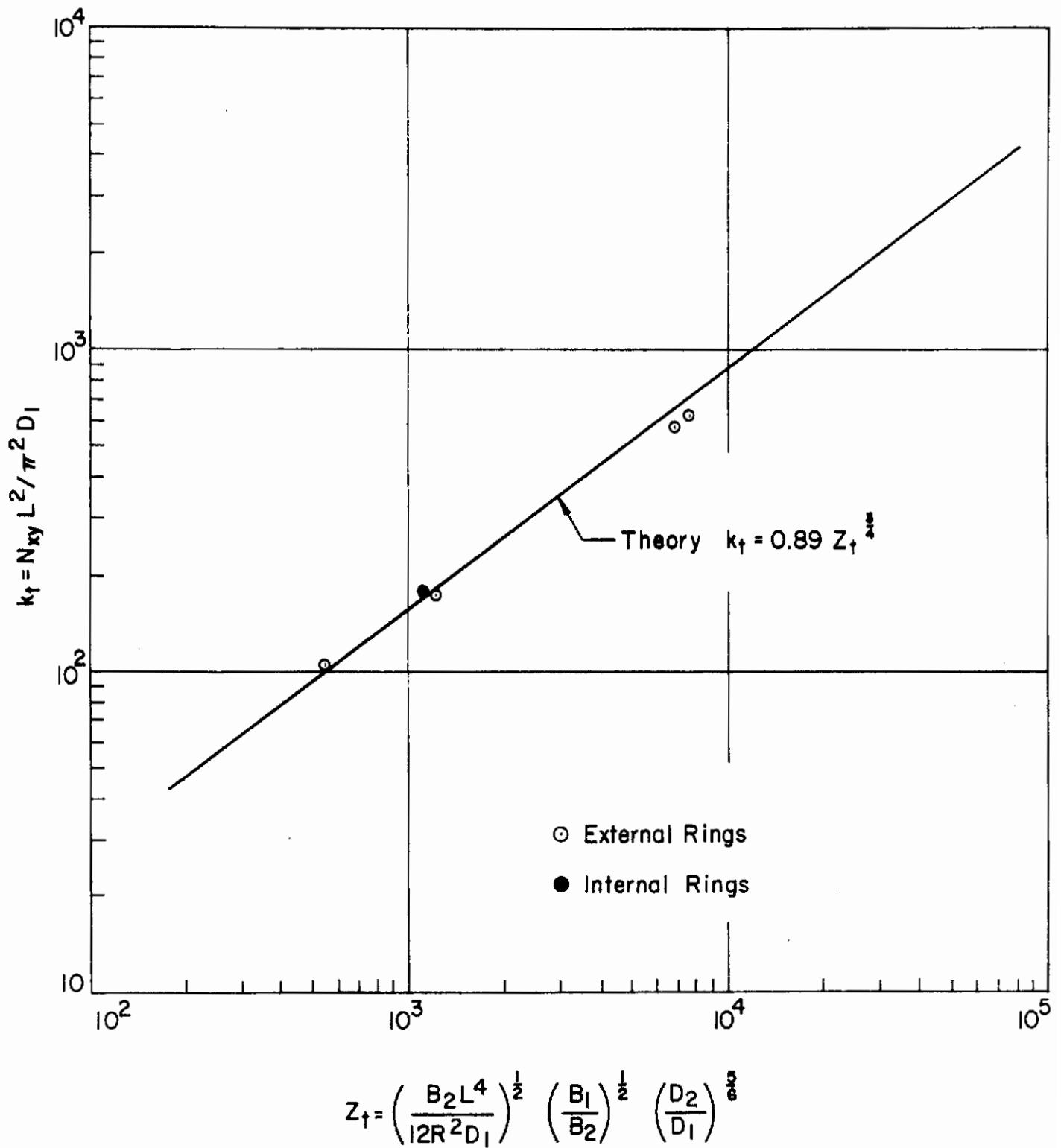
16

The plot shows:

Y-axis: $k_t = N_{xy} L^2 / \pi^2 D_1$ ranging from 10 to 10^4

X-axis: ranging from 10^2 to 10^5

Theory $k_t = 0.89 \, Z_t^{\frac{3}{4}}$

⊙ External Rings
● Internal Rings

$$Z_t = \left(\frac{B_2 L^4}{12 R^2 D_1} \right)^{\frac{1}{2}} \left(\frac{B_1}{B_2} \right)^{\frac{1}{2}} \left(\frac{D_2}{D_1} \right)^{\frac{5}{6}}$$

Fig. 2.12   Correlation of Theory and Experiments for Ring Stiffened Cylinders Under Torsion

17

$$Z_t = \left(\frac{B_2 L^4}{12 R^2 D_1} \right)^{\frac{1}{2}} \left(\frac{B_1}{B_2} \right)^{\frac{1}{2}} \left(\frac{D_2}{D_1} \right)^{\frac{5}{6}}$$

△ Longitudinally Stiffened – external

▲ Longitudinally Stiffened – internal
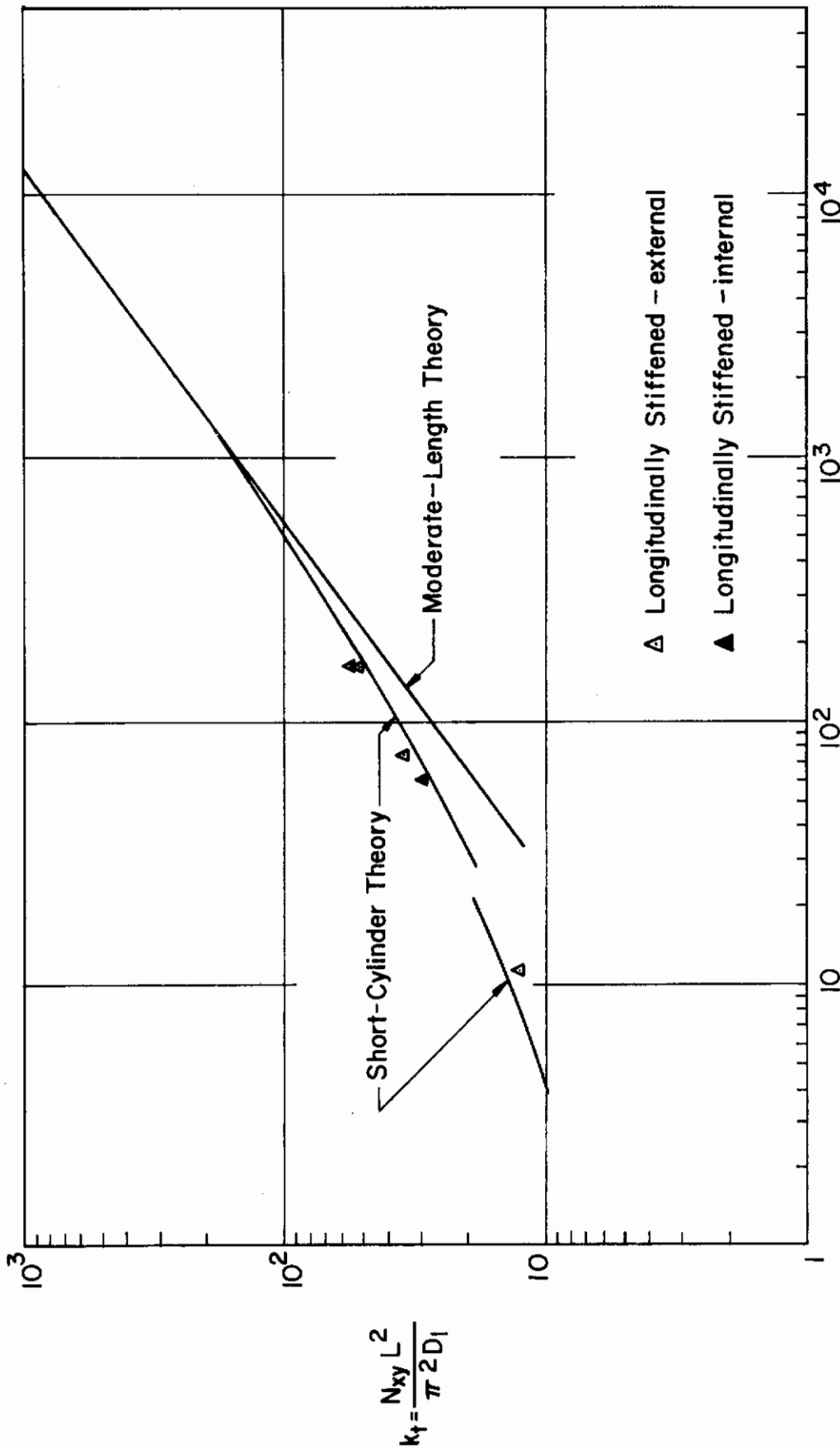
Fig. 2.13   Correlation of Theory and Experiments for Longitudinally Stiffened Cylinders Under Torsion

$$k_t = \frac{N_{xy} L^2}{\pi^2 D_1}$$

18
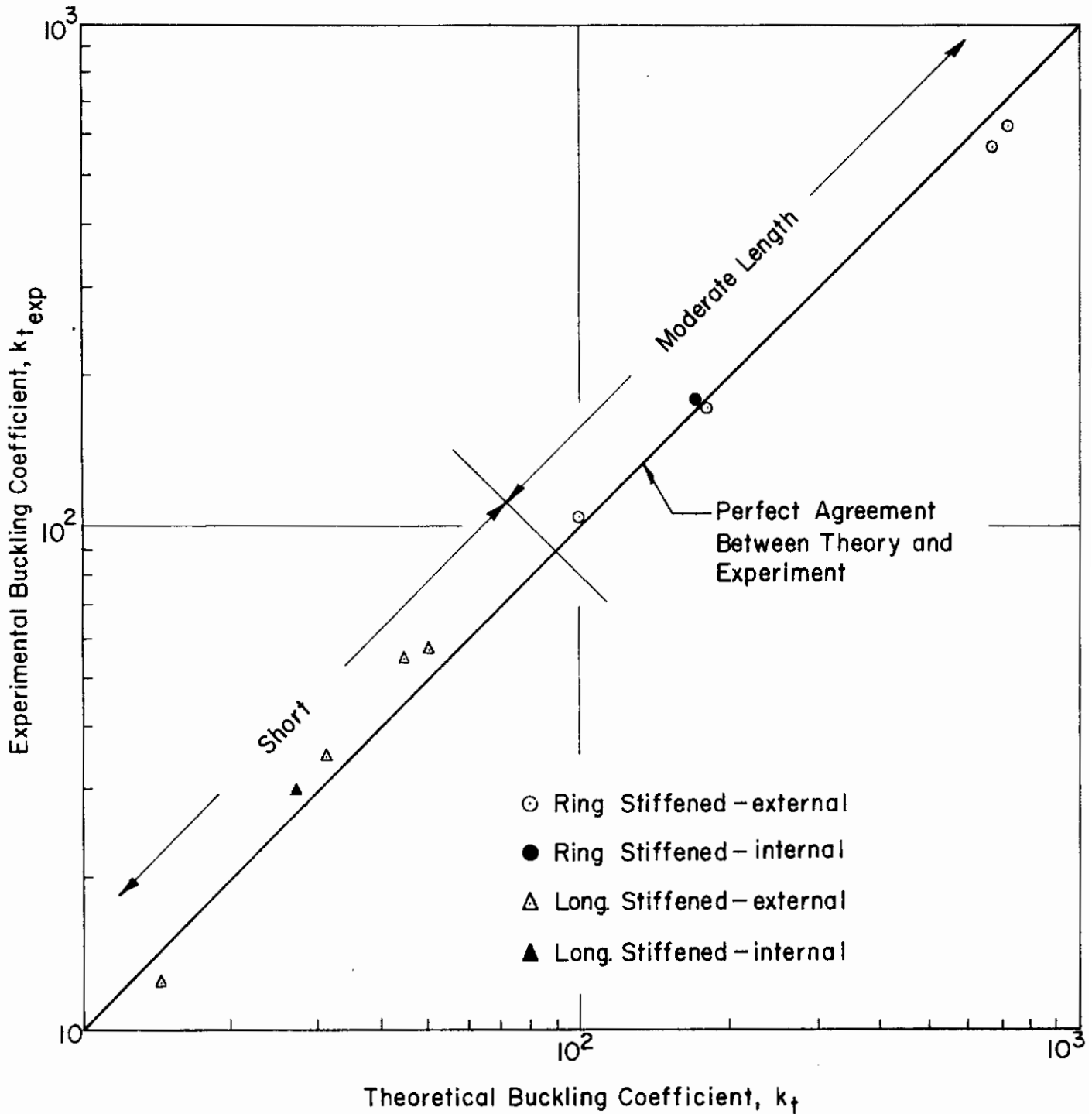
Fig. 2.14 Correlation of Theory and Experiments for Stiffened Cylinders Under Torsion

19

The longitudinally stiffened cylinders were in the short rather than moderate length region and consequently the theory presented in Ref. 1 was utilized to compute the short cylinder results shown in Figure 2.13. The corresponding test points are plotted in Figure 2.13 and it can be observed that good correlation is obtained.

The data on all torsion cylinders are summarized in Figure 2.14 where k_t experimental is plotted against k_t theoretical. In this form both short and moderate length cylinder data are presented in a unified form and the excellent correlation can be observed over the entire test range. Again it is apparent that the stiffener location has no effect upon the test results.

Hydrostatic Pressure

Correlation of experiments with theory for hydrostatic pressure loading is presented in Figure 2.15. It is to be noted that in this case the experimental data are for buckling since failure occurred at a higher pressure in all cases.

The test data for ring stiffened and longitudinally stiffened cylinders are shown in Figure 2.15. Two theoretical curves are presented: one for simply supported boundary conditions from Refs. 1 and 2 and a second for clamped boundary conditions. The derivation of the latter is presented in Appendix B. In contrast with moderate length stiffened cylinders under axial compression or torsion where several longitudinal wavelengths occur, only one half wavelength occurs for the hydrostatic pressure case. As a consequence, boundary conditions play a significant role in the moderate length region for the latter.

The boundary conditions in the experiments closely approximated clamped edges, and it is interesting to observe in Figure 2.15 that the test data correlate excellently with the theoretical curve for clamped edges. It is to be noted that in the long history of testing clamped cylinders under hydrostatic pressure, this is apparently the first time that such good correlation of theory and experiment has been achieved. The data on all cylinders under hydrostatic pressure again indicate that the stiffener location has no significant effect upon the test results.

Figure 2.16 presents a summary of the pressure test results in a different form. The abscissa of the figure is the theoretical buckling coefficient for clamped boundary conditions, and the ordinate is the cylinder buckling coefficient

20
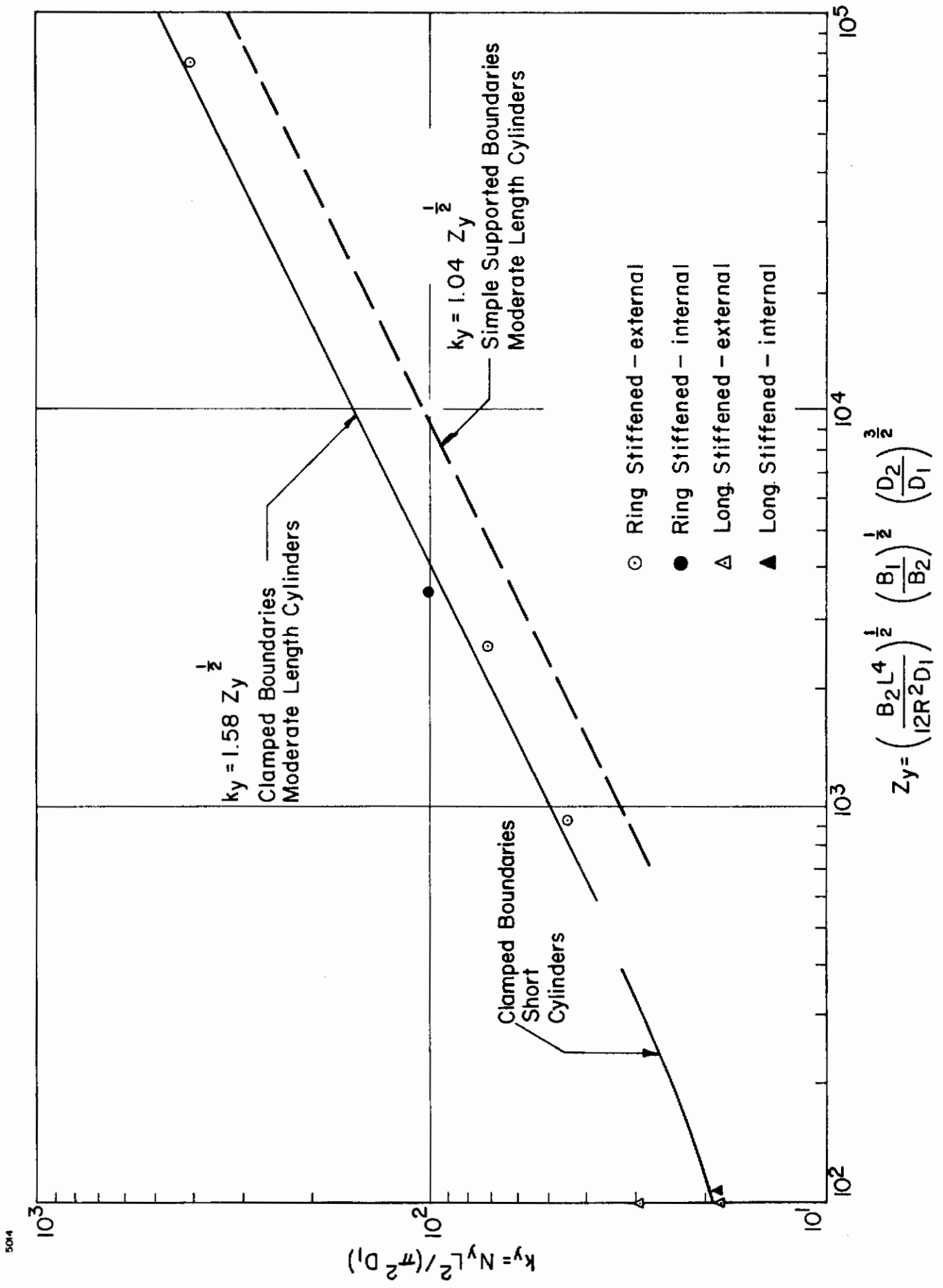
Fig. 2.15   Correlation of Theory and Experiments for Stiffened Cylinders Under Hydrostatic Pressure

$k_y = 1.04\ Z_y^{\frac{1}{2}}$
Simple Supported Boundaries
Moderate Length Cylinders

$k_y = 1.58\ Z_y^{\frac{1}{2}}$
Clamped Boundaries
Moderate Length Cylinders

Clamped Boundaries
Short
Cylinders

$Z_y = \left(\dfrac{B_2 L^4}{12 R^2 D_1}\right)^{\frac{1}{2}} \left(\dfrac{B_1}{B_2}\right)^{\frac{1}{2}} \left(\dfrac{D_2}{D_1}\right)^{\frac{3}{2}}$

$k_y = N_y L^2 / (\pi^2 D_1)$

⊙ Ring Stiffened − external
● Ring Stiffened − internal
△ Long. Stiffened − external
▲ Long. Stiffened − internal

504

21
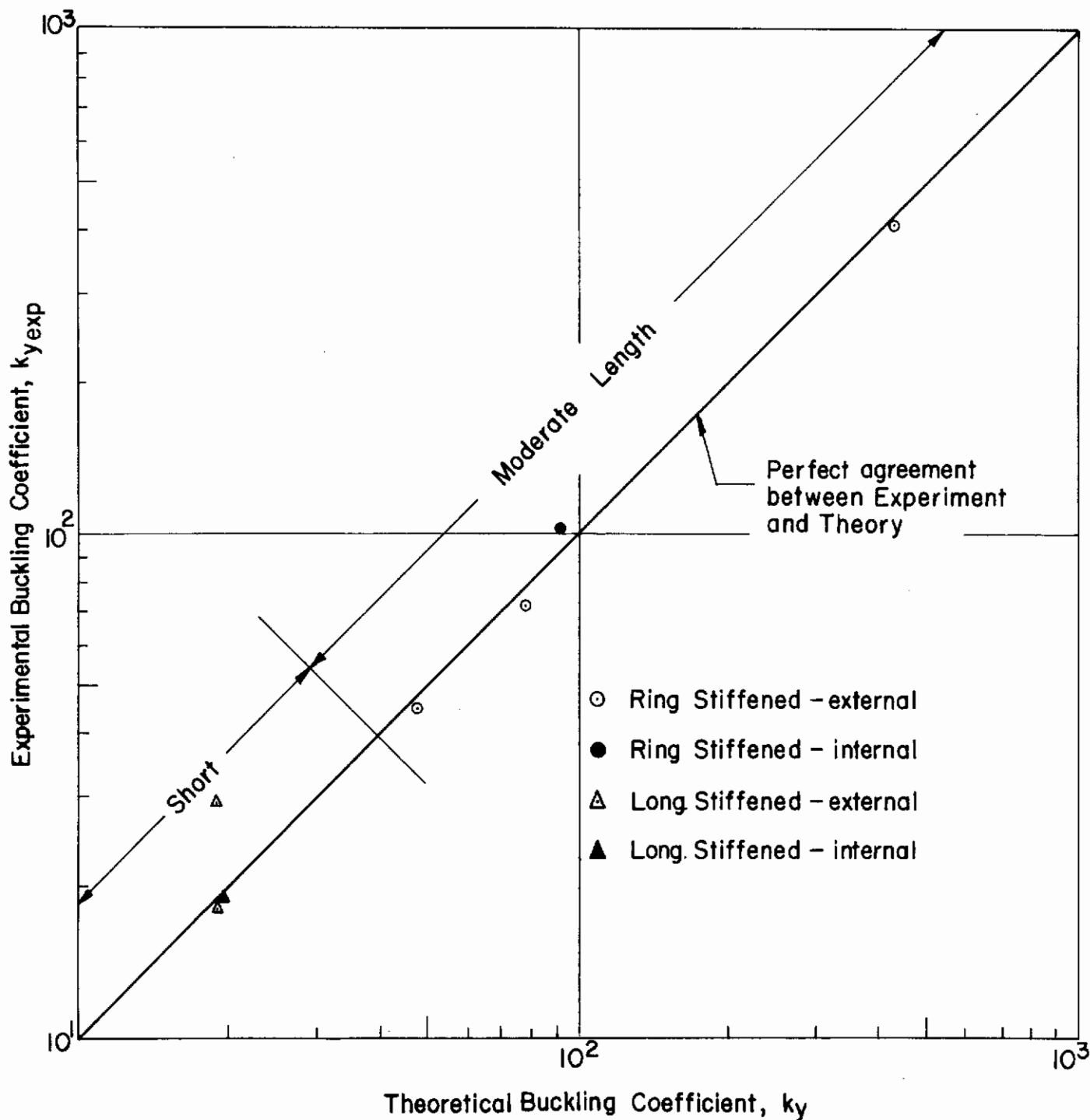
Fig. 2.16   Correlation of Theory and Experiments for Stiffened Cylinders Under Hydrostatic Pressure

22

as determined from experiments. As indicated, the experimental data for ring stiffened and longitudinally stiffened cylinders lie close to the solid line which represents perfect agreement between experiment and theory.

Program Achievements

To conclude this section on correlation of theoretical and experimental results, the excellent agreement between linear orthotropic stability theory using computed section properties and test results under a variety of loading conditions conclusively demonstrates the validity of the linear theory except possibly for longitudinally stiffened cylinders under axial compression with values of α approaching unity. In the latter case, an examination of the post buckling behavior indicates a sensitivity to imperfections similar to that characteristically obtained for isotropic cylinders.

In addition to this major objective, the following represent other achievements of this phase of the program:

a.   The stability behavior of ring stiffened cylinders under axial compression is accurately predicted by linear stability theory for values of α as low as 1.5, the smallest value tested in this program. This is relatively close to an isotropic cylinder ($\alpha = 1$) and indicates that even with a small degree of circumferential stiffening, linear theory is accurate.

b.   The stability behavior of longitudinally stiffened cylinders under axial compression is accurately predicted by the newly discovered $m = 1$ asymmetric mode of linear orthotropic theory. Excellent correlation is obtained at low values of α but as α approaches unity a sensitivity to imperfections characteristic of isotropic cylinders ($\alpha = 1$) appears.

c.   The behavior of grid stiffened (longitudinals plus rings) cylinders in compression can be characterized in terms of α.

d.   An unusually high experimental to theoretical stress ratio was obtained for the machined isotropic cylinder in compression tested in this program.

e.   The stability of ring and longitudinally stiffened cylinders under torsion and hydrostatic pressure is accurately predicted by linear orthotropic stability theory for the short and moderate length cylinder ranges.

23

f.   It has been demonstrated by the experimental results and confirmed by the orthotropic theory developed herein that boundary conditions are of considerable importance for moderate length and short cylinders under hydrostatic pressure.

g.   The test results for ring and longitudinally stiffened cylinders under all loading conditions indicate that the stiffener location, whether external or internal, has no significant effect for the ranges of variables used in this program.

3. EXTENSIONAL AND FLEXURAL RIGIDITIES

Introduction

Of particular significance in correlating the experimental and theoretical results of this program are accurate methods of determining the pertinent extensional and flexural shell rigidities of the cylinders tested. As a consequence, this section is devoted to a general discussion of the assumptions and analytical methods used, as well as certain experimental procedures that were employed to verify calculations of shearing and twisting rigidities.

The geometric parameters of the stiffened cylinders used in this program are illustrated in Figure 3.1. Because of the nature of the stiffening systems used, and to effect a considerable simplification in the computations, it was assumed that $\nu = 0$, except for the isotropic cylinders. As a consequence, the extensional rigidities B_i and flexural rigidities D_i reduce to those shown in Table 3.1 for stiffened cylinders.

Membrane Axial Rigidity

Procedures were presented by Dow, Libove and Hubka (Ref. 7) and by Crawford and Libove (Ref. 8) for determination of the membrane elastic constants of plates with waffle-like stiffening. These procedures for membrane axial rigidity involve a combination of theoretical analysis and selected experimental measurements.

The plate membrane rigidity equations of Ref. 7 involve relations for calculating t_s and t_f. Each of these quantities is essentially the sum of the shell thickness, t, and the effective additions provided by the ribs.

$$t_s = t + u_s \Delta t_s + u_f \Delta t_f \tag{3.1}$$

where u_s and u_f are coefficients to be determined experimentally in a manner prescribed in Ref. 7 while Δt_s and Δt_f are the incremental equivalent thicknesses provided by the stiffeners.

Experimental measurements of t_s were reported in Ref. 7 on waffle plates with stiffeners at various angles. In order to calculate t_s theoretically, it was first necessary to determine u_s and u_f in a semi-empirical manner. The data lie approximately 15 percent about the theoretical curve determined in that fashion

25
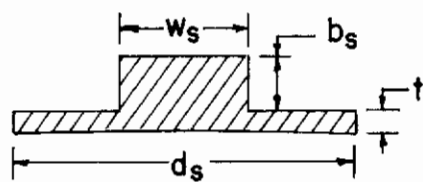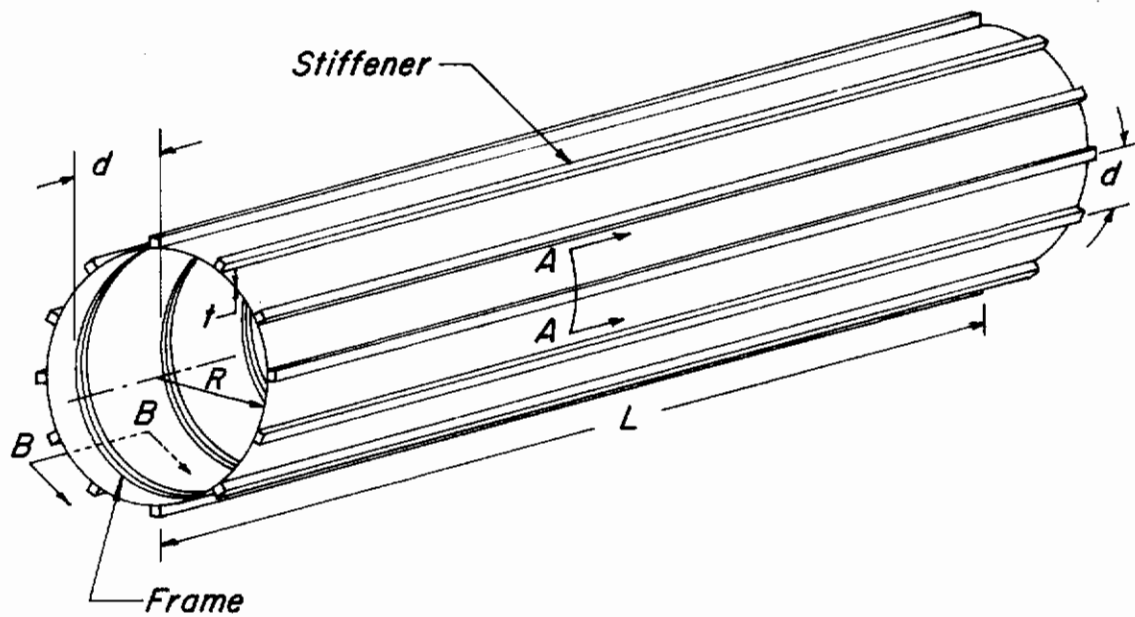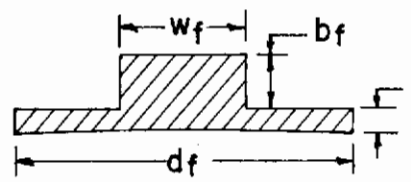
Fig. 3.1   Orthotropic Cylinder Geometric Parameters

Table 3.1

Extensional and Flexural Rigidities for Stiffened Cylinders

$B_1 = E\, t_s$ membrane axial rigidity in longitudinal direction

$B_2 = E\, t_f$ membrane axial rigidity in circumferential direction

$B_3 = 2E\, \overline{t}$ membrane shear rigidity (average)

$D_1 = E\, I_s$ bending rigidity in longitudinal direction

$D_2 = E\, I_f$ bending rigidity in circumferential direction

$D_3 = EJ/2$ twisting rigidity (average)

for stiffening systems ranging from 0° to 90° to the longitudinal direction with the best agreement (5 percent deviation) for longitudinal stiffening.

An examination of these data indicated that for this program in which the stiffeners were oriented in either the 0° or 90° directions, the formulas for t_s and t_f given in Table 3.2 were of sufficiently high precision.

Membrane Shear Rigidity

The membrane shear rigidity is the effective shear thickness of the stiffened cylinder wall, $\bar{t}$. It is defined by the relation between shear loading and shear deformation,

$$q/\bar{t} = \tau = G\gamma \tag{3.2}$$

In this program the value of $\bar{t}$ was determined by measurements of γ using 45° electrical resistance strain rosettes, and by calculation of q from torsion tests of cylinders later used for stability testing. As a consequence, the following relations are available:

$$q = T/2A \tag{3.3}$$

$$\gamma = (\epsilon_1 - \epsilon_2) \tag{3.4}$$

From Equations (3.2) to (3.4), the effective shearing thickness

$$\bar{t} = (1/2AG)T/(\epsilon_1 - \epsilon_2) \tag{3.5}$$

In a given test, the quantity 2AG was a calculated constant for a given cylinder. The value of $T/(\epsilon_1 - \epsilon_2)$ was determined from the slope of the plot of the applied torque as a function of the difference of the 45° diagonal strains, $(\epsilon_1 - \epsilon_2)$ (See Figure 3.2). The determination of T involved the load applied by the testing machine and the lever arms of the torsion jig, arranged as shown in Figure 3.3. The values of ϵ_1 and ϵ_2 were obtained as averages over several stiffeners by cementing long strain gages to the unstiffened face of the shell wall.

The experimental data for $\bar{t}$ as a function of α obtained in this program are shown in Figure 3.4. Also shown for comparison with the test data is an effective $\bar{t}$ computed from the relation:

$$\bar{t}/b = (1/2b)(t_s + t_f) \tag{3.6}$$

28
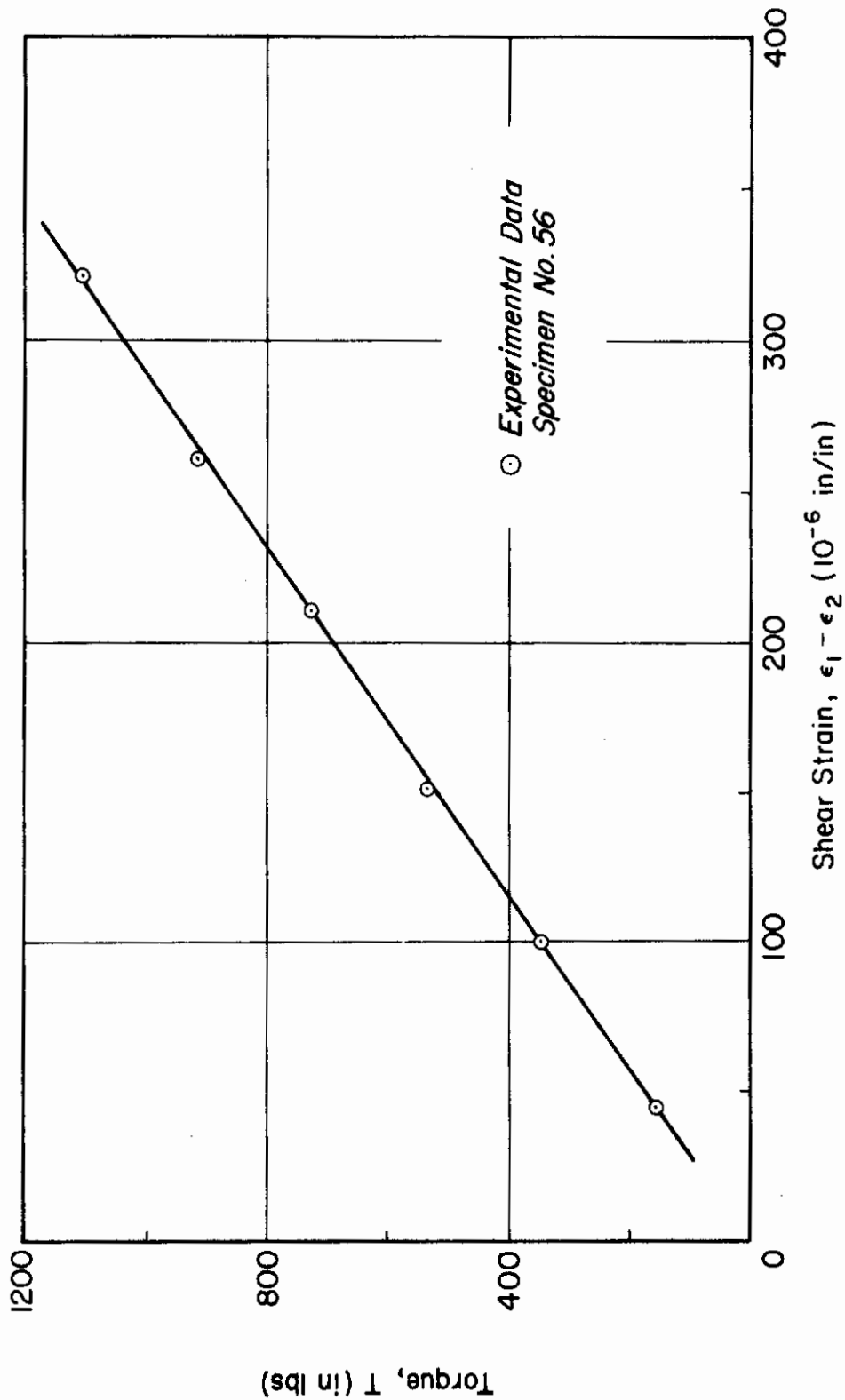
Fig. 3.2 Typical Torque vs Shear Strain Measurements Used to Determine Cylinder Effective Shear Stiffness

The plot axes:
- Vertical axis: Torque, T (in lbs)
- Horizontal axis: Shear Strain, $\epsilon_1 - \epsilon_2$ (10^{-6} in/in)
- Legend: ⊙ Experimental Data Specimen No. 56

5017

29

ARA TEST MACHINE

TEST SPECIMEN

STRAIN
GAGE

STRAIN GAGE
RECORDER
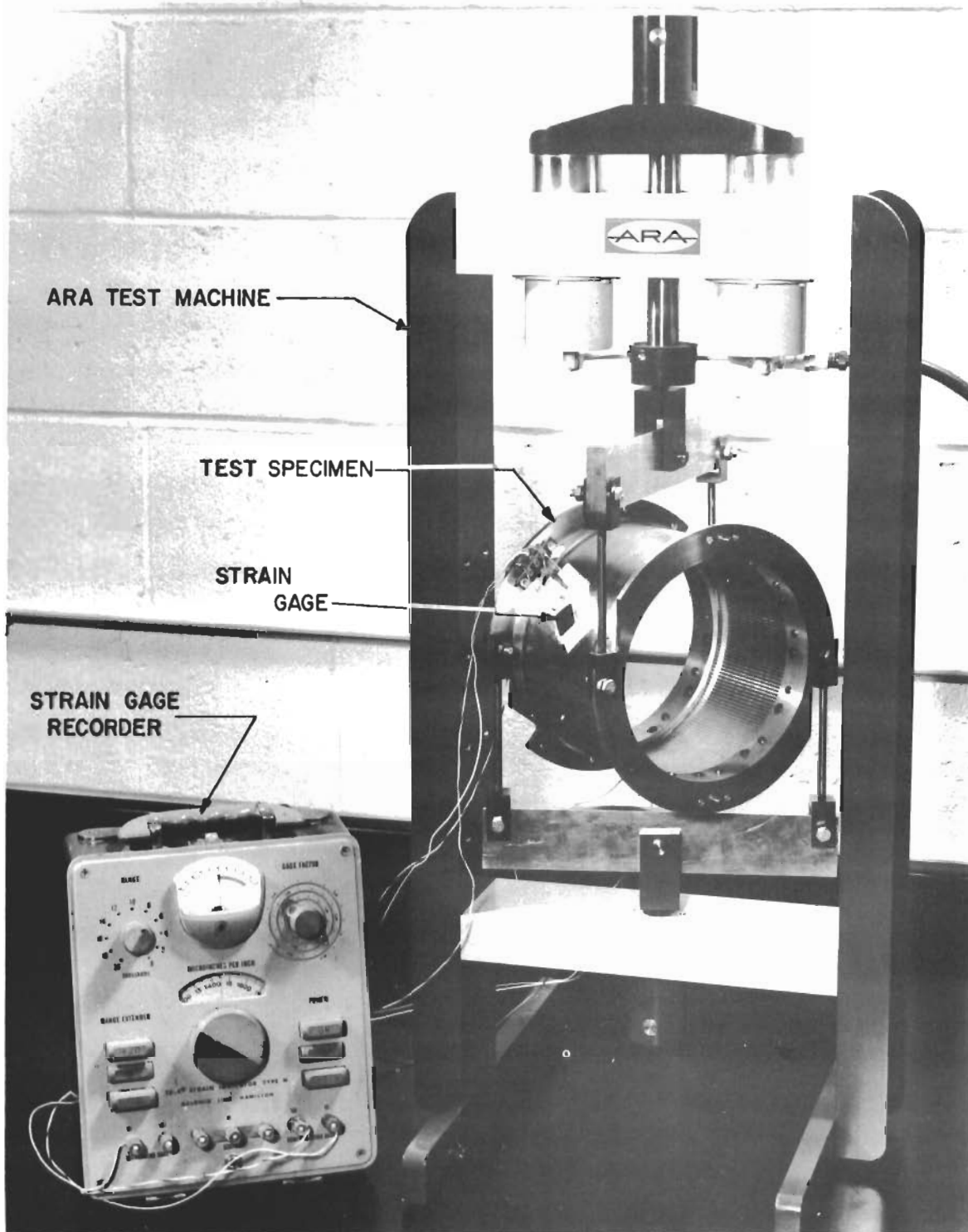
Fig. 3.3   Test Arrangement for Determination of Effective Shear Thickness
for Longitudinally Stiffened Cylinder.

30

w/d = 0.5

$$\frac{\bar{t}}{b} = \frac{1}{2b}(t_s + t)$$

$\bar{t}$ = Effective Shear Thickness
b = Stiffener Height
t_s = Area of Sheet and Stiffener per Unit Width
t = Sheet Thickness
w = Stiffener Width
d = Stiffener Spacing
I_s = Moment of Inertia of Sheet and Stiffener per Unit Width
I = Moment of Inertia of Sheet per Unit Width

Effective Shear Thickness Parameter, $\bar{t}/b$

Geometry Parameter, $a = t_s I/(t\, I_s)$
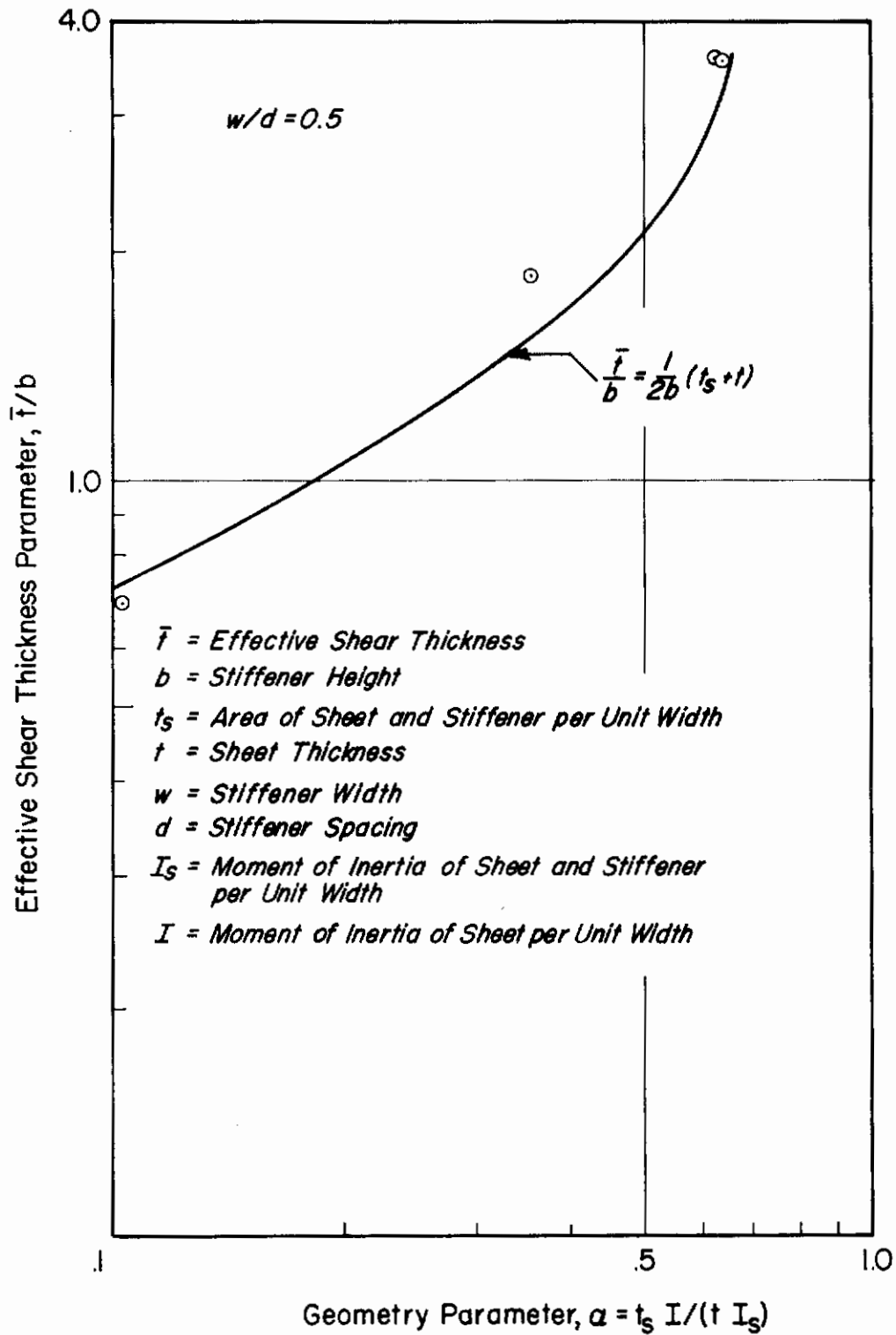
Fig. 3.4   Effective Shear Thickness vs Geometry for Longitudinally Stiffened Cylinders

5018

31

It can be observed that Equation (3.6) is in relatively good agreement with the test data over the range of variables used. As a consequence, Equation (3.6) was used to compute $\overline{t}$ in this program.

Bending Rigidity

Through application of the semiempirical procedure described in Ref. 7, the bending rigidities of waffle grid plates were determined and compared to experimental data. Excellent agreement was found for plates loaded by bending moments orthogonal with the stiffening system. However, departures were found for stiffening in other directions with the largest discrepancy occurring for 45° stiffeners. Other bending investigations conducted by Hoppmann (Ref. 9) and by Hoppman, Huffington and Magness (Ref. 10) on longitudinally stiffened plates indicated that theory and experiment correlated within 6 percent.

As a result of these investigations, the straight forward calculation of bending rigidities I_s and I_f presented in Table 3.2 were deemed to be of sufficient accuracy for this program.

Torsional Rigidity

Because of uncertainties in calculating twisting rigidities on the basis of the available literature, the torsional rigidities of the shell walls of representative stiffened cylinders were determined directly from torque/twist experiments on stiffened flat plates. The technique involved a testing machine designed especially for these measurements as described in Ref. 11. An accuracy of within 2.5 percent was established by correlating test results on isotropic plates with theory. The use of plate data to obtain shell wall rigidities is a satisfactory approximation for the relatively large R/t values of the cylinders used in this program.

Long flat stiffened plate models representative of the dimensional ratios employed on the stiffened cylinders of this test program were machined of 6061-T6 aluminum alloy. These models were tested in the machine described in Ref. 11 and utilized similar test procedures in which J was determined from the slope of the torque/twist data using the relation

$$J = T/G(d\theta/dx) \tag{3.7}$$

TABLE 3.2

Summary of Equations for the Determination of Geometrical and Rigidity Parameters from Cylinder Measurements

Ring Stiffened Cylinder

(3.15)** $t_s = t$ (3.16) $b = t/(t/b)$ (3.17) $t_f = b(w/d + t/b)$ (3.18) $I_s/b^3 = (1/12)(t/b)^3$

(3.19) $\bar{t} = (1/2)(t_s + t_f)$

(3.20) $I_f/b^3 = (1/3)(t/b)^3 + w/d\,[(1/12)+(t/b+.5)^2] - (w/d)[t/b+.5+(.5)(t/b)^2/(w/d)]^2\,[1+(t/b)/(w/d)]^{-1}$

(3.21) $J/b^3 = (1/3)\left\{(t/b)^3[1-(w/d)] + [(t/b)+1]^3(w/d)F^\phi\right\}$

Longitudinally Stiffened Cylinder

(3.22) $t_f = t$ (3.23) $b = t/(t/b)$ (3.24) $t_s = b(w/d + t/b)$ (3.25) $I_f/b^3 = (1/12)(t/b)^3$

(3.26) $\bar{t} = (1/2)(t_s + t_f)$

(3.27) $I_s/b^3 = (1/3)(t/b)^3 + (w/d)[(1/12)+(.5+t/b)^2] - (w/d)[.5+t/b+.5\,(t/b)^2/(w/d)]^2[1+(t/b)/(w/d)]^{-1}$

(3.28) $J/b^3 = (1/3)\left\{(t/b)^3[1-(w/d)]+[(t/b)+1]^3(w/d)F^\phi\right\}$

Grid Stiffened Cylinder

(3.29) $b_f = t/(t/b_f)$ (3.30) $b_s = t/(t/b_s)$ (3.31) $t_f = b_f(w_f/d_f+t/b_f)$ (3.32) $t_s = b_s(w_s/d_s+t/b_s)$ (3.33) $\bar{t} = (1/2)(t_s+t_f)$

(3.34)* $J/b_s^3 = (1/4)\left\{(t/b_s)^3(1-w_s/d_s)+(t/b_s+1)^3(w_s/d_s)F^\phi\right\}+(1/12)(1+b_f/b_s+t/b_s)^3$

(3.35)△ $J/b_s^3 = (1/4)(b_f/b_s)^3\left\{(t/b_f)^3(1-w_f/d_f)+(t/b_f+1)^3(w_f/d_f)F^\phi\right\}+(1/12)(1+b_f/b_s+t/b_s)^3$

(3.36) $I_f/b_f^3 = (1/3)(t/b_f)^3+(w_f/d_f)[(1/12)+(.5\,t/b_f)^2]-(w_f/d_f)[.5+t/b_f+.5\,(t/b_f)^2/(w_f/d_f)]^2[1+(t/b_f)/(w_f/d_f)]^{-1}$

(3.37) $I_s/b_s^3 = (1/3)(t/b_s)^3+(w_s/d_s)[(1/12)+(.5+t/b_s)^2]-(w_s/d_s)[.5+t/b_s+.5\,(t/b_s)^2/(w_s/d_s)]^2[1+(t/b_s)/(w_s/d_s)]^{-1}$

**Equation Number ϕ See Figure 3.6   *$\alpha \leq 1.0$ △$\alpha > 1.0$

It was desired to evolve a general analytical procedure for the purposes of calculating J directly from the geometric properties of the cross section. For this purpose, the following approximate analysis was devised. The torsional rigidity of a long twisted flat strip is given by (Ref. 12)

$$J = \overline{L}t^3/3 \tag{3.8}$$

For the shorter strips which it is assumed comprise the stiffened plate cross section as indicated in Figure 3.5, a correction must be applied to Equation (3.8) in the form (Ref. 12)

$$J = F\overline{L}t^3/3 \tag{3.9}$$

where: $F = 1 - 0.63 \, (t/\overline{L})$; for $\overline{L}/t >> 3$. $\tag{3.10}$

For the system of elements shown in Figure 3.5, it was assumed that the following relation could be used where now the correction factor F is as yet unspecified.

$$3J = \overline{L}t^3 + Fwh^3 \tag{3.11}$$

With $\overline{L} = (d-w)$, Equation (3.11) can be written as:

$$J/b^3 = (1/3)(t/b)^3 \, (1-w/d) + (F/3)(t/b+1)^3 \, (w/d) \tag{3.12}$$

The factor F, was determined from Equation (3.12) using the measured value of J and the geometric properties of the specimens tested. The data were then plotted as a function of b/w as shown in Figure 3.6. By fairing a smooth curve through these data, and then utilizing that curve to calculate J for the test specimens, excellent agreement was obtained between this method of calculation and experimental data as shown in Figure 3.7. For the longitudinal and ring stiffened test cylinders, Equation (3.12) in conjunction with Figure 3.6 was used to calculate J.
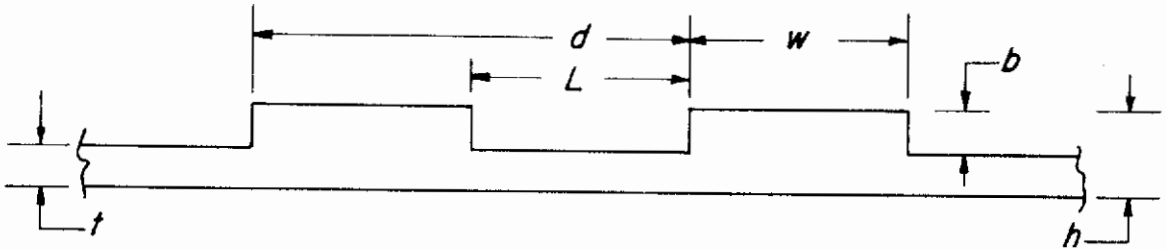
(a) Section of Wall
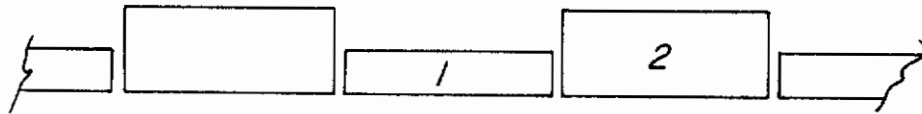
$$3J = Lt^3 + Fwh^3$$

(b) Rigidity Relation

Fig. 3.5 Division of Stiffened Shell or Plate Into Elements for Calculation of Torsional Stiffness Parameter

5019

35
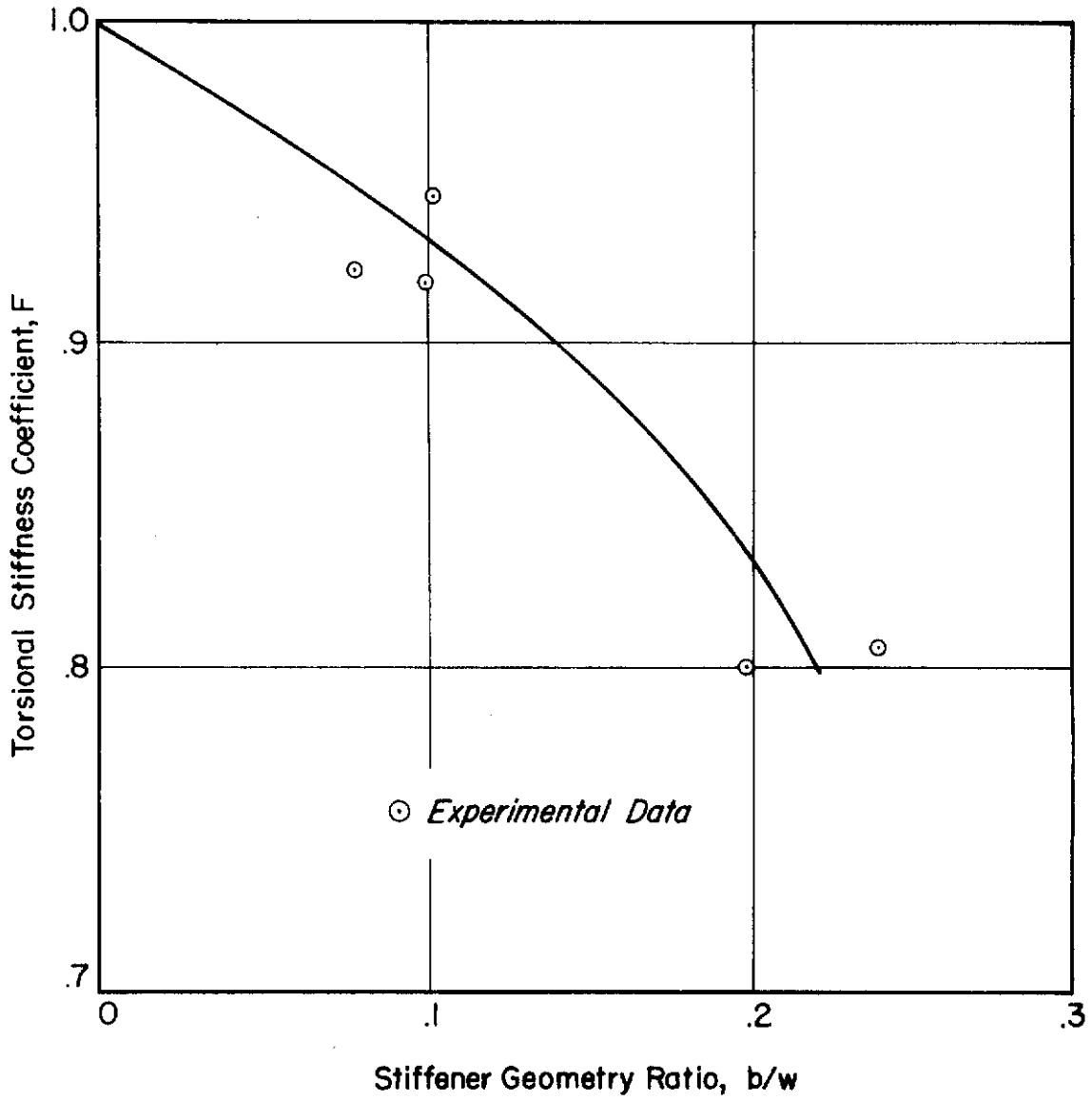
Fig. 3.6   Torsional Stiffness Coefficient From Stiffened Plate Twist Experiments

502c

36
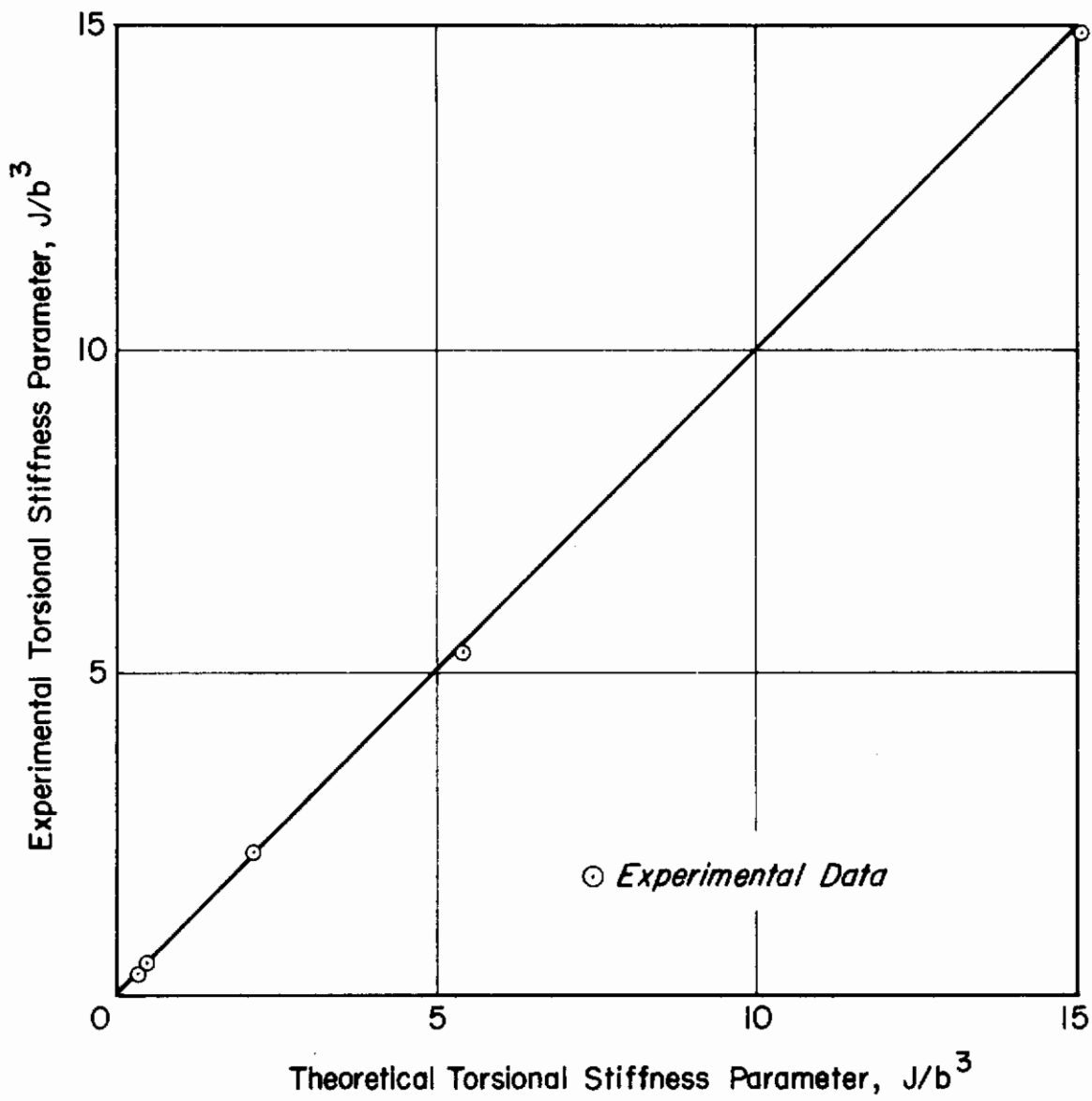
Fig. 3.7   Correlation of Theory and Experiment for Flat Orthotropic Plates Under Torsion

For the grid stiffened cylinders, a test was conducted on a flat square plate representative of an $\alpha = 1$ design. The test arrangement is shown in Figure 3.8. As indicated the plate was supported on three corners and load applied via dead weights at the fourth corner. This load together with its reactions at the plate supports produce a twisting moment on the plate. The four dial gage indicators placed at prescribed points on the specimen surface allow the measurement of the specimen twist per unit length.

The test procedure consisted of hanging weights from the chain and recording the dial gage readings corresponding to each weight increment. The reduced data was then plotted on a curve of torque vs twist per unit length, and the specimen torsional stiffness was found from the slope of the curve using Equation (3.7).

The reproducibility of the test results was confirmed by data obtained from several test runs. It was also determined that the torque-twist results were essentially the same for two different grid placements (4 and 6 inch squares) of the dial gages. Further evaluation of this experimental arrangement and procedure was obtained by conducting torsion tests on an isotropic plate. It was found that test results for the isotropic plate agreed with theoretical values within 8 percent.

In order to generalize the plate test results for other grid geometries, an empirical relationship for cylinder cross section torsional stiffness was postulated as follows:

$$J = J_o + \Delta J_o \qquad (3.13)$$

In this formulation J_o is the torsional stiffness based on one set of stiffening elements only (either longitudinal or ring depending on the cylinder α) and is found from Equation (3.12). The increment in torsional stiffness, ΔJ_o, realized through the addition of a second stiffening array was considered to follow a relationship of the following form:

$$\Delta J_o = K [h^3/3 - J_o]$$

where $\qquad\qquad\qquad\qquad\qquad\qquad\qquad\qquad\qquad\qquad\qquad (3.14)$

$$h = t + b_s + b_f$$

This equation expresses the increment in torsional stiffness as a fraction, K, of the difference between the maximum possible isotropic unit torsional stiffness and the torsional stiffness for a unidirectional stiffener array system.

38

From torsion tests on the grid stiffened flat plate, a value for K of 0.25 was indicated. This value together with Equations (3.12), (3.13) and (3.14) was then used to determine the empirical equations for the torsional stiffness of the grid stiffened cylinders (characterized by either longitudinal or ring stiffened α values) presented in Table 3.2.
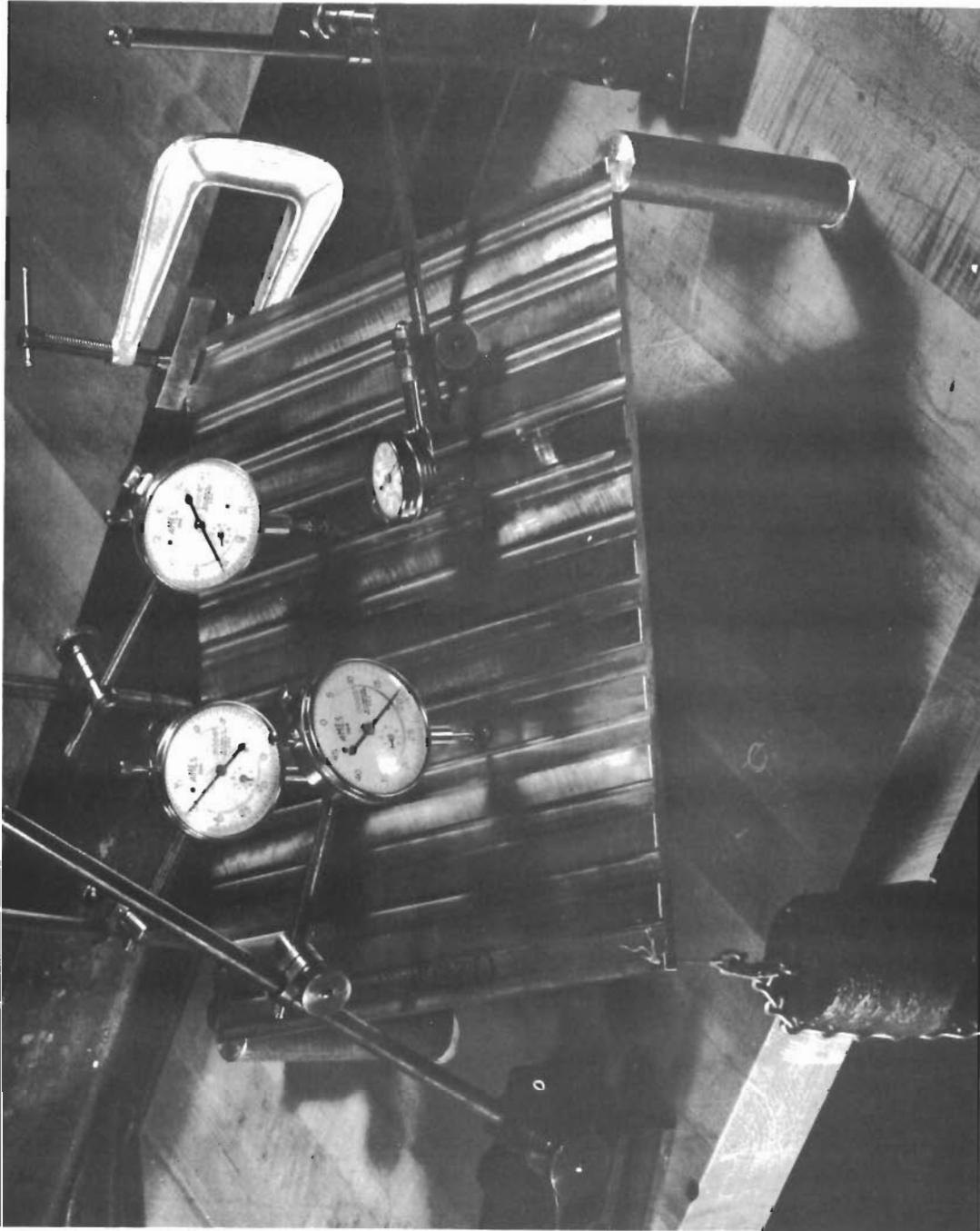
Fig. 3.8   Test Arrangement for Conducting Torsional Stiffness Measurements on a Grid Stiffened Flate Plate.

4. AXIAL COMPRESSION TESTS

Design and Fabrication of Test Specimens

Three types of cylinder configurations, ring stiffened, longitudinally stiffened, and grid stiffened designs, were employed to obtain experimental data on the general instability of orthotropic cylinders in axial compression. With regard to design for general instability, cylinder geometries were such that other possible failure modes such as buckling of the skin between stiffeners, local buckling of the stiffeners, and Euler buckling corresponded to stress levels greater than the critical stress for general instability. Also, a monolithic type of construction technique was employed so as to eliminate design consideration of failure modes associated with attachments of the stiffener to the sheet. Uncertainties in cylinder behavior associated with material property effects were minimized by designing the specimens to fail at a stress level below the proportional limit of the material. Consideration of the effect of stiffener location on cylinder behavior was achieved by designing ring stiffened and longitudinally stiffened specimens with stiffeners on either the outside (externally stiffened) or inside (internally stiffened) cylinder wall.

Geometrical constraints associated with the manufacture and testing of the specimens also influenced the detailed design. For example, the specimens were fabricated on a lathe which limited the maximum cylinder diameter to about 13 inches. Furthermore, the capacity of the ARA testing machine is 12,000 lbs. which places a maximum limitation on the cylinder cross sectional area for a given design failure stress.

In order that possible interactions between the loading platens of the testing machine and the test specimen would not influence cylinder buckling behavior, each test specimen was integrally reinforced at its ends by a heavy ring. The end reinforcing rings also stiffened the cylinder wall and facilitated machining the specimen to close tolerances.

For ring stiffened cylinders, effort was focused on investigating cylinder behavior for specimens characterized by $\alpha < 10$ and particularly for cylinders with $\alpha \leq 3.0$. Since previous work on the general instability of ring stiffened cylinders (Ref. 4) included test data in the α range between 3 and 20, this selection for design α resulted in a minimum duplication of test effort and also gave test data in an unexplored α region. The longitudinally stiffened designs had cross sectional dimensions similar to that for the ring stiffened cylinders and corresponded to $0.1 < \alpha < 1.0$. This

arrangement allowed a meaningful comparison of test results on the basis of stiffener orientation (longitudinal vs ring stiffened). Finally, the α range for the grid stiffened design $(0.5 \leq \alpha \leq 2.0)$ was chosen so as to bracket that for the ring stiffened and longitudinally stiffened cylinders in the vicinity of $\alpha = 1.0$.

Further considerations leading to the detailed design of the test specimens are presented below for the ring stiffened cylinder configuration. The design technique, however, was applied to both the longitudinally stiffened and grid stiffened configurations.

A typical repeating element of the cylinder wall of a ring stiffened cylinder is shown in Section B-B of Fig. 3.1. For this configuration it can be shown that α is a function of the stiffener width/skin width ratio (w/d) and the skin thickness/stiffener height ratio (t/b). A typical curve of this relationship generated for w/d = 0.5 is presented as Fig. 4.1. (One observes from the ordinate of the figure that the design curve also applies for longitudinally stiffened cylinders.) Once the design α is specified, therefore, the thickness ratio t/b follows directly from curves such as shown by Fig. 4.1 for a given w/d ratio.

For a given α and either w/d or t/b the theoretical buckling stress is a function of material properties and the cylinder radius/skin thickness ratio (R/t). This relationship is illustrated by the curve in Fig 4.2A for an aluminum material $(E = 10^7)$, $\alpha = 1.5$, w/d = 0.5, and assuming moderate-length cylinder behavior. One observes from the curve that the buckling stress decreases as the R/t ratio increases. Manufacturing considerations favor the selection of low values for the design R/t since for a given radius this results in the largest wall thickness and attendant ease for dimensional control. However, it is desirable to keep the buckling stress below the material proportional limit as noted earlier, and this criterion together with curves such as Fig. 4.2A establish the lower limit for R/t.

Specimen design for moderate-length cylinder behavior is achieved by control of the curvature parameter, Z_x. For a given α and R/t, Z_x is a function of the length/radius ratio (L/R). Fig 4.2B shows a typical plot of this relationship for $\alpha = 1.5$ and R/t = 380. Information given in Reference 1 show that moderate-length cylinder behavior is associated with $Z_x > 10$, and this condition together with curves such as shown in Fig 4.2B establish a lower limit for the L/R ratio. For this investigation specimen designs for a given α and R/t were chosen to include a range of Z_x by selecting several values for L/R.

In summary, the detailed design of test specimens was achieved as follows: for a given design α and w/d, the required t/b ratio was determined from curves such as shown in Figure 4.1. Once the material of construction and the design buckling stress was established, the required R/t ratio was determined for a given α with the

42
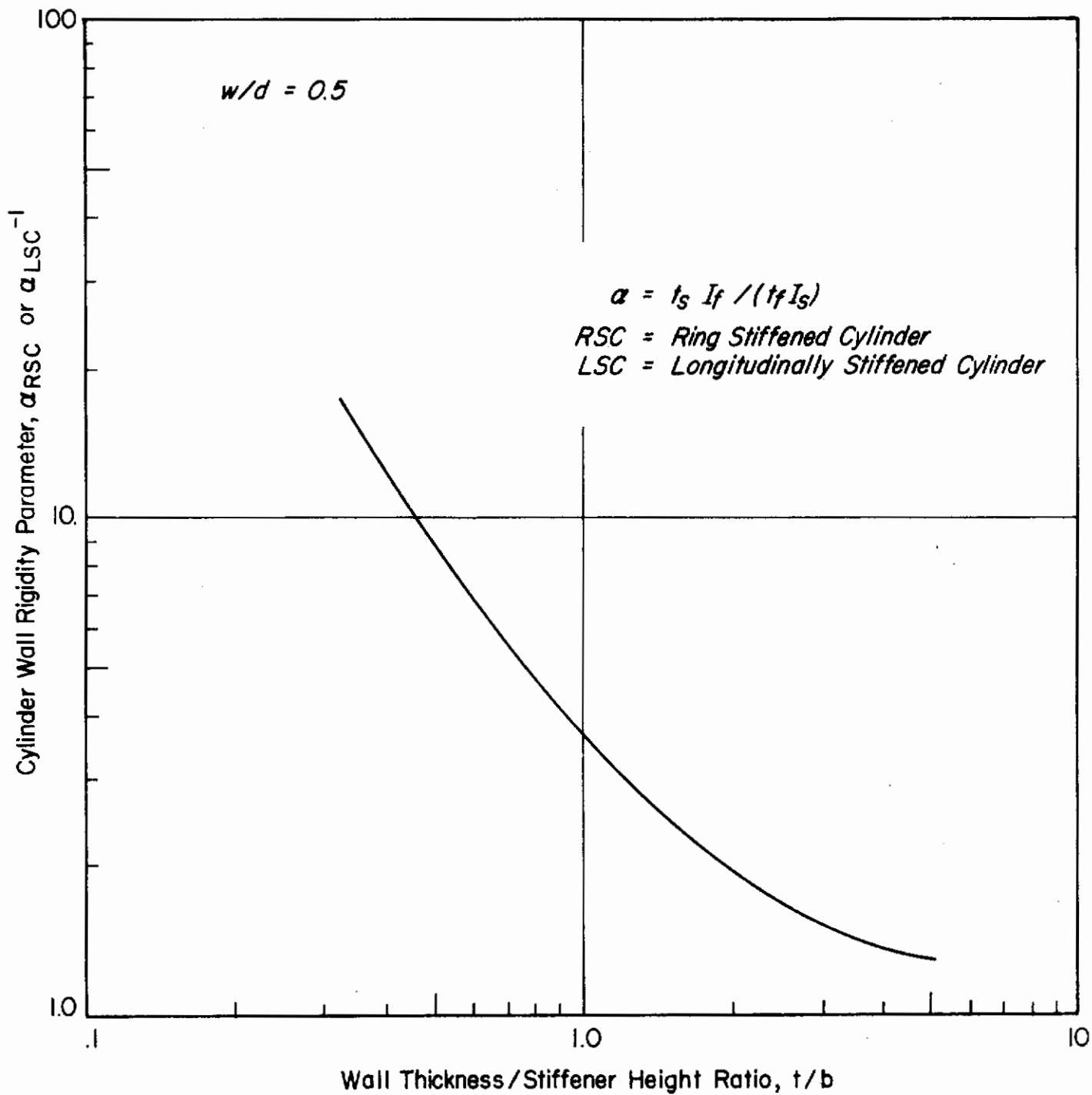
Fig. 4.1   Cylinder Wall Ridigity Parameters vs Ratio Cross Sectional
Dimensions

43

(A)

(B)
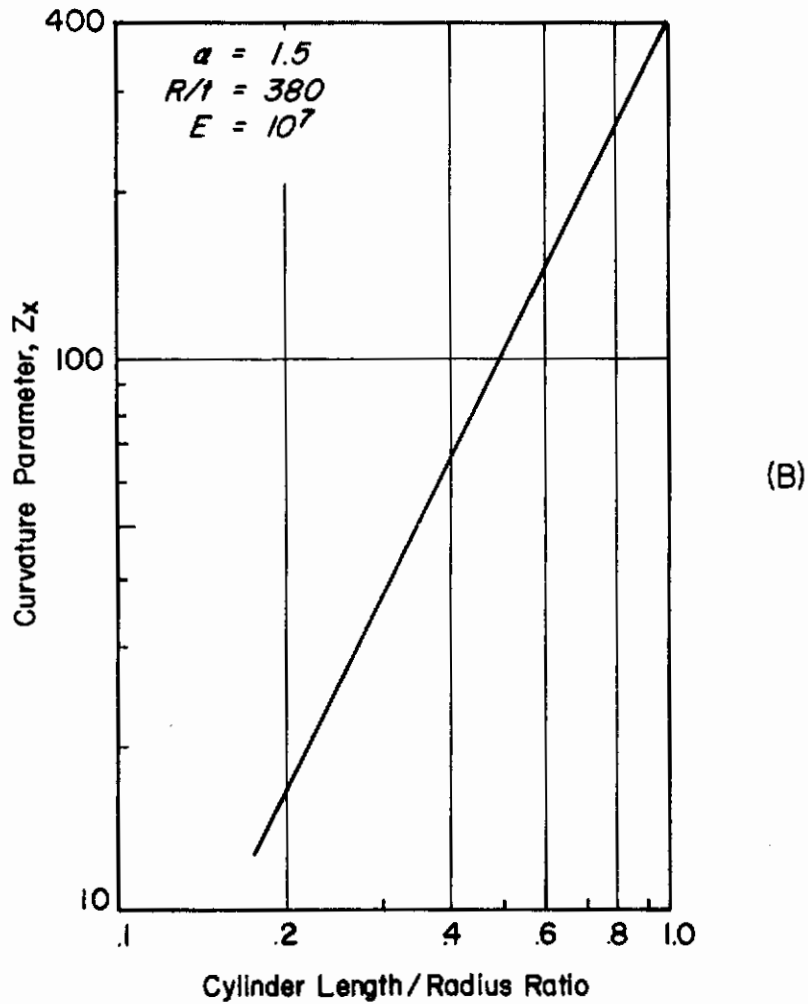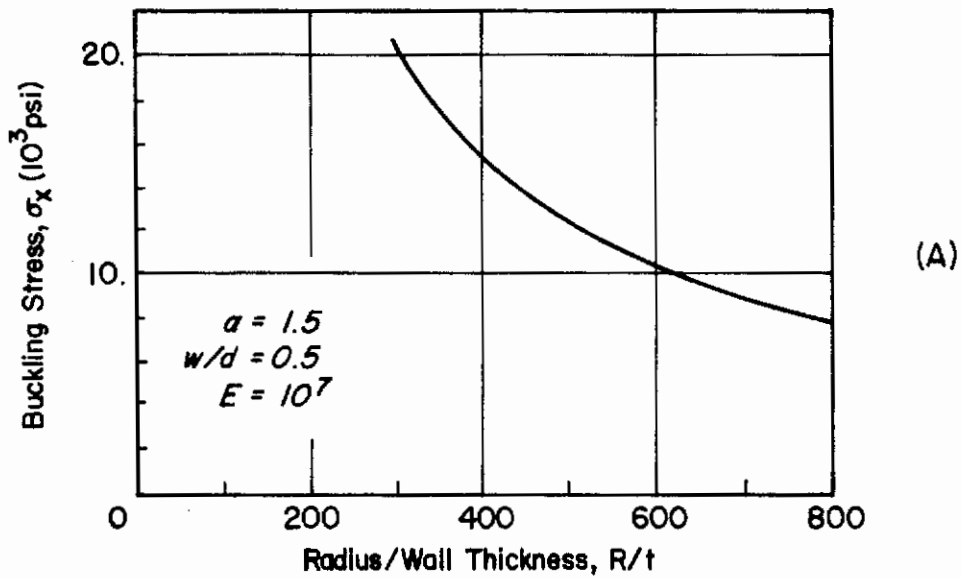
Fig. 4.2   Typical Design Curves for Axial Compression Specimens

44

aid of curves similar to Fig. 4.2A. Finally, the moderate-length cylinder criterion for ring stiffened cylinders was satisfied by choosing values for the L/R ratio from curves such as Fig. 4.2B such that $Z_x > 10$. The design procedure based on moderate-length cylinder theory was also used for the longitudinally stiffened cylinders as noted previously. Subsequent examination of the specimen geometries, however, revealed that these cylinders were subject to buckling in a short-cylinder asymmetric mode as discussed below.

Although much experimental data is available in the literature for isotropic cylinders under axial compressive loading, it appeared that a more meaningful evaluation of the orthotropic cylinder data of this report would result if some isotropic cylinder results were obtained for test conditions similar to that for the orthotropic cylinders. Accordingly, a few tests were performed on isotropic cylinders. The test specimens were designed to fail at a stress of 20,000 psi and had a nominal Z of 400 which is in the moderate-length cylinder region. The cylinder ends were reinforced by integral rings to facilitate specimen fabrication and minimize interactions between the loading platens of the testing machine and the cylinder wall.

All of the test specimens were machined on a lathe from a 6061-T6 aluminum tube. In order to ensure an even distribution of circumferential axial load during the test, extreme care was exercised in the fabrication of each specimen such that the cylinder walls would be concentric with the axis of the cylinder, and that the cylinder ends would be flat, square, and parallel. The circular rings which provided the stiffening elements for the ring stiffened cylinders were formed into the cylinder wall by a threading operation. The longerons for the longitudinally stiffened specimens were formed in the cylinder wall by cutting closely spaced slots along the cylinder axis. For the externally stiffened cylinders, these slots were cut by a slitting saw held in a Domore grinder which was adapted to the lathe carriage so as to transverse parallel to the cylinder axis on an automatic feed. Accurate control over the circumferential slot spacing was obtained by adapting a Brown and Sharpe index head to the lathe spindle. Since space requirements precluded the use of the grinder for fabrication of the internally stiffened cylinders, the slots for these specimens were cut using a broaching operation with the tool attached to a long boring bar. In this case, hand feeding the carriage with many small cuts per slot resulted in the best dimensional control for the specimen. As before, the slot spacing was achieved using the index head. Fabrication of the grid stiffened cylinders was achieved through a combination of the manufacturing techniques described. For these specimens, the longitudinal stiffeners were formed on the outside cylinder wall with the Domore grinder, and the ring stiffeners were threaded on the inside cylinder wall.

45

Test Arrangement and Procedure

Extreme care was used in the axial compression test arrangement to ensure that a uniform distribution of axial load was applied to the test specimen. A picture of the test arrangement without the test specimen is presented as Fig 4.3. The loading platens shown, which transfer the load from the machine to the specimen, are steel cylindrical disks which were ground flat to within 0.3×10^{-3} in. With a small load induced in the testing machine to take up slippage between parts, the platens were aligned in parallel to within 0.2×10^{-3} in. by means of the jacks shown between the carriage and upper loading plate. An aluminum disc was mounted on the lower loading platen which allowed the test specimen to be aligned concentric with the centroid of the applied load within approximately 10.0×10^{-3} in.

During the test, load was applied slowly to the specimen until buckling occurred. Stops were provided between the loading platens to limit the post buckling axial shortening of the specimen. A post failure picture of a longitudinally stiffened cylinder in the test machine is shown in Fig. 4.4. Post-failure photographs of test specimens representative of each cylinder configuration are shown in Fig. 4.5.

As indicated, the axial compression tests were performed with the cylinder ends bearing flat-ended directly against the loading platens. It is possible that some radial cylinder end restraint was provided by the centering disk on the lower load platen. Both cylinder ends had integral reinforcing rings, and the effective cylinder length was chosen as the distance between rings. The exact nature of the cylinder boundary conditions at the end reinforcing ring-cylinder interface are not known; however, for moderate length cylinders characterized by several buckle wavelengths along the cylinder axis, the boundary conditions should be relatively unimportant.

Accuracy of Experimental Data

The maximum load sustained by a specimen during a compression test was recorded by an indicator on the dial of the pressure gage of the ARA testing machine. This maximum test load corresponded to failure of the test specimen. The testing machine pressure gage was calibrated in 0.25 psi increments and could easily be read to this precision.

Other experimental data involved measurements of the test specimen geometry-- e.g., cylinder length (L), radius (R), wall thickness (t), total height (h), stiffener width (w), and stiffener spacing (d). The length and radius were measured by a vernier caliper which could be read within 0.5×10^{-3} in. As indicated above the cylinder length was measured between the cylinder end reinforcing rings. Wall thickness and total height measurements were made using a pointed micrometer

46

Contrails

ARA TESTING MACHINE
UPPER LOADING PLATEN
ALIGNMENT JACK
STOPS
DISC FOR CENTERING TEST SPECIMEN
LOWER LOADING PLATEN
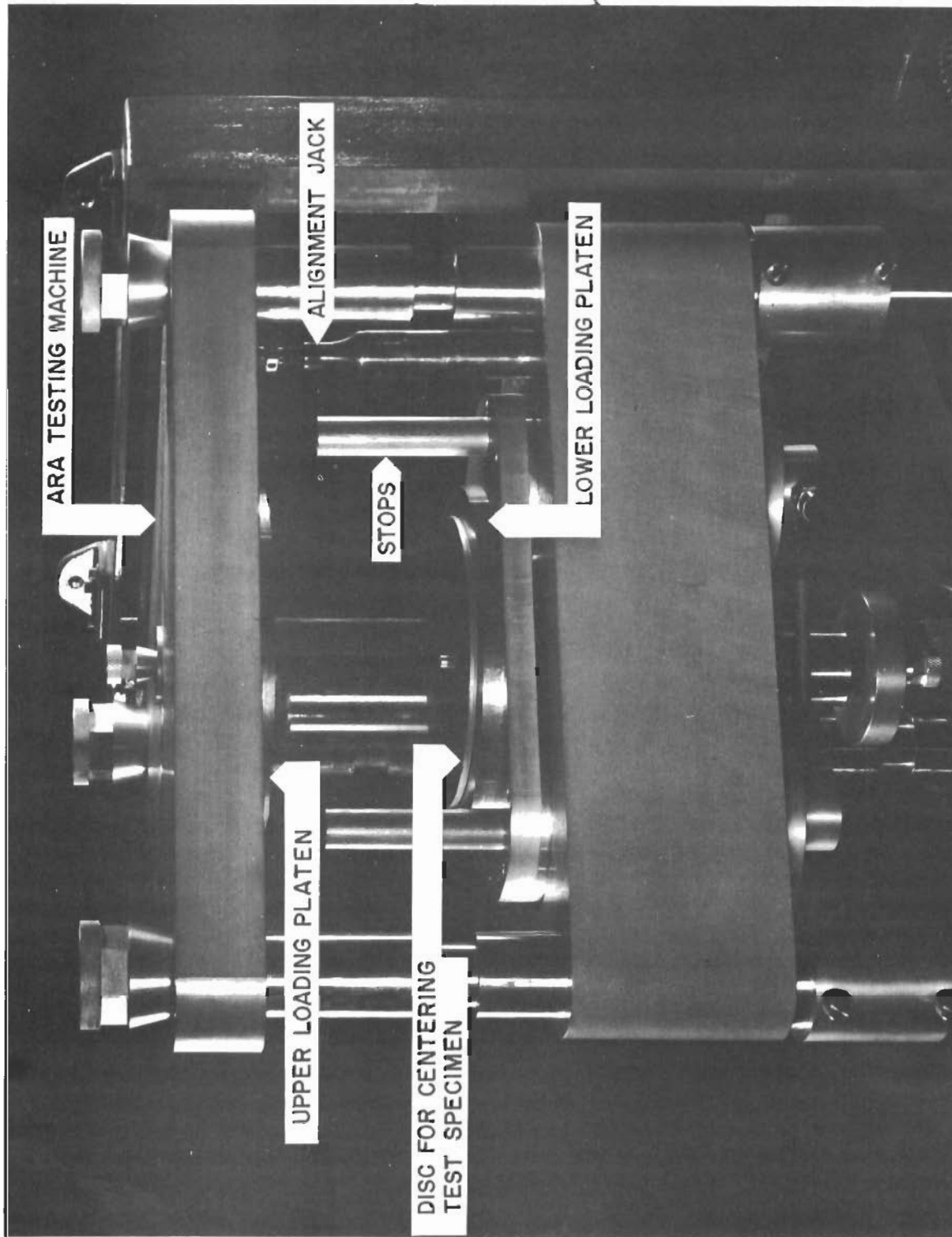
Fig. 4.3 Axial Compression Test Fixture.

Approved for Public Release
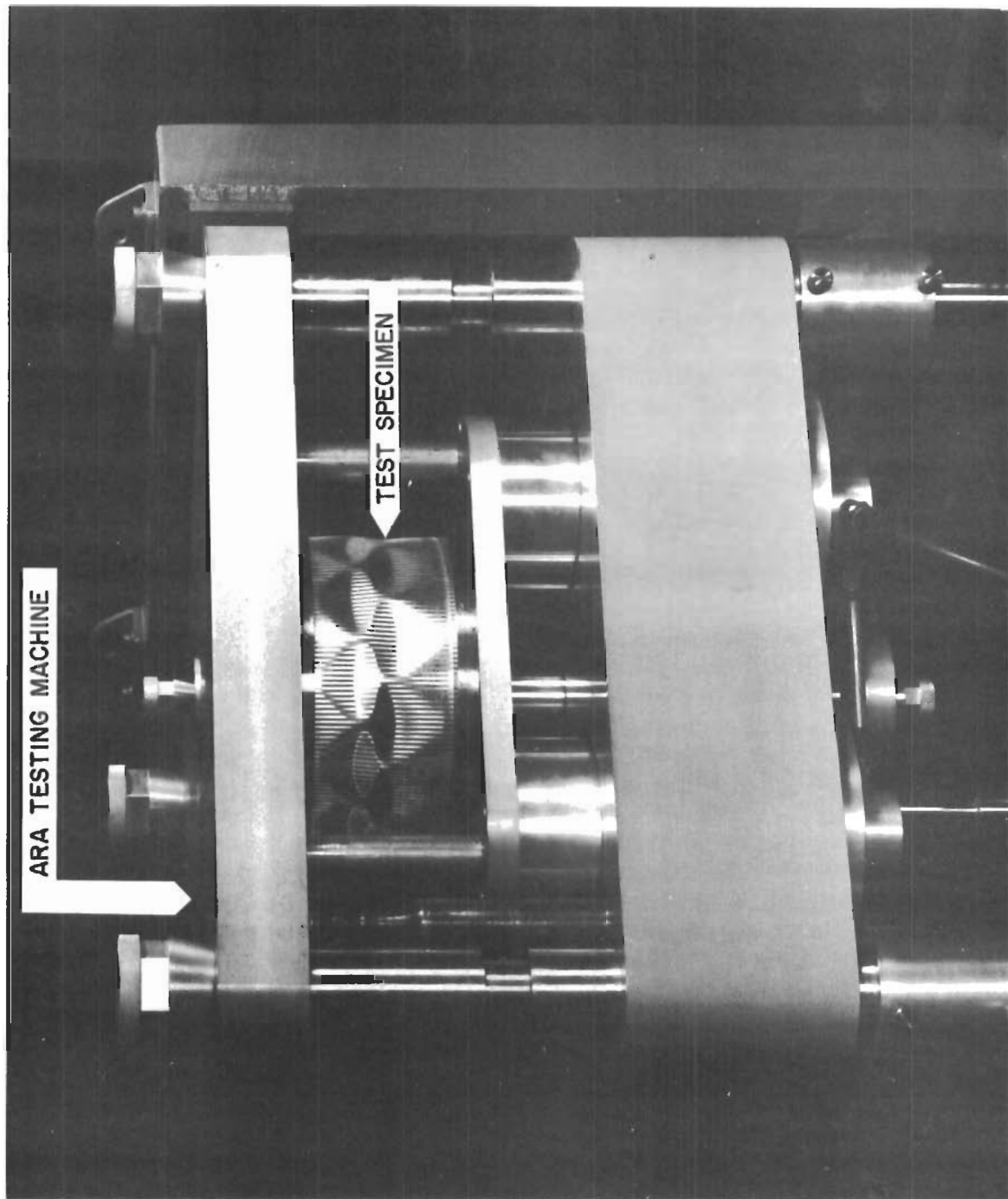
Fig. 4.4   Post Failure Axial Compression Test Specimen.

48

Ring
Stiffened Cylinder
(Spec. No. 7)

Longitudinally
Stiffened Cylinder
(Spec. No. 36)
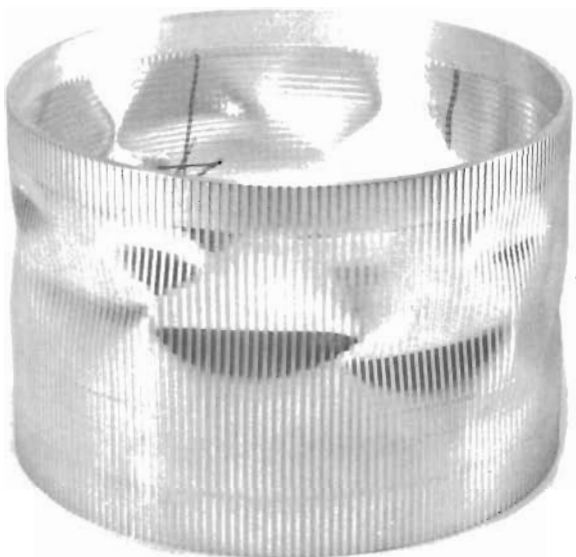
Grid
Stiffened Cylinder
(Spec. No. 58)

Isotropic
Cylinder
(Spec. No. 29)

Fig. 4.5   Post Failure Compression Specimens Representative of all
Stiffener Configurations.

49

which could be read to an estimated accuracy of 0.2×10^{-3} in. Stiffener width and stiffener spacing measurements were also made with a micrometer but because of the difficulty of making the measurements, they could only be estimated to within 2.0×10^{-3} in. Uniformity of the stiffener spacing and stiffener width for ring stiffening elements was maintained by the lathe thread pitch and cutting tool dimensions, respectively. For longitudinal stiffening elements, accurate control over these dimensions was insured by the indexing head and the cutting tool size.

Summarized in Table 4.1, considering all specimens for a given cylinder configuration, are minimum, average, and maximum values for all measured parameters, estimated measurement error as given above, and the indicated percent error based on maximum, average, and minimum values for a given parameter. These latter quantities are indicative of the quality of the measured data for a given cylinder configuration. One observes from the table that the measurements of failure load are accurate within approximately 1% and that the geometric parameter subject to the greatest uncertainty is the cylinder wall thickness which has a maximum possible measurement error of 4.5%.

Reduction of Test Data on Failure of Cylinders

Axial compression test results were evaluated on the basis of load, stress, and buckling coefficient. The failure load ($P_{x_{exp}}$) was obtained by multiplying the testing machine pressure gage reading at specimen failure by the machine calibration factor. A value for the experimental failure stress ($\sigma_{x_{exp}}$) was then determined by dividing the failure load by the average cross sectional area of the test specimen which was calculated using the cylinder radius and average values for the effective cross section thickness (t_s). This thickness was based on measurements of the wall thickness and total height for the orthotropic cylinders and on measurements of the wall thickness for the isotropic cylinders. The procedure used to obtain these measurements is described below. From the above, the experimental failure stress is thus

$$\sigma_{x_{exp}} = P_{x_{exp}} / (2\pi R t_{s_{av.}}) \tag{4.1}$$

Values for the experimental buckling coefficient were determined by dividing the failure stress by a cylinder material and geometry parameter (F_x). Thus,

$$k_{x_{exp}} = \sigma_{x_{exp}} / F_x \tag{4.2}$$

As indicated in Ref. 3,

$$F_x = \pi^2 E I_s / [(t_s L^2)(1 - \nu^2] \tag{4.3}$$

50

Substitution of Equation (4.3) in (4.2) gives

$$k_{x_{exp}} = \sigma_{x_{exp}} [t_s L^2 / (\pi^2 E I_s)] (1 - \nu^2) \qquad (4.4)$$

It is noted that Equations (4.1) through (4.4) were applied for reduction of isotropic as well as orthotropic cylinder test data.

The parameters I_s and t_s were calculated using equations presented in Table 3.2 and based on cylinder measurements obtained as described below. Also shown in Table in Table 3.2 are equations used to determine values for other geometrical and rigidity parameters which appear in subsequent equations. A detailed discussion of techniques for determining cylinder section properties is presented in Section 3.

All data were reduced based on $E = 10.1 \times 10^6$ psi which corresponds to an aluminum 6061-T6 material. For the orthotropic cylinders, Poisson's ratio was assumed equal to zero. However, for the isotropic cylinders a value of $\nu = 0.3$ was used.

The cylinder dimensions subject to the greatest variation due to fabrication were the wall thickness and stiffener height. For ring stiffened cylinders where variations in characteristic values for wall thickness (t) and the wall thickness/stiffener height ratio (t/b) could be significant with regard to interpretation of test data, it was desirable to evaluate the test results based on average and minimum values for these parameters. For longitudinally and grid stiffened cylinders where the effect of variations in these parameters was less pronounced, the test data was reduced using average values. The isotropic cylinder test results were also sensitive to values used for cylinder wall thickness; hence, this data was reduced using average and minimum values for this parameter.

Pre-test measurements of both the cylinder wall thickness and the total height at a stiffener (t+ b) were made at six circumferential locations near each end of the orthotropic specimens. For ring stiffened and longitudinally stiffened cylinders, this resulted in a total of twelve measurements each for the wall thickness and total height. For grid stiffened designs, this procedure gave twelve measurements each for the wall thickness, total height at a frame, and total height at a longeron. The wall thickness of the isotropic cylinders was also measured at six circumferential locations near each specimen end. It is noted that in general all specimens (both isotropic and orthotropic) exhibited some taper such that the average dimensions at

51

one end of the specimen exceeded those at the other end. For longitudinally stiffened and grid stiffened designs, the value for wall thickness and stiffener height used to reduce the test data was found from the average of the pre-test measurements as noted previously.

Post failure examination of the ring stiffened cylinders revealed that in general the specimens buckled around an annular location near the end of the specimen with the smaller average dimensions. In such cases six additional measurements each for the wall thickness and total height were made near the buckled region. Average and minimum values for t and t/b were then computed based on 12 measurements near the buckled region (six pre-test measurements plus six post failure measurements). The minimum values were computed assuming a Gaussian distribution of t or t/b variation about the mean and establishing a 2σ deviation below the mean as representative of the minimum value. Hence, minimum values for these parameters are based on the criterion that 90 percent of the values should exceed the minimum value.

For ring stiffened cylinders where the buckle location could not be attributed to a particular location on the specimen, minimum and average values for wall thickness and stiffener height were based on the pre-test measurements.

Minimum and average values for the wall thickness were also calculated for the isotropic cylinders based on the pre-test measurements. As for the ring stiffened cylinders, minimum values for wall thickness were computed assuming a Gaussian distribution of thickness variation about the mean and establishing a 2σ deviation below the mean as representative of the minimum value.

In summary, for longitudinally stiffened and grid stiffened cylinders, values for the experimental buckling stress and buckling coefficient were determined using Eqs. (4.1) and (4.4) wherein geometric parameters were based on average values of pre-test measurements of the test specimen geometry. For ring stiffened and isotropic cylinders, the experimental buckling stress (Eq. 4.1) was based on the experimental buckling load and the average cross sectional area of the specimen. However, average and minimum values for the experimental buckling coefficient were determined from Eq. (4.4) based on average and minimum values for test specimen geometry. For ring stiffened cylinders, specimen geometrical parameters were usually determined from measurements in the vicinity of the buckled region; however, for a few specimens, the location of incipient buckling was not definitive and these

parameters were based solely on pre-test measurements. For the isotropic cylinders, the region of initial buckling could not be clearly identified, and average and minimum values for cylinder geometric parameters were based on pre-test measurements. A summary of material, geometrical and rigidity parameters for the axial compression test specimens is presented in Tables 4.2, 4.3 and 4.4, and the experimental structural parameters are presented in Tables 4.5 and 4.6.

Calculation of Theoretical Structural Parameters

From Reference 3, the theoretical buckling stress for an orthotropic cylinder under axial compressive loading is

$$\sigma_x = k_x(\pi^2 E I_s/t_s L^2)(1-\nu^2)^{-1} \tag{4.5}$$

where k_x is the theoretical buckling coefficient. For moderate length cylinders the buckling coefficient is related (See Ref. 3) to the cylinder curvature parameter, Z_x, as follows:

$$k_x = .702(1-\nu^2)^{1/2}Z_x \tag{4.6}$$

where
$$Z_x = ZU = (12^{-1/2})(t_f/I_s)^{1/2}(L^2/R)U \tag{4.7}$$

In the above equation, U is a coefficient which is a function of three cylinder geometry parameters, α, γ and δ which for $\nu = 0$ are defined as

$$\alpha = t_s I_f/(t_f I_s)$$

$$\gamma = (1/4)(\bar{t}/t_f)(J/I_s) \tag{4.8}$$

$$\delta = \bar{t}^2/(t_s t_f)$$

Physically, U = 1.0 corresponds to axisymmetric buckling and U ≠ 1.0 is characteristic of buckling in the asymmetric moderate length mode.

Substitution of Eqs. (4.6) and (4.7) in (4.5) gives the following equation for the theoretical buckling stress for moderate length cylinders

$$\sigma_x = [2E(t_f I_s)^{1/2}/(R t_s)](1-\nu^2)^{-1/2}U \tag{4.9}$$

The theoretical buckling load was determined by multiplying the buckling stress by the average cross sectional area of the cylinder. Thus,

$$P_x = \sigma_x (2 \pi R t_{s\ av.})\qquad(4.10)$$

Substitution of Eq. (4.7) in (4.6) gives the following equation for the theoretical buckling coefficient for moderate length cylinders

$$k_x = .203\,(t_f/I_s)^{1/2}(L^2/R)(1-\nu^2)^{1/2}U\qquad(4.11)$$

Methods for calculating U are presented in Reference 3 and apply for the α, γ domains as follows (See Appendix A)

a) $\alpha > 1.0$, all γ

b) $\alpha \leq 1.0$, $\gamma < \alpha$

In particular, the coefficient U has a value of 1.0 for specimen geometries characterized by the $\alpha - \gamma$ relationship noted.

$$\alpha > 1.0,\ \gamma \geq 1.0\qquad(4.12)$$

Subsequent examination of the test specimen geometry (See Tables 4.5 and 4.6) revealed that all the ring stiffened specimens and also grid stiffened Specimen No. 57 satisfied the condition of Eq. (4.12). Hence, for these specimens values for the theoretical structural parameters were based on $U = 1.0$. One grid stiffened design (Specimen No. 58) had $\alpha = 1.0$ and $\gamma = 1.55$ for which either axisymmetric (U = 1.0) or asymmetric short cylinder buckling (see below) is possible; however, the axisymmetric buckling mode was found to correspond to a minimum value for the buckling coefficient for this specimen.

For the ring stiffened cylinders, average and minimum values for the theoretical curvature parameter, buckling stress, buckling load, and buckling coefficient were determined using Eqs. (4.7), (4.9), (4.10), and (4.11), respectively, and based on average and minimum values for test specimen geometry. Structural parameters for the grid stiffened cylinders (Specimens No. 57 and 58) were calculated using the above equations but based on average values for specimen geometry. As indicated

54

by Eq. (4.10) the average cross sectional area of the test specimen was used to calculate the theoretical buckling load in all cases.

As shown in Appendix A, specimen geometries characterized by $\alpha \leq 1.0$, $\gamma \geq \alpha$ are subject to short cylinder behavior wherein buckling may occur in the $m = 1.0$ asymmetric mode. The longitudinally stiffened cylinders and Grid Stiffened Cylinder No. 61 of this report were found to have minimum values for the theoretical buckling coefficient corresponding to this failure mode. Equations relating the buckling coefficient (k_x) and curvature parameter (Z_x) to a wavelength parameter $\overline{\beta}$ and orthotropic cylinder parameters α, γ and δ are derived in Appendix A and presented below.

$$Z_x^2 = [1 + 2(\overline{\beta}^2/\delta) + (\overline{\beta}^4/\delta)]^2 (\gamma + \alpha\overline{\beta}^2)[(1 + \overline{\beta}^2) \ 12(1 - \nu^2/\pi^4) \ ]^{-1} \qquad (4.13)$$

$$k_x = 1 + 2\gamma(\overline{\beta}^2/\delta) + \alpha(\overline{\beta}^4/\delta) + [1 + 2(\overline{\beta}^2/\delta) + (\overline{\beta}^4/\delta)](\gamma + \alpha\overline{\beta}^2)(1 + \overline{\beta}^2)^{-1} \qquad (4.14)$$

For a given specimen geometry and assumed values of $\overline{\beta}$, a curve of k_x vs Z_x was constructed through use of Eqs. (4.13) and (4.14). The theoretical value for the buckling coefficient was then determined from the curve for the design value of Z_x.

Representative results based on this procedure are illustrated by Figure 4.6. The solid curve shown is a theoretical k_x vs Z_x relationship based on the $m = 1.0$ asymmetric buckling mode and was determined using an average value of δ, α, and γ for the specimens indicated. The dotted curve shows the corresponding values for k_x based on the axisymmetric buckling mode. Also shown are experimental values for the buckling coefficient for several specimens. One observes that the $m = 1.0$ asymmetric buckling theory corresponds to lower values for the theoretical buckling coefficient and that the test data is in good agreement with theory.

Once theoretical values for the short cylinder asymmetric buckling coefficient were determined using the graphical procedure described, the associated buckling stress and load were calculated from Eqs. (4.5) and (4.10), respectively. Geometrical parameters in these equations were calculated based on average values for specimen geometry.

For isotropic cylinders under axial compressive loading the equation for the theoretical buckling stress is (Ref. 13)

$$\sigma_x = .577 \ (Et/R)(1 - \nu^2)^{-1/2} \qquad (4.15)$$
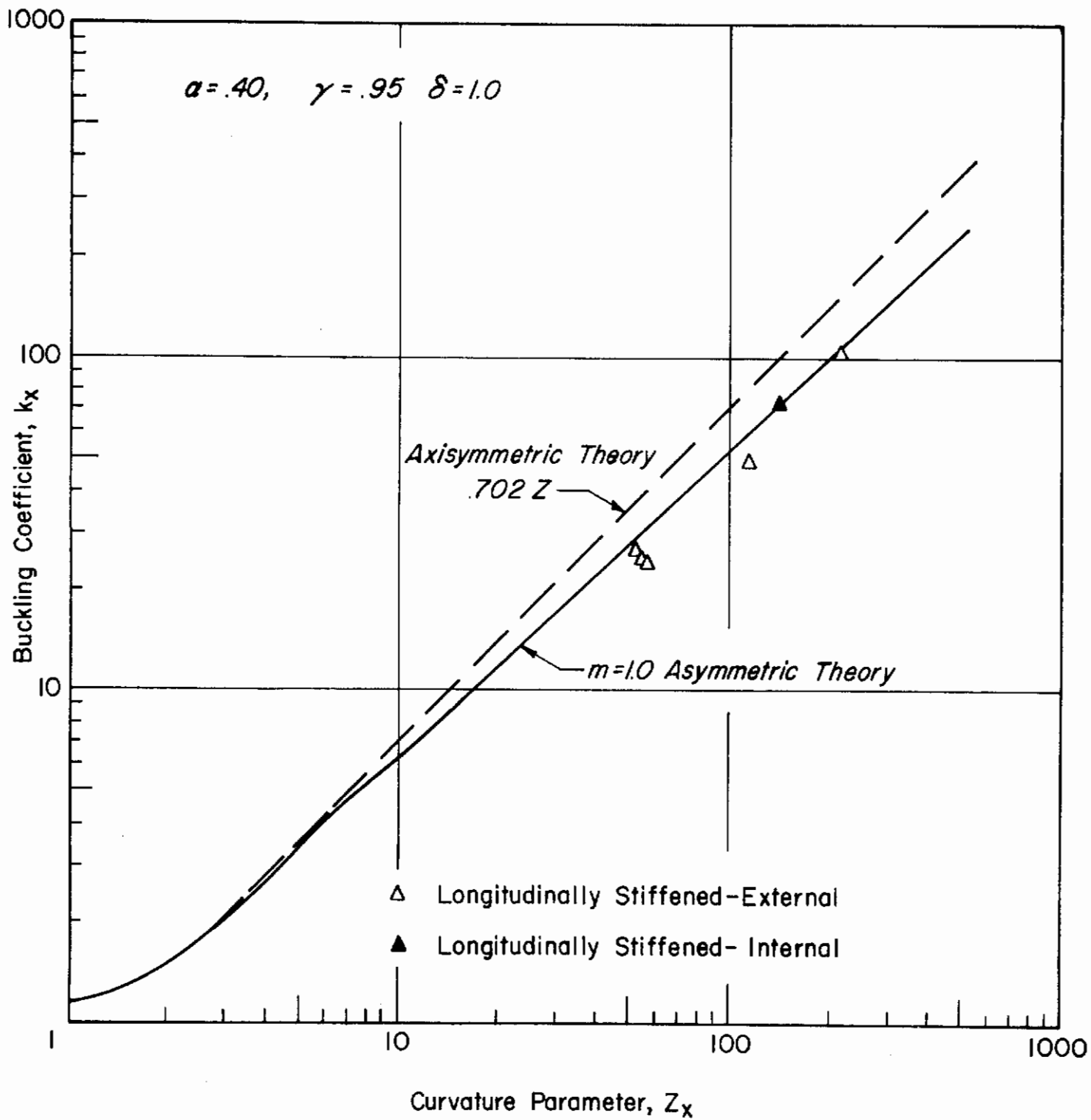
Fig. 4.6   Typical Curve of Theoretical Buckling Coefficient for m = 1.0 Asymmetric Mode

The theoretical buckling load was found by multiplying the buckling stress by the average cylinder cross sectional area (See Eq. 4.10).

From Reference 13 the theoretical buckling coefficient for an isotropic cylinder is

$$k_x = .702 \, (L/R)^2 (R/t)(1 - v^2)^{1/2} \tag{4.16}$$

Average and minimum values for the theoretical buckling stress, buckling load and buckling coefficient were determined for the isotropic cylinders using Eqs. (4.15), (4.10) and (4.16) respectively, and based on average and minimum values for test specimen geometry.

Material properties appearing in all the above equations were evaluated as follows: a value of 10.1×10^6 psi was used for Young's modulus (E). For all isotropic cylinders, $v = 0$ was assumed, whereas for isotropic cylinders, $v = .3$.

A summary of values for the theoretical structural parameters is presented in Tables 4.5 and 4.6.

TABLE 4.1

Accuracy of Experimental Data for Axial Compression Tests
Considering all Specimens for a Given Configuration

Ring Stiffened Cylinders

Parameter Units	P_{exp} psi	L in.	R in.	t	h	w	d
					10^{-3} in.		
Minimum Value	19	1.77	3.80	4.5	14.4	51	111
Average Value	59	2.84	3.80	8.6	16.6	52.2	111
Maximum Value	104	3.96	3.80	12.5	19.0	55	111
Measurement Error	.25	$.5 \times 10^{-3}$	$.5 \times 10^{-3}$	.2	.2	2.0	2.0
% Error (1)	1.3	.03	.013	4.5	1.4	3.9	1.8
% Error (2)	.42	.017	.013	2.3	1.2	3.8	1.8
% Error (3)	.24	.013	.013	1.6	1.1	3.6	1.8

Longitudinally Stiffened Cylinders

Parameter Units	P_{exp} psi	L in.	R in.	t	h	w	d
					10^{-3} in.		
Minimum Value	43.2	1.98	3.80	4.5	12.0	60	119
Average Value	89	3.12	3.80	11.1	17.0	60.3	119
Maximum Value	133.5	4.00	3.80	14.1	20.8	62	119
Measurement Error	.25	$.5 \times 10^{-3}$	$.5 \times 10^{-3}$	.2	.2	2.0	2.0
% Error (1)	.6	.03	.013	4.5	1.7	3.3	1.7
% Error (2)	.3	.016	.013	1.8	1.2	3.3	1.7
% Error (3)	.19	.013	.013	1.4	.96	3.2	1.7

Grid Stiffened Cylinders

Parameter Units	P_{exp} psi	L in.	R in.	t	h_1	h_2	w_1	w_2	d_1	d_2
						10^{-3} in.				
Minimum Value	96	3.78	3.80	6.0	11.1	11.1	57	49	119	111
Average Value	110	3.79	3.80	9.6	15.9	17.5	57.5	50	119	111
Maximum Value	126	3.80	3.80	11.0	17.8	21.8	58	51	119	111
Measurement Error	.25	$.5 \times 10^{-3}$	$.5 \times 10^{-3}$	.2	.2	.2	2.0	2.0	2.0	2.0
% Error (1)	.26	.013	.013	3.3	1.8	1.8	3.5	4.1	1.7	1.8
% Error (2)	.23	.013	.013	2.1	1.3	1.1	3.5	4.0	1.3	1.8
% Error (3)	.20	.013	.013	1.8	1.1	.92	3.5	3.9	1.3	1.8

Isotropic Cylinders

Parameter Units	P_{exp} psi	L in.	R in.	t
				10^{-3} in.
Minimum Value	52	3.92	3.80	9.8
Average Value	55.1	3.94	3.80	10.6
Maximum Value	60.5	3.95	3.80	11.7
Measurement Error	.25	$.5 \times 10^{-3}$	$.5 \times 10^{-3}$	.2
% Error (1)	.48	.013	.013	2.0
% Error (2)	.45	.013	.013	1.9
% Error (3)	.41	.013	.013	1.7

(1) Based on minimum measured values
(2) Based on average measured values
(3) Based on maximum measured values

58

TABLE 4.2

Material, Geometrical and Rigidity Parameters for Axial Compression Ring Stiffened Cylinders

Spec. No.	L	R	w	d	Based On Average Properties t	t/b	b	t_s	t_f	$\bar{t}$	I_s/b^3	I_f/b^3	J/b^3	Based on Minimum Properties t	t/b	b	t_s	t_f	$\bar{t}$	I_s/b^3	I_f/b^3	E
Col.	2	3	4	5	6	7	8	9	10	11	12	13	14	15	16	17	18	19	20	21	22	23
Ref.	--	--	--	--	--	--	(3.16)*	(3.15)	(3.17)	(3.19)	(3.18)	(3.20)	(3.21)	--	--	(3.16)	(3.15)	(3.17)	(3.19)	(3.18)	(3.20)	--
Units	in.	in.	10^{-3} in.	10^{-3} in.	10^{-3} in.			10^{-3} in			10^{-2} in^3/in			10^{-3} in.			10^{-3} in.			10^{-2} in^3/in		10^6 psi
5	2.00	3.80	51	111	10.2	1.312	7.7	10.2	13.7	12.0	18.8	68.0	209	9.8	1.220	8.0	9.8	13.5	11.7	15.1	60	10.1
6	2.00	3.80	51	111	4.8	.484	10.0	4.8	9.4	7.1	.95	17.5	44.2	4.4	.437	10.1	4.4	9.1	6.8	.7	16	10.1
7	3.00	3.80	51	111	9.7	1.253	7.8	9.7	13.3	11.5	16.4	62.0	189	8.9	1.144	8.6	8.9	12.5	10.7	12.5	54	10.1
8	3.00	3.80	51	111	5.5	.529	10.4	5.5	10.3	7.9	1.23	19.0	48.	4.6	.431	10.6	4.6	9.4	7.0	.66	15.7	10.1
9	1.77	3.80	51	111	12.1	2.64	4.6	12.1	14.2	13.2	153.0	285.	1022	11.3	2.35	4.8	11.3	13.6	12.5	108.	220.	10.1
10	3.93	3.80	51	111	11.8	2.46	4.8	11.8	14.0	12.9	124.0	242	864	11.0	2.18	5.1	11.0	13.4	12.2	86.3	188.	10.1
11	2.99	3.80	51	111	12.0	3.04	4.0	12.0	13.9	13.0	234.	390	1470	11.7	2.67	4.4	11.7	13.7	12.7	158.5	295.	10.1
12	2.10	3.80	51	111	5.3	.496	10.6	5.3	10.1	7.7	1.02	17.9	44.3	4.5	.414	10.7	4.5	9.4	7.0	.59	15.2	10.1
17	2.40	3.80	51	111	4.9	.477	10.3	4.9	9.6	7.3	.91	17.3	43.	4.6	.441	10.5	4.6	9.4	7.0	.71	16.0	10.1
18	3.96	3.80	53	111	5.2	.511	10.2	5.2	10.1	7.7	1.11	19.1	48.5	4.3	.418	10.2	4.3	9.2	6.8	.61	15.4	10.1
19	3.95	3.80	53	111	10.0	1.23	8.7	10.0	13.9	12.0	15.5	63.0	189	9.8	1.164	8.4	9.8	13.8	11.8	13.2	54.	10.1
20	2.95	3.80	53	111	9.4	1.061	8.8	9.4	13.6	11.5	9.96	48.6	143	8.6	.912	9.5	8.6	13.1	10.9	6.33	38.	10.1
32	2.98	3.80	55	111	9.9	1.208	8.2	9.9	14.0	12.0	14.7	62.0	191	8.9	1.016	8.7	8.9	13.3	11.1	8.71	47.	10.1
33	1.96	3.80	55	111	5.7	.559	10.1	5.7	10.7	8.2	1.45	21.5	56.5	5.2	.500	10.4	5.2	10.4	7.8	1.04	19.	10.1
34	3.52	3.80	55	111	11.6	2.52	4.6	11.6	13.9	12.8	133.	270.	976	10.9	1.84	5.9	10.9	13.9	12.4	51.9	137.	10.1

*Equation Number

TABLE 4.3

Material, Geometrical and Rigidity Parameters for Axial Compression Longitudinally Stiffened Cylinders

Specimen Number	L	R	w	d	t	t/b	b	t_f	t_s	$\bar{t}$	I_f/b^3	I_s/b^3	J/b^3	E
Col.	2	3	4	5	6	7	8	9	10	11	12	13	14	15
Ref.	--	--	--	--	--	--	(3.23)*	(3.22)	(3.24)	(3.26)	(3.25)	(3.27)	(3.28)	--
Units	in.	in.		10^{-3} in.	10^{-3} in.			10^{-3} in.			10^{-2} in^3/in^3			10^6 psi
13	1.98	3.80	60	119	10.5	1.555	6.8	10.5	14.0	12.3	31.4	97.0	321	10.1
14	1.99	3.80	60	119	10.4	1.404	7.4	10.4	14.1	12.3	23.1	80.0	257	10.1
15	2.00	3.80	60	119	12.0	2.89	4.2	12.0	14.1	13.1	201.	370.	1340	10.1
16	2.03	3.80	60	119	13.3	3.58	3.7	13.3	15.1	14.2	382.	630.	2300	10.1
22	4.00	3.80	60	119	5.8	.631	9.2	5.8	10.4	8.1	2.09	24.8	68.6	10.1
23	3.00	3.80	60	119	5.5	.538	10.2	5.5	10.6	8.1	1.29	20.8	55.3	10.1
24	4.00	3.80	60	119	10.0	1.28	7.8	10.0	13.9	12.0	17.5	68.	215	10.1
25	3.00	3.80	60	119	10.0	3.09	3.3	10.0	11.7	10.9	246.	435.	1600	10.1
26	1.99	3.80	60	119	10.9	1.435	7.6	10.9	14.8	12.9	24.6	83.	270	10.1
27	3.03	3.80	60	119	11.8	1.46	8.1	11.8	15.8	13.8	26.0	86.	276	10.1
28	2.00	3.80	60	119	6.3	.664	9.5	6.3	11.1	8.7	2.44	26.0	69.6	10.1
31	4.00	3.80	60	119	12.9	3.43	3.7	12.9	14.7	13.8	336.	560.	2060	10.1
36	3.00	3.80	57	119	13.5	3.50	3.8	13.5	15.3	14.4	357.	590.	2180	10.1
38	2.99	3.80	60	119	12.1	2.53	4.8	12.1	14.5	13.3	135.	270.	964	10.1
41	3.38	3.80	60	119	12.1	1.528	7.9	12.1	16.0	14.1	29.7	94.	304	10.1
43	3.49	3.80	57	119	6.2	.564	11.0	6.2	11.5	8.9	1.5	21.5	54.8	10.1

*Equation Number

60

TABLE 4.4

Material, Geometrical and Rigidity Parameters for Axial
Compression Grid Stiffened and Isotropic Cylinders

Grid Stiffened Cylinders

Specimen Number	L	R	w_s	d_s	t	t/b_s	b_s	w_f	d_f	t/b_f	b_f	t_s	t_f	$\bar{t}$	I_s/b_s^3	I_f/b_f^3	J/b_s^3	E
Col.	2	3	4	5	6	7	8	9	10	11	12	13	14	15	16	17	18	19
Ref.	--	--	--	--	--	--	(3.30)*	--	--	--	(3.29)	(3.32)	(3.31)	(3.33)	(3.37)	(3.36)	**	--
Units	in.	in.	←		10^{-3} in.		→	←		10^{-3} in.				→	← 10^{-3} in. →		10^{-2} in^3/in^3 →	10^6 psi
57	3.79	3.80	58	119	9.9	1.96	5.0	49	111	.89	11.1	12.4	14.8	13.6	154	36	1252	10.1
58	3.80	3.80	57	119	10.2	1.73	5.9	49	111	1.65	6.1	12.9	12.8	12.9	120	105	744	10.1
61	3.78	3.80	58	119	8.7	1.08	8.1	51	111	1.38	6.3	12.7	11.6	12.1	52	74	310	10.1

Isotropic Cylinders

Specimen Number	L	R	t_{av}	t_{min}	ν	E
Col.	2	3	4	5	6	7
Units	in.	in.	←	10^{-3} in. →	--	10^6 psi
21	3.95	3.80	10.2	9.8	.3	10.1
29	3.95	3.80	11.3	10.6	.3	10.1
30	3.92	3.80	10.2	9.5	.3	10.1

*Equation Number

**(3.34) for Spec. No. 58 and 61
(3.35) for Spec. No. 57

61

5. TORSION TESTS

Design and Fabrication of Test Specimens

Torsion tests were performed on ring stiffened and longitudinally stiffened cylinders. The geometry of the test specimens covered the same α range as the axial compression tests. For ring stiffened cylinders, this corresponded to $1 < \alpha < 10$, and for longitudinally stiffened cylinders, $0.1 < \alpha < 1.0$. As before, specimens were proportioned such that failure occurred in the general instability mode. For a monolithic type of construction, this criterion was satisfied by a design for which the shear buckling stress of the skin between the stiffeners exceeded the general instability stress. The nominal design value for the general instability stress was chosen well below the proportional limit in shear of the cylinder material.

Considerations leading to the detailed design of the test specimens were similar to those described for the compression tests. For example, the stiffener α vs t/b relationship for a given w/d is the same as shown in Fig. 4.1, and for a given design α the corresponding t/b ratio was obtained from the figure. However, the theoretical buckling stress for a given α is a function not only of material properties and the radius/thickness ratio but also of the cylinder length/radius ratio. Whenever possible, moderate-length cylinder behavior was assured for a given α and R/t by selection of the proper L/R ratio. For ring stiffened cylinders, the moderate-length cylinder criterion was realized with reasonable design values for L/R; however, for longitudinally stiffened cylinders, it was necessary to design for short-cylinder behavior in order to keep the L/R ratio and associated cylinder lengths compatible with machining tolerances desired for other cross sectional dimensions. For example, it was found that for cylinder lengths greater than $1.5\,R$, effects of machine taper and cylinder wall eccentricity induced by the cutting tool bearing against the thin wall specimen introduced excessively large variations in wall thickness and stiffener height.

Typical design curves for a ring stiffened torsion specimen are presented in Fig. 5.1. Shown in the figure are the variation of torsional buckling stress (assuming moderate-length cylinder behavior) and curvature parameter with cylinder radius/thickness ratio for a given design α, L/R, w/d, and E. For the indicated geometry, it can be shown that moderate-length cylinder behavior corresponds to $Z_t > 400$, and the corresponding minimum value for R/t is 250 as deduced from the Z_t vs R/t curve. Specimen design for moderate-length cylinder behavior is, therefore, obtained by

64

selecting a design $R/t \geq 250$ and utilizing the τ curve shown in Fig. 5.1 to determine the critical buckling stress.

Problems associated with the design of longitudinally stiffened cylinders for moderate-length behavior are illustrated by the curves of Fig. 5.2. In this figure curves of Z_t vs R/t are presented for a ring stiffened ($\alpha = 1.5$) and longitudinally stiffened cylinder ($\alpha = .67$) with the same cross sectional proportions. One observes from the figure that for the same R/t ratio the value of curvature parameter is markedly decreased for the longitudinally stiffened as compared with the ring stiffened configuration. In addition to this reduction in Z_x, the minimum value for Z_x corresponding to moderate-length cylinder behavior is increased (from 400 to 2,000) for the longitudinally stiffened cylinder. Because of these effects, it was expedient to select geometrical proportions for longitudinally stiffened torsion specimens which corresponded to short-cylinder behavior. Evaluation of test results, however, required a more involved procedure than for the ring stiffened designs and is described below.

The test specimens were fabricated on a lathe from an aluminum 6061-T6 tube using a procedure described previously (See Section 4). Reinforcing rings were machined on each end of the test specimen to facilitate the adaptation of the cylinder to the torsion test apparatus.

Test Arrangement and Procedure

A torsion jig was designed such that the application of an axial load to the jig by the testing machine resulted in torsion loading in the test specimen. The details of the test arrangement are shown in Fig. 5.3. A structure consisting of a base plate, two vertical channel sections, and a pin supports the dead weight of the specimen and the loading platens and facilitates the alignment of the specimen in the testing machine. A couple load was applied to the specimen loading platen through two whiffletrees. Pin attachments between the platens and cylinder end rings allowed the torsion loading to be transferred to the test specimen.

During the test, load was applied gradually to the specimen until failure occurred. Post failure rotations were limited by a stop arrangement on the loading fixture.

Post failure photographs of two torsion specimens representative of ring and longitudinally stiffened designs are shown in Fig. 5.4.
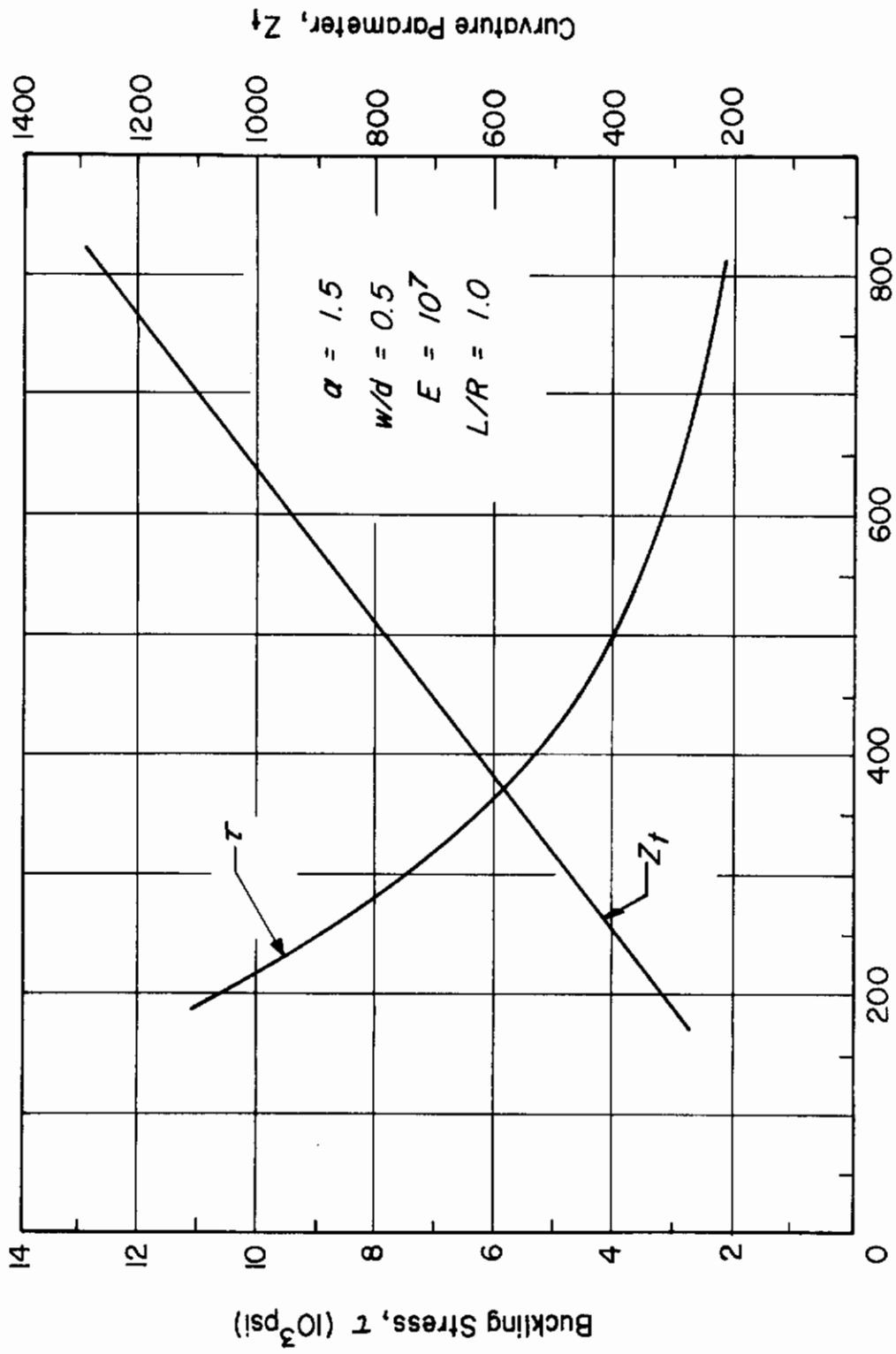
Fig. 5.1   Typical Design Curves for Torsion Specimens

$$a = 1.5$$
$$w/d = 0.5$$
$$E = 10^7$$
$$L/R = 1.0$$

Curvature Parameter, Z_t

Radius/Wall Thickness, R/t

Buckling Stress, τ (10^3psi)

5025

66

Fig. 5. 2   Curvature Parameter vs Radius/Wall Thickness Ratio for Ring and Longitudinally Stiffened Cylinders With Equal Skin-Stiffener Proportions

Fig. 5.3   Torsion Test Arrangement.

Labels in figure: ARA TESTING MACHINE, SUPPORT STRUCTURE, LOADING PLATENS, TEST SPECIMEN, WHIFFLETREE

68
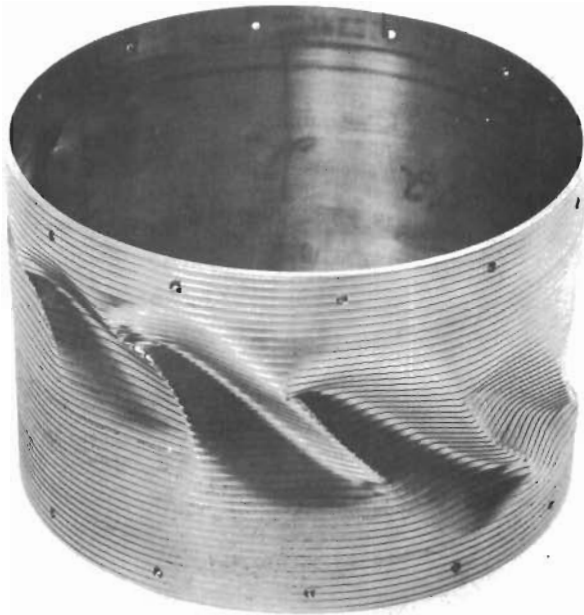
Ring
Stiffened Cylinder
(Spec. No. 52)
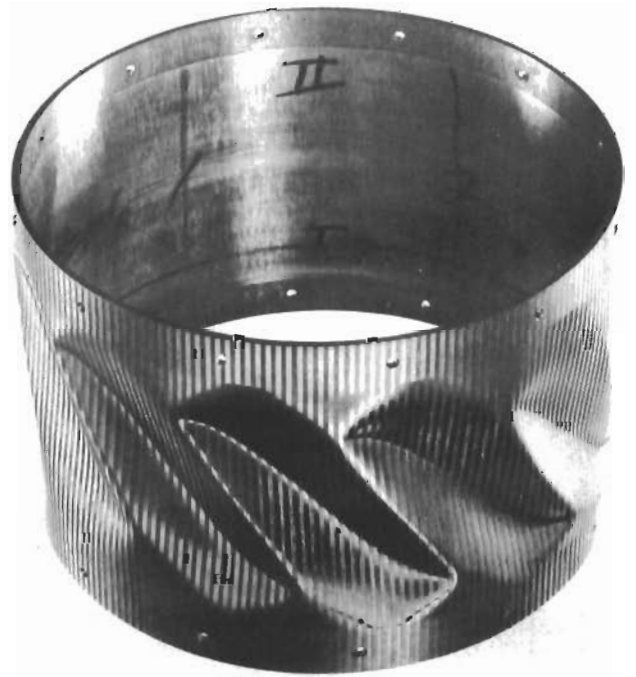
Longitudinally
Stiffened Cylinder
(Spec. No. 46)

Fig. 5.4   Post Failure Torsion Specimens.

Accuracy of Experimental Data

The maximum axial load applied to the torsion jig was indicated by a dial on the pressure gage of the testing machine and was read to a precision of 0.25 psi. For the ring stiffened specimen designs, failure occurred at pressures in the 23 to 46 psi range and the precision is approximately within 1% or better. One longitudinally stiffened cylinder failed at a test machine pressure loading of 8.75 psi which is accurate to within approximately 3%. However, the other specimens failed at testing machine pressure loadings in the 34 to 47 psi range which gives accuracies within 1%. Since the couple load distance can be measured from the test fixture within an accuracy of 1%, the torque loading corresponding to specimen failure was measured to approximately the same precision as the testing machine pressure load at failure.

Other experimental data were cylinder length, radius, wall thickness, and total height. Techniques for performing these measurements together with estimated measurement error were the same as for the axial compression tests (See Section 4). Tabulated below, (Table 5.1), considering all torsion test specimens, are minimum, average, and maximum values for each measurement, estimated measurement error, and the corresponding % error in the data. These latter values indicate the quality of the data. One observes that the geometric parameter most susceptable to measurement error was the cylinder wall thickness and had a maximum error of approximately 4%.

Table 5.1

Accuracy of Experimental Data for Torsion Tests

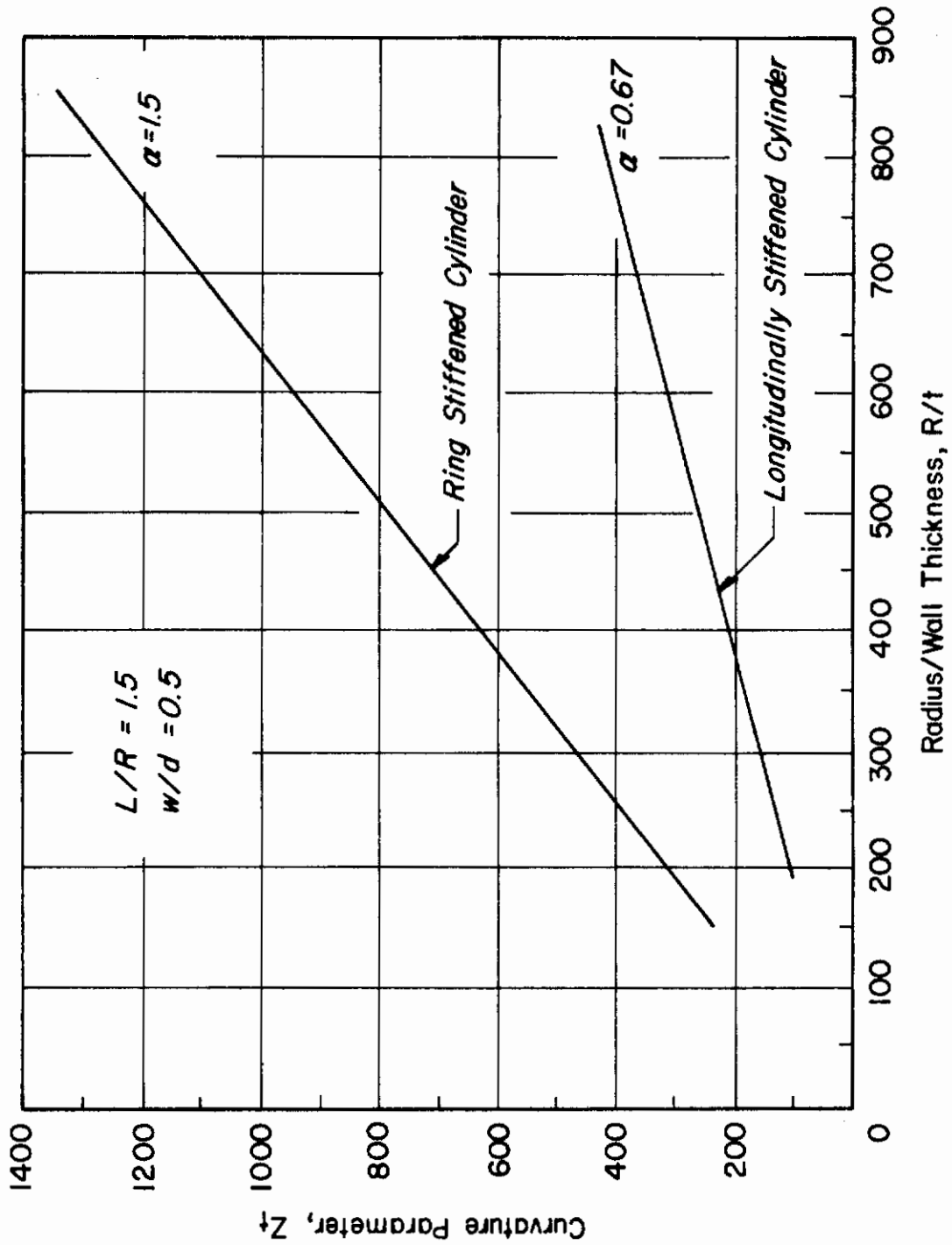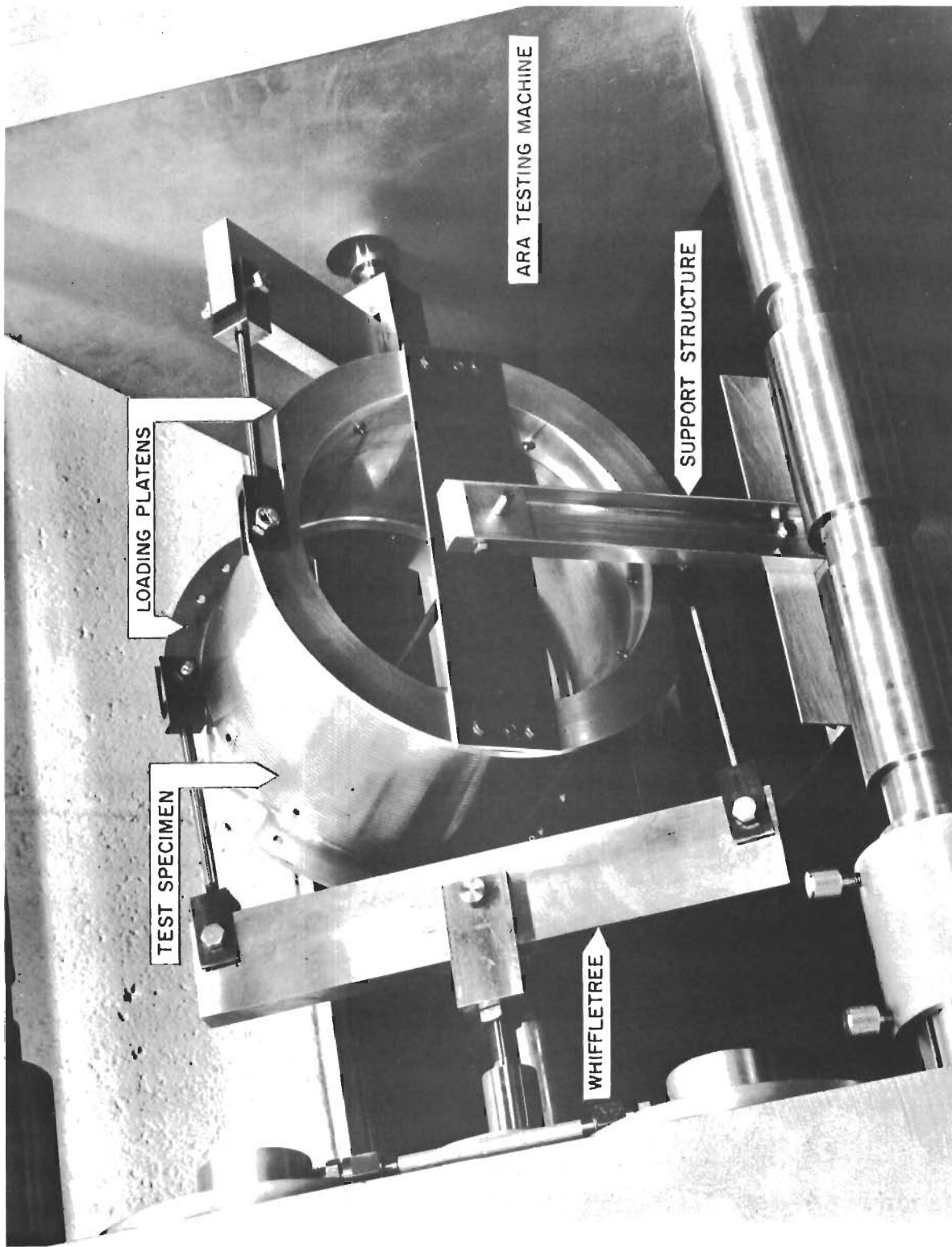| Parameter	L	R	w	d	t	h
Minimum Value (in.)	3.74	3.80	.051	.111	.0051	.0090
Average Value (in.)	3.76	3.80	.055	.115	.0092	.0146
Maximum Value (in.)	3.78	3.80	.060	.119	.0135	.0271
Measurement Error (10^{-3} in.)	.5	.5	2.0	2.0	.2	.2
% Error (1)	.01	.01	3.9	1.8	3.9	2.2
% Error (2)	.01	.01	3.6	1.7	2.2	1.4
% Error (3)	.01	.01	3.3	1.7	1.5	.74

(1) Based on minimum values (2) Based on average values (3) Based on maximum values

Reduction of Test Data on Failure of Cylinders

Experimental data determined from failure of the test specimens included the specimen failure torque load, failure stress, and corresponding buckling coefficient. The experimental value for the critical torque load (T_{exp}) was determined from the

70

testing machine pressure loading at specimen failure (p_{exp}), the testing machine calibration factor (C), and the geometry of the torsion jig. For these tests, C = 53.1 lbs/psi, and one half the load applied by the testing machine was distributed to each side of the torque loading platen at a couple arm of 8.4 in. Hence,

$$T_{exp} = (p_{exp} \times C/2)(8.4) = 223 p_{exp} \qquad (5.1)$$

The experimental value for failure stress (τ_{exp}) was determined by dividing the unit shear (q) in the cylinder wall using Bredt's formula (Ref.14) by the effective shear thickness of the specimen ($\bar{t}$).

Thus,

$$q = T_{exp}/2A \qquad (5.2)$$

$$\text{where} \qquad A = \text{cross sectional area of test specimen enclosed by the cylinder radius}$$

$$\text{and} \qquad \tau_{exp} = q/\bar{t} \qquad (5.3)$$

For the test specimens, the cross sectional area was 45.3 in^2 based on a cylinder radius of 3.80 in., and the effective shear thickness was found experimentally (See Section 3) to be approximately equal to the mean wall thickness per unit width $[.5(t_s + t_f)]$. Substitution of Eq. (5.2) in (5.3) together with the above values for A and $\bar{t}$ gives

$$\tau_{exp} = (T_{exp}/45.3)(t_s + t_f)^{-1} \qquad (5.4)$$

This equation was used for the determination of the experimental torsional buckling stress.

In a manner analogous to that used for the axial compression test data reduction, the experimental value for the torsional buckling coefficient ($k_{t_{exp}}$) was determined by dividing the experimental buckling stress (τ_{exp}) by a factor (F_t) which is a function of cylinder material and geometry properties. For $\nu = 0$, this factor is given in Reference 1 as

$$F_t = \pi^2 E I_s / (\bar{t} L^2) \qquad (5.5)$$

71

From the above, the equation for experimental buckling coefficient is

$$k_{t_{exp}} = \tau_{exp}[\overline{t} L^2 / \pi^2 E I_s)]$$ (5.6)

Eqs. (5.1), (5.4), and (5.6) were used to determine experimental values for torque load, torsional failure stress, and torsional buckling coefficient, respectively.

Cylinder cross sectional parameters appearing in the above equations (t_s, t_f, I_s) were determined using average values of specimen measurements. In a manner similar to that used for compression specimens, six circumferential measurements each for wall thickness and total height were made at both ends of the specimen. An average value for t and t/b based on the twelve measurements for each parameter was then used in conjunction with equations presented in Table 3.2 to determine values for thickness and bending stiffness parameters. The data was reduced based on $E = 10.1 \times 10^6$ psi.

A summary of the material, geometrical, and rigidity parameters for the test specimens is presented in Table 5.2. Experimental values for the structural parameters are given in Table 5.3.

Calculation of Theoretical Structural Parameters

As shown in Reference 1 the theoretical torsional buckling stress (τ) is given by

$$\tau = k_t \pi^2 E I_s / \overline{t} L^2$$ (5.7)

where k_t is the theoretical buckling coefficient. This equation was obtained assuming $\nu = 0$.

From Bredt's formula (Ref. 14), the critical torque load (T) is related to the buckling stress as follows

$$T = 2A\overline{t}\tau$$ (5.8)

Substitution of Eq. (5.7) in (5.8) gives the following equation for the theoretical torque load corresponding to torsional buckling

$$T = k_t 2\pi^2 E I_s A/L^2$$ (5.9)

72

One observes from Eqs. (5.7) and (5.9) that both the buckling stress and torque are a function of the buckling coefficient. Values for this parameter are dependent on whether a specimen is characterized by short-cylinder or moderate-length cylinder behavior. For example, for moderate-length cylinders the buckling coefficient from Reference 1 is given by

$$k_t = 0.89 Z_t^{3/4} \tag{5.10}$$

where

$$Z_t = Z(I_f/I_s)^{5/6} (t_s/t_f)^{1/2} \tag{5.11}$$

and

$$Z = (12^{-1/2}) (t_f)^{1/2} (L^2/R) \tag{5.12}$$

For specimens which are characterized by short-cylinder behavior, a more involved procedure is necessary to determine the buckling coefficient. The method . is presented in Reference 1 and summarized as follows: from an equation presented in Reference 1 for a given specimen geometry, the buckling coefficient can be expressed as a function of the length parameter Z_t and two wavelength parameters m and β. A minimum value for k_t always coincides with m = 1.0 which physically represents one buckle half wave length along the cylinder axis. With m = 1.0, a minimum value for the buckling coefficient is determined graphically by assuming a value for the other wavelength parameter (β) and plotting the resultant k_t vs Z_t relationship. The procedure is repeated for other assumed values of the wavelength parameter β. The final curve of minimum k_t vs Z_t is determined by fairing a curve through minimum values of k_t for each β.

Fig. 5.5 is presented to illustrate this procedure. The abscissa of the curve is the length parameter, Z_t, and the ordinate is the buckling coefficient k_t. Shown on the figure are many short k_t vs Z_t segments which represent possible values for this relationship for a given β. The minimum value for k_t is determined by constructing the envelope of the minimum values for each β segment (Curve B). It is noted that these curves were constructed for a specific specimen geometry (Specimen 47). Also shown in the figure is a curve of k_t vs Z_t for specimens which are characterized by moderate-length cylinder behavior (Curve A). One observes that the short-cylinder and moderate-length cylinder curves coincide for $Z_t \approx 1000$. For this particular specimen, short-cylinder buckling coefficients apply for $Z_t < 1000$ and moderate-length cylinder buckling coefficients apply for $Z_t > 1000$.

73
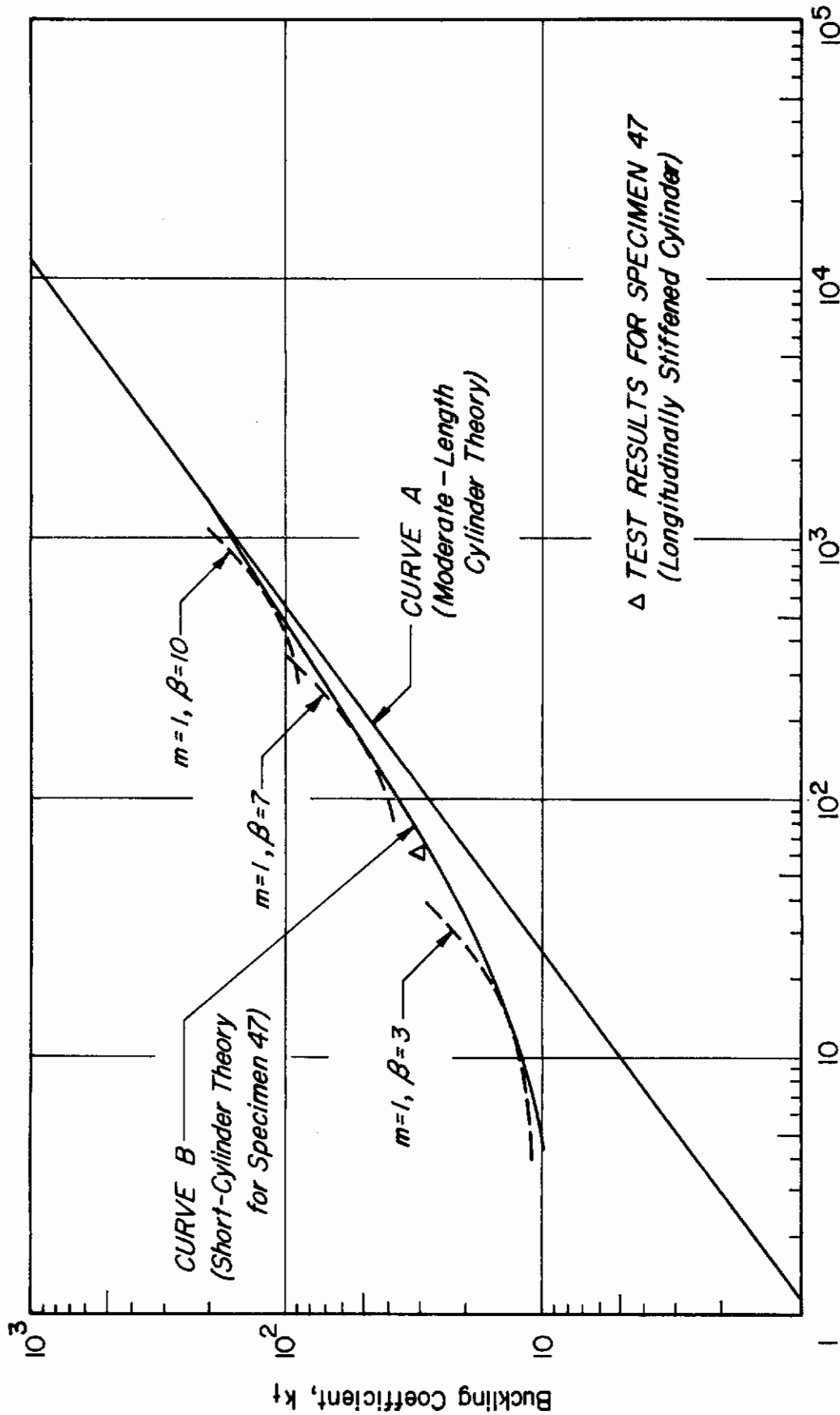
Fig. 5.5   Typical Buckling Coefficients vs Curvature Parameter for
Short-Length Cylinders in Torsion

74

As noted previously, the ring stiffened cylinder designs were in the moderate-length region. Accordingly, for these specimens theoretical values for the buckling stress, torque loading, and buckling coefficient were obtained using Eqs. (5.7), (5.9), and (5.10) through (5.12), respectively. The longitudinally stiffened specimens were characterized by short-cylinder behavior. For these specimens, the buckling coefficient was determined by a graphical procedure described above. Once the buckling coefficient was established, values for buckling stress and the corresponding torque was calculated using Eqs. (5.7) and (5.9).

Theoretical values for the structural parameters are summarized for all specimens in Table 5.3.

TABLE 5.2

Material, Geometrical and Rigidity Parameters for Torsion Test Specimens

Specimen Number	Type	L	R	w	d	t	t/b	b	t_s	t_f	$\bar{t}$	I_s/b^3	I_f/b^3	J/b^3	α	E
Col.	2	3	4	5	6	7	8	9	10	11	12	13	14	15	16	17
Ref.	--	--	--	--	--	--	--		Table 3.2						Eq. (4.8)	--
Units		in.	in.	$\leftarrow 10^{-3}$ in. $\rightarrow$					$\leftarrow 10^{-3}$ in.			$\leftarrow 10^{-2}$ in^3/in^3 $\rightarrow$				10^6 psi
35	RSC$^\phi$	3.77	3.80	56	111	11.8	2.75	4.3	11.8	13.9	12.9	173	330	--	1.61	10.1
37		3.75		53		10.1	1.23	8.2	10.1	12.9	11.5	15.5	64	--	3.22	
39		3.78		54		5.6	.538	10.4	5.6	10.7	8.1	1.3	20.8	--	1.90	
40*		3.76		54		10.1	1.32	7.6	10.1	13.8	12.0	19.4	73	--	2.84	
52	RSC	3.77		53	111	5.4	.516	10.5	5.4	10.4	7.9	1.4	19.8	--	9.00	
44	LSC$^\Delta$	3.74		56	119	5.9	1.55	3.8	7.7	5.9	6.8	97	31.2	315	.42	
45		3.75		56		11.1	1.40	7.9	14.8	11.1	13.0	80	22.8	242	.38	
46		3.77		57		13.0	3.68	3.5	14.6	13.0	13.8	680	415	2430	.69	
47*		3.76		57		11.1	1.25	8.9	15.3	11.1	13.2	66	16.1	194	.34	
49	LSC	3.74	3.80	58	119	8.3	.469	17.7	16.9	8.3	12.6	17.9	.86	38.8	.098	10.1

*   Internally Stiffened

φ   Ring Stiffened Cylinder

Δ   Longitudinally Stiffened Cylinder

76

TABLE 5.3

Summary of Structural Parameters for Torsion Tests

Specimen Number	Type	T_{exp}	T	τ_{exp}	τ	k_{texp}	k_t	Z_t
Col.	2	3	4	5	6	7	8	9
Ref.	--	--	Eq.(5.9)	Eq.(5.4)	Eq.(5.7)	Eq.(5.6)	**	Eq.(5.11)
Units	--	← 10^3 in. lbs. →		← 10^3 psi →		--	--	--
35	RSC φ	9.03	8.65	7.74	7.40	105	100	540
37		9.37	9.85	9.00	9.45	172	180	1200
39		5.25	6.07	7.14	8.26	580	670	6790
40*		9.70	9.34	8.95	8.61	178	170	1120
52	RSC	5.13	5.85	7.16	8.16	630	720	7490
44	LSC Δ	1.95	1.70	3.18	2.76	58	50	160
45		8.92	7.85	7.58	6.66	35	31	74
46		10.38	8.4	8.3	6.72	56	45	160
47*		8.81	8.03	7.36	6.71	30	28	61
49	LSC	7.65	9.06	6.70	7.94	12.3	14.5	11

φ Ring Stiffened Cylinder

Δ Longitudinally Stiffened Cylinder

* Internally Stiffened

** Eq. (5.10) for RSC
    See Text for LSC

6. HYDROSTATIC PRESSURE TESTS

Design and Manufacture of Test Specimens

Experimental data were obtained for the stability of ring stiffened and longitudinally stiffened cylinders under hydrostatic pressure loading. Cylinder geometries covered the same α range as those for compression and torsion tests. For ring stiffened cylinders, this corresponded to $1 < \alpha < 10$ and for longitudinally stiffened cylinders the α range was $0.1 < \alpha < 1.0$. Specimens were of a monolithic design and were proportioned such that local buckling of the skin between stiffeners was suppressed and that the specimen failed in a general instability mode. The critical design stress for the test specimens was selected well below the proportional limit of the material which simplified cylinder behavior with regard to material property effects. In addition, the cylinders were designed such that the external pressure loading corresponding to buckling was less than 10 psi. This allowed a simple test arrangement wherein a vacuum pump could be used to induce external pressure loading on the test specimen.

Specimen cross section proportions for a given design α were obtained from curves such as shown in Fig. 4.1. Once the design α and material of construction is fixed, the buckling stress (σ_y) and corresponding critical pressure (p_y) is a function primarily of the R/t ratio of the specimen; this relationship is illustrated by curves in Fig. 6.1 for a ring stiffened cylinder with simple support boundary conditions and $L/R = 1.0$. The σ_y and p_y curves of Fig. 6.1 are based on the assumption that the specimen exhibits moderate-length cylinder behavior. This assumption is valid providing the cylinder-length parameter Z_y has a value greater than 100 (Ref. 1). For a given L/R and α, Z_y is also a function of R/t and a curve illustrating this relationship is shown in Fig. 6.1 for the design parameters noted. A minimum design value for R/t therefore corresponds to the minimum Z_y for moderate-length cylinder behavior. Based on a limiting value for Z_y of 100, one observes that the R/t ratios corresponding to the σ_y and p_y curves of Fig. 6.1 are in the moderate-length cylinder range.

In summary, once the design α is established the required t/b ratio follows from curves such as Fig. 4.1 for a given w/d. Consideration of the desired buckling pressure and stress together with curves such as shown in Fig. 6.1 allow the determination of a value for R/t for a given α, material of construction, and L/R. Finally, the Z_y value corresponding to the design R/t is examined using a curve such as
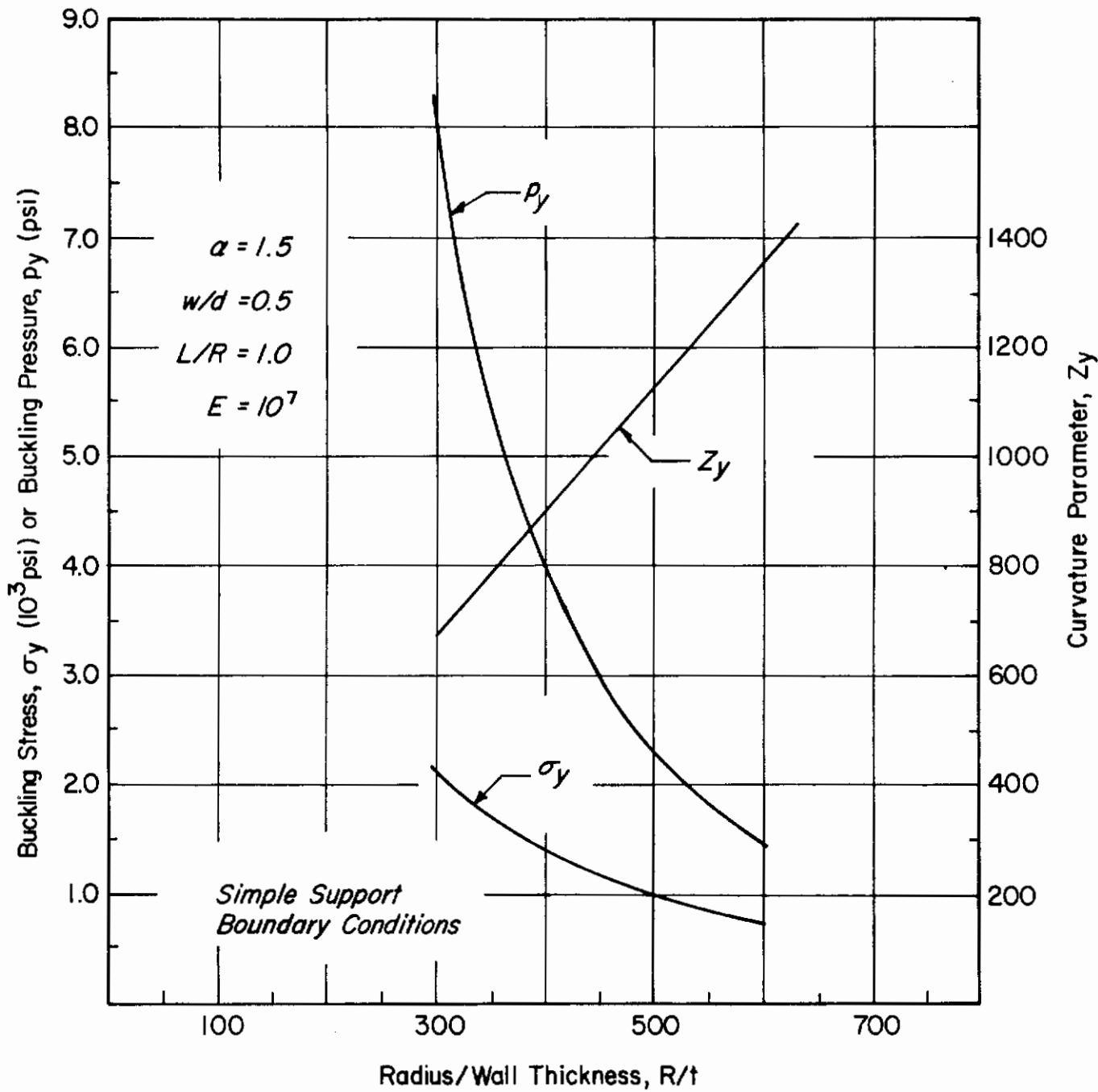
78

Fig. 6.1   Typical Design Curves for Hydrostatic Pressure Test Specimens

shown in Fig. 6.1 to verify that the design proportions correspond to moderate-length cylinder behavior.

As in the case for torsion test specimens, the design of longitudinally stiffened cylinders for moderate length cylinder behavior required excessively large values for L/R based on manufacturing considerations. For these specimens, it was expedient to obtain the detailed design configuration using the procedure described above and based on moderate length theory. The evaluation of the test results, however, was accomplished based on short-cylinder theory as described below.

All of the test specimens were machined on a lathe from an aluminum 6061-T6 tube using a technique described previously (See Section 4). Reinforcing rings were integrally machined on both ends of the test specimen to facilitate installation of the specimen in the test fixture.

Test Arrangement and Procedure

A schematic of the test arrangement used to perform the hydrostatic pressure tests is shown in Fig. 6.2. As indicated, end closures were assembled top and bottom to the cylinder test specimen. This assembly was made pressure tight via "O" rings which were pressed against the cylinder and end closures by means of seal rings bolted to the end closures. Air was evacuated from the test chamber at a controlled rate through a hose in the top end closure which produced an external hydrostatic pressure loading on the test specimen. The magnitude of the differential pressure loading was measured by a mercury or water manometer which was also attached to the chamber by a hose on the top end closure.

By means of a bleed valve attached to the vacuum pump hose, pressure loading was applied gradually to the test specimen until buckling occurred. The pressure loading at the instant of cylinder buckling was recorded by an observer monitoring the manometer. Photographs of representative test specimens buckled under hydro-static loading are shown in Fig. 6.3.

Accuracy of Experimental Data

Buckling of the test specimens corresponded to manometer readings in the range from 14.8 to 28.3 in. of mercury and for one specimen, 65.8 in. of water. The manometer scale was graduated in tenths of an inch, and the pressure loading was applied sufficiently slow so that the scale could be read to this accuracy. Based on a reading accuracy of 0.1 in., the indicated accuracy of the measured buckling pressure is within 0.7%.
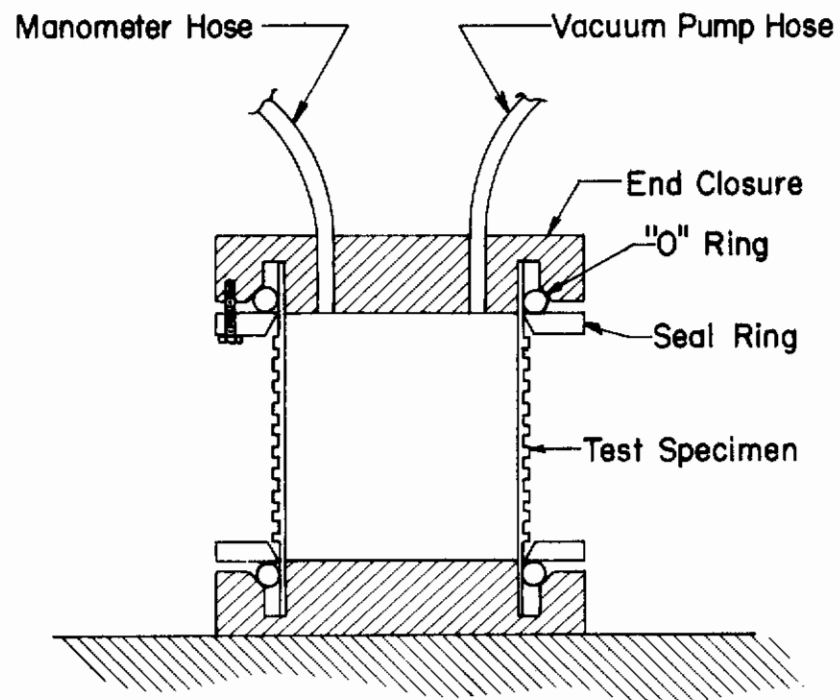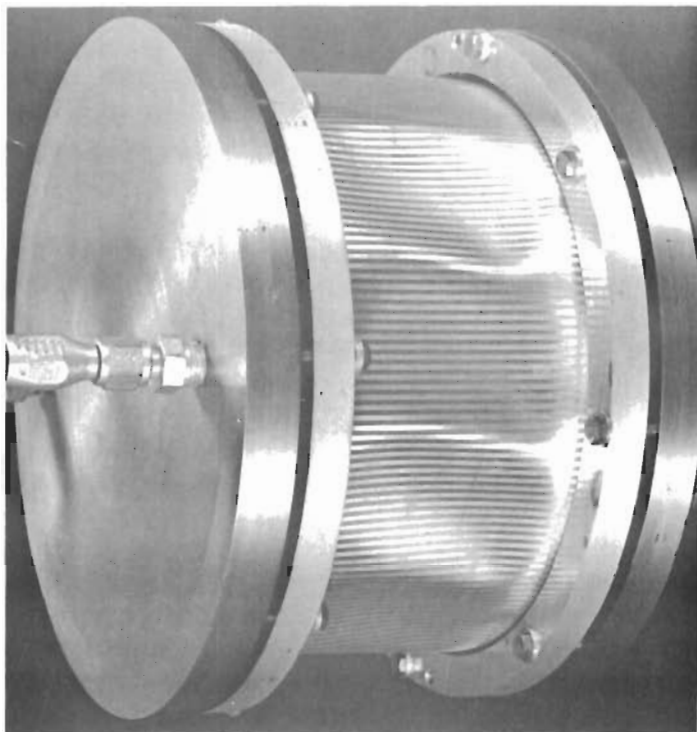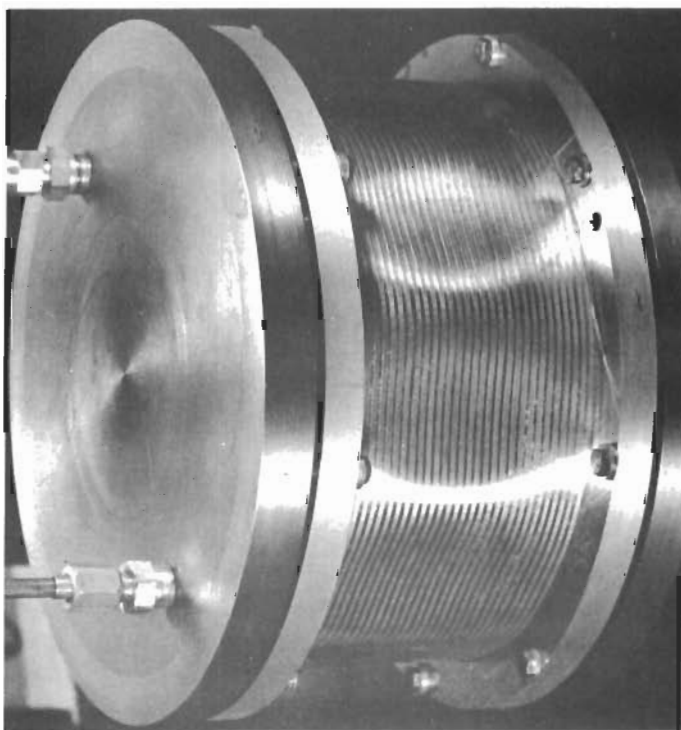
Fig. 6.2   Hydrostatic Pressure Test Arrangement

81

Longitudinally
Stiffened Cylinder
(Spec. No. 51)

Ring
Stiffened Cylinder
(Spec. No. 48)

Fig. 6.3   Post-Failure Hydrostatic Pressure Specimens.

82

Measurements of cylinder geometry also formed part of the experimental data and included cylinder length, radius, stiffener width, stiffener spacing, wall thickness, and total height. Methods for making the measurements and the estimated measurement error were the same as for the axial compression tests (See Section 4). Tabulated below (Table 6.1) are minimum, average, and maximum values for these parameters based on measurements of all test specimens together with the estimated measurement error. Also shown are values for the percent measurement error and are indicative of the quality of the data. One observes from the table that the measurement most susceptable to error was the cylinder wall thickness.

Table 6.1

Accuracy of Experimental Data for Hydrostatic Pressure Tests

Parameter	L	R	w	d	t	h
Min. Value (in.)	3.75	3.80	51×10^{-3}	111×10^{-3}	5.0×10^{-3}	11.5×10^{-3}
Av. Value (in.)	4.07	3.80	56×10^{-3}	114×10^{-3}	9.6×10^{-3}	16.1×10^{-3}
Max. Value (in.)	5.73	3.80	60×10^{-3}	119×10^{-3}	11.2×10^{-3}	18.1×10^{-3}
Measurement error (10^{-3} in.)	.5	.5	2.0	2.0	0.2	0.2
% Error (1)	.01	.01	3.9	1.8	4.0	1.7
% Error (2)	.012	.01	3.5	1.75	2.1	1.2
% Error (3)	----	.01	3.3	1.7	1.8	1.1

(1) Based on min. values (2) Based on average values (3) Based on max. values

Reduction of Test Data on Buckling of Cylinders

The structural parameters significant to interpretation of test results are buckling pressure ($p_{y_{exp}}$), buckling stress ($\sigma_{y_{exp}}$), and buckling coefficient ($k_{y_{exp}}$). The experimental buckling pressure was read directly from the manometer attached to the test specimen. Values for the other parameters, however, were computed from measurements of the critical pressure and cylinder geometry.

Values for the experimental buckling stress were obtained using the following relationship:

$$\sigma_{y_{exp}} = p_{y_{exp}} R/t_f \qquad (6.1)$$

The experimental buckling coefficient was determined by dividing the buckling stress as given by Eq. (6.1) by a material and geometrical parameter given in Ref. 1 as:

$$F_y = \pi^2 EI_s/(t_f L^2) \qquad (6.2)$$

83

This results in the following equation for buckling coefficient

$$k_{y\ exp} = p_{y\ exp}t_f^2L^2/(\pi^2EI_sR) \qquad (6.3)$$

Equation (6.3) is based on the assumption that $\nu = 0$. A value for E of 10.1×10^6 psi was used for reducing the test data.

The geometrical and rigidity parameters appearing in the above equations were based on the average of pre-test measurements of the specimen geometry. As for compression and torsion specimens, six circumferential measurements each of the wall thickness and total height at a stiffener were made at both ends of the cylinder. Average values of wall thickness and wall thickness/stiffener height ratio were than determined, and these parameters together with equations presented in Table 3.2 were used to calculate values for thickness and bending stiffness parameters. A summary of the material, geometrical and rigidity parameters for the hydrostatic pressure test specimens is presented as Table 6.2. Experimental values for the structural parameters for the specimens are summarized in Table 6.3.

Calculation of Theoretical Structural Parameters

Based on the assumption that $\nu = 0$, the theoretical buckling stress is related to the buckling coefficient and cylinder material and geometry parameters as shown.

$$\sigma_y = k_y\pi^2EI_s/(t_fL^2) \qquad (6.4)$$

Values for the buckling coefficient are dependent on whether the cylinder geometry is characterized by moderate-length or short-cylinder behavior. For moderate-length cylinders with simply support boundary conditions, results given in Reference 1 show that the buckling coefficient has the following form:

$$k_y = 1.039\ Z_y^{1/2} \qquad (6.5)$$

where
$$Z_y = (I_f/I_s)^{3/2}(t_s/t_f)^{1/2}Z \qquad (6.6)$$

and
$$Z = (12^{-1/2})(t_f/I_s)^{1/2}(L^2/R) \qquad (6.7)$$

Eq. (6.5), (6.6), and (6.7) were derived in Reference 1 for an orthotropic cylinder subject to lateral pressure only. However, results presented in Reference 15 show that for moderate length cylinders, the critical pressure for a cylinder subject to hydrostatic or lateral pressure loading are essentially equal.

84

Hence, the above equations are also valid for determining the buckling coefficient for a moderate length cylinder under hydrostatic pressure loading.

Theoretical results presented in Appendix B show that for clamped cylinder end boundary conditions in the moderate length cylinder range the equation for k_y is:

$$k_y = 1.58 \, Z_y^{1/2} \tag{6.8}$$

Theoretical values for the buckling coefficient were determined for both simple support and fixed boundary conditions using Eq. (6.5) or (6.8) and Eqs. (6.6) and (6.7). Corresponding values for the theoretical buckling stress were then caluclated using Eq. (6.4). Finally, the theoretical buckling pressure was determined for both edge conditions from the following equation:

$$p_y = \sigma_y t_f / R \tag{6.9}$$

As indicated previously the longitudinally stiffened cylinder designs were in the short-cylinder range. For these specimens, the buckling coefficient for simple support cylinder end boundary conditions was determined from an equation and method presented in Reference 1. The method involves the use of a graphical procedure and is similar to that described for obtaining torsional buckling coeffic- ients in the short-cylinder range (See Section 5).

The buckling coefficient for clamped support cylinder end boundary conditions was determined using equations presented in Appendix B of this report. For a given cylinder geometry and material, Eq. (B.8) was used to calculate the curvature para- meter Z for an assumed value of the wave length parameter β. This value of β was also substituted in Eq. (B.9) to obtain the associated minimum value for the buckling coefficient. In this manner, curves of theoretical buckling coefficient were generated as a function of Z_t for a given cylinder geometry. From such k_t vs Z_t curves, the theoretical buckling coefficient was readily determined for a given design value for Z_t. Once the buckling coefficient was known the associated buckling stress and critical external pressure was calculated using Eqs. (6.4) and (6.9).

Fig. 6.4 is presented to illustrate typical curves of buckling coefficient vs curvature parameter as determined using the procedures described above. Shown in the figure are theoretical values for buckling coefficient based on short-cylinder theory for both the simple support and clamped boundary condition and were generated for a particular specimen geometry (Specimen No. 51). Also indicated is the test result for the specimen. One observes the good correlation between experiment and theory based on clamped boundary conditions.

85

Curve A – Short-Cylinder Theory – Clamped Boundary Conditions
Curve B – Short-Cylinder Theory – Simple Support Boundary Conditions
Curve C – Moderate-Length Cylinder Theory – Clamped Boundary Conditions

Curve A

Curve C

Curve B

$\triangle$ Test Results for Specimen 51
(Longitudinally Stiffened Cylinder)

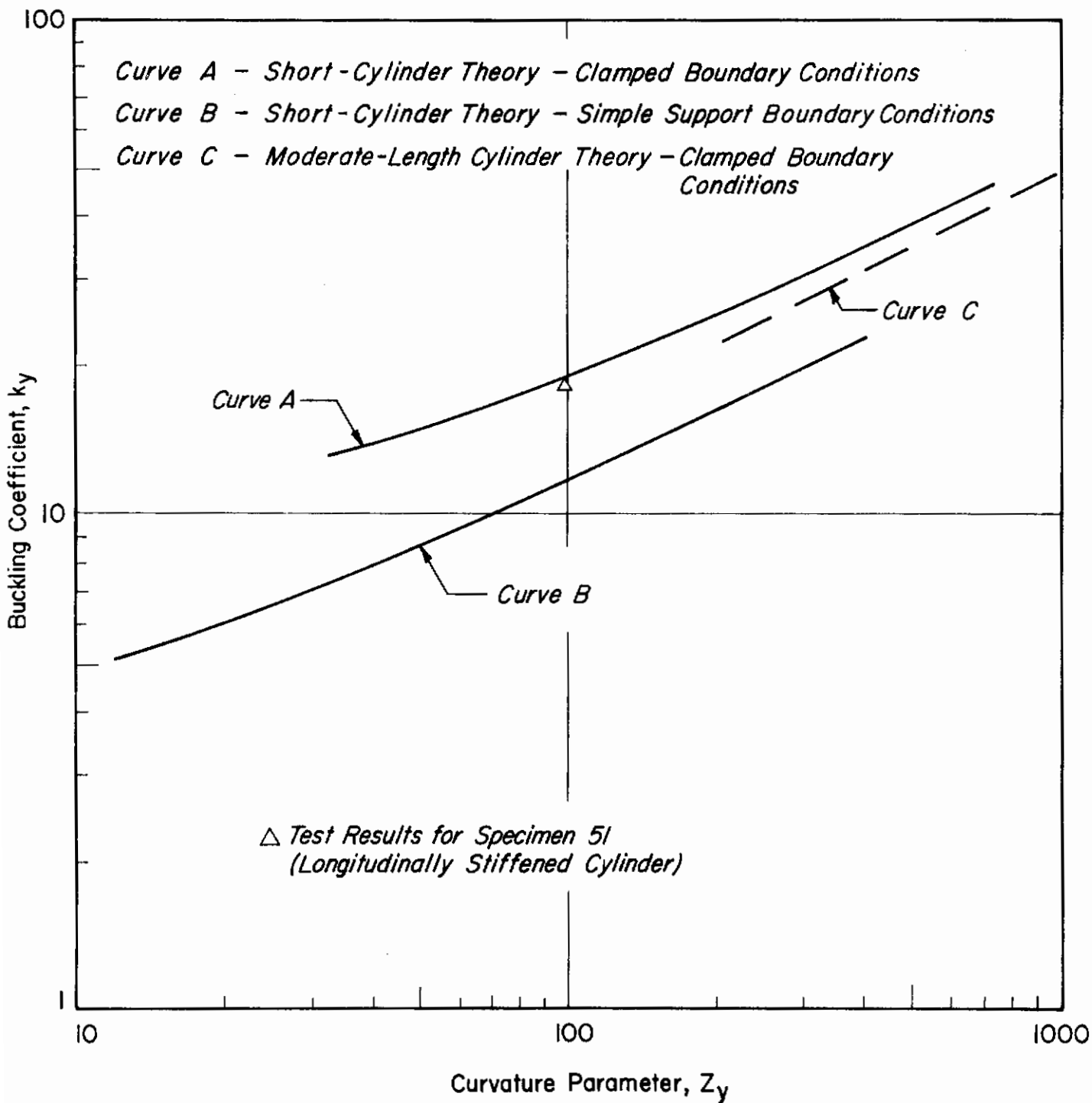Buckling Coefficient, k_y

Curvature Parameter, Z_y

Fig. 6.4   Typical Buckling Coefficient vs Curvature Parameter for
Short-Length Cylinders Under Hydrostatic Pressure

5030

86

A summary of the theoretical structural parameters is presented in Table
6.3 for all specimens and for clamped and simply supported edge boundary conditions.

TABLE 6.1

Material, Geometrical and Rigidity Parameters for Hydrostatic Pressure Test Specimens

Specimen Number	Type	L	R	w	d	t	t/b	b	t_s	t_f	I_s/b^3	I_f/b^3	α	E
Col.	2	3	4	5	6	7	8	9	10	11	12	13	14	15
Ref.	--	--	--	--	--	--	--		← Table 3.2 →				Eq.(4.8)	--
Units	--	in.	in.	← 10⁻³ in. →			--	--	← 10⁻³ in. →		← 10⁻² in³/in³ →		--	10⁶ psi
48	RSC$^\phi$	3.83	3.80	51	111	11.3	2.62	4.3	11.3	13.3	150	295	1.68	10.1
50		3.77		56	111	10.5	1.35	7.8	10.5	14.4	20	75	2.68	
54 *		3.83		53	111	9.8	1.19	8.3	9.8	13.8	14	61	3.1	
55	RSC	3.81		54	111	5.4	.45	11.9	5.4	11.2	0.77	17.4	10.9	
51	LSC$^\Delta$	3.75		61	119	12.3	2.98	4.1	14.5	12.3	400	220	.65	
53*		3.76		60	119	11.3	2.92	3.9	13.2	11.3	380	208	.64	
56	LSC	5.73	3.80	60	119	6.8	1.30	5.3	9.5	6.8	71	18.3	.36	10.1

φ Ring Stiffened Cylinder

Δ Longitudinally Stiffened Cylinder

* Internally Stiffened

88

TABLE 6.2

Summary of Structural Parameters for Hydrostatic Pressure Tests

Specimen Number	Type	$P_{y\,exp}$	$\sigma_{y\,exp}$	$k_{y\,exp}$	Z_y	Simple Support $\triangle$			Clamped $\triangle$		
						P_y	σ_y	k_y	P_y	σ_y	k_y
Col	2	3	4	5	6	7	8	9	10	11	12
Ref.	--	--	Eq.(6.1)	Eq.(6.3)	Eq.(6.6)	Eq.(6.9)	Eq.(6.4)	**	Eq.(6.9)	Eq.(6.4)	***
Units		psi	psi	--	--	psi	psi	--	psi	psi	--
48	RSC$^\phi$	9.31	2660	43	930	6.86	1960	32	10.4	2980	49
50		12.1	3180	69	2520	9.16	2410	52	13.9	3660	79
54*		13.8	3820	98	3500	8.73	2410	62	13.3	3660	94
55	RSC	9.1	3080	390	76200	6.74	2290	290	10.3	3480	440
51	LSC$^\triangle$	9.16	2820	18	100	6.17	1900	12	9.8	3020	19
53*		7.22	2440	18	107	5.00	1690	12	8.2	2760	19.7
56	LSC	2.37	1320	29	100	1.02	570	12	1.6	900	19

$\triangle$ Cylinder End Boundary Conditions

ϕ Ring Stiffened Cylinder

$\triangle$ Longitudinally Stiffened Cylinder

* Internally Stiffened

** Eq. (6.5) for RSC
See Text for LSC

*** Eq. (6.8) for RSC
See Text for LSC

APPENDIX A

A DISCRETE AXIAL-BUCKLE SOLUTION FOR THE STABILITY OF ORTHOTROPIC CYLINDERS UNDER AXIAL COMPRESSION

Introduction

In Ref. 3, a solution for the general instability of orthotropic cylinders under compression was obtained on the basis that for moderate length cylinders, the number of buckles along the axis of the cylinder m, was large enough that it could be treated as a continuous parameter along with β, the ratio of the buckle length in the axial direction to that in the circumferential direction. The buckling coefficient k, was treated as a function of two variables m and β for obtaining a minimum value. From the requirements of stationariness, a quadratic equation was obtained for β^2 in terms of the orthotropicity parameters γ, α and δ and exclusive of Z_x, the curvature parameter.

As a consequence of the above quadratic equation it was found that for certain combinations of γ, α and δ, β was imaginary; hence for these γ, α and δ combinations the moderate length solution or more precisely m-continuous solution, did not apply. However, since the axisymmetric solution was independent of γ, α, δ and β, it was assumed that the axisymmetric solution prevailed in the regions where the moderate length solution failed. These above conclusions, based on the quadratic equation, are shown in Figure 1 of Ref. 3. The shaded regions therein represent the combinations of γ and α (with $\delta = 1$) for which the quadratic equation yields imaginary values for β. This figure also shows that the asymmetric solution is higher than the axisymmetric solution in the region bounded by $\gamma \geq 1$ and $\alpha \leq 1$.

The present analysis considers the problem on the basis that m need not be continuous but has an integer value; in particular m = 1. As a result of letting m be equal to 1, it has been found that real solutions (i.e., with real β values) are obtainable in the shaded zones in Figure 1 of Ref. 3 and also that in the strip $\gamma \geq 1$ $\alpha \leq 1$ there may be asymmetric solutions lower than the axisymmetric solutions depending upon the value of γ and the curvature parameter, Z_x.

90

The m = 1 Asymmetric Solution

From Ref. 3 we can write the following expression for the $k_{asy_{m=1}}$ solution:

$$k_{asy_{m=1}} = 1 + 2\left[(D_3/D_1)(1-\nu) + \nu/2\,(1+D_2/D_1)\right]\beta^2 + (D_2/D_1)\,\beta^4$$

$$+ \left[12Z_x^2\,(1-\nu^2)/\pi^4\right]\left[1 + 2\left\{(B_2/B_3)(1+\nu) - (\nu/2)(1+B_2/B_1)\right\}\beta^2\right.$$

$$\left. + (B_2/B_1)\,\beta^4\right]^{-1} \tag{A.1}$$

where: $\quad k = N_x L^2/\pi^2 D_1 \qquad Z_x = B_2 L^4/12 R^2 D_1 \qquad \beta = nL/\pi R$

Using the following definitions of Ref. 3,

$$\alpha = B_1 D_2/B_2 D_1$$

$$\gamma = \left[(D_3/D_1)(1-\nu) + (\nu/2)(1+D_2/D_1)\right] / \left[(B_2/B_3)(1+\nu) - (\nu/2)(1+B_2/B_1)\right]$$

$$\delta = B_2/\left[B_1\left\{(B_2/B_3)(1+\nu) - (\nu/2)(1+B_2/B_1)\right\}^2\right]$$

and $\quad \bar{\beta}^2 = B_2\left[B_1\left\{(B_2/B_3)(1+\nu) - (\nu/2)(1+B_2/B_1)\right\}\right]^{-1}\beta^2$

which were used for the $k_{asy_{m-cont}}$ solution, we can rewrite Eq. (A.1) to obtain the following:

$$k_{asy_{m=1}} = 1 + 2\gamma\,(\bar{\beta}^2/\delta) + \alpha(\bar{\beta}^4/\delta)$$

$$+ (12Z_x^2(1-\nu^2)/\pi^4)\left[1 + 2(\bar{\beta}^2/\delta) + (\bar{\beta}^4/\delta)\right]^{-1} \tag{A.2}$$

By differentiating k with respect to $\bar{\beta}^2$, we obtain for the stationariness of k, the following expression for Z_x

$$\left[12\,(1-\nu^2)/\pi^4\right]Z_x^2 = \left[1 + 2\,(\bar{\beta}^2/\delta) + (\bar{\beta}^4/\delta)\right]^2\,(\gamma + \alpha\bar{\beta}^2)\,(1 + \bar{\beta}^2)^{-1} \tag{A.3}$$

Substituting Eq. (A.3) into (A.2), we obtain for a stationary value of k, the following:

$$k_{asy_{m=1}} = 1 + 2\,\gamma(\bar{\beta}^2/\delta) + \alpha(\bar{\beta}^4/\delta)$$

$$+ \left[1 + 2\,(\bar{\beta}^2/\delta) + (\bar{\beta}^4/\delta)\right]\,(\gamma + \alpha\bar{\beta}^2)\,(1 + \bar{\beta}^2)^{-1} \tag{A.4}$$

91

Eqs. (A.3) and (A.4) constitute the basic equations for the $m = 1$ asymmetric solution. For a cylinder with specified α, γ, δ, $k_{asy_{m=1}}$ and the corresponding Z_x can be found by assuming values of $\overline{\beta}$ and solving Eqs. (A.3) and (A.4). Typical results for Zone II are illustrated in Figure (A.2) and are compared with the axisymmetric solution, $k_{axi} = .702 \, Z_x \, (1 - \nu^2)^{1/2}$ and also the asymmetric solution with m continuous, $k_{asy_{m=cont.}} = .702 \, Z_x \, (1 - \nu^2)^{1/2}$ U of Ref. 3. It can be observed that the $m = 1$ solution does indeed result in lower values of k. This incidently coincides quite closely with the region used for the longitudinally stiffened cylinders of this program.

Significance of m = 1 Solution in Other Zones

A critical evaluation of the significance of the $m = 1$ solution in other zones of Figure A.1 was undertaken relative to the asymmetric $m = $ cont. and axisymmetric modes. The conclusions are as follows for longitudinally stiffened cylinders which constitute Zones I, II, and III.

Zone I: $\alpha \leq 1$; $\gamma \geq 1$

As shown in Figure A.3, we find that in this zone, as γ increases, either the axisymmetric or the asymmetric $m = 1$ solution applies depending upon Z_x.

Zone II: $\alpha \leq 1$; $\alpha \leq \gamma \leq 1$

As shown in Figure A.2, $k_{asy_{m=1}}$ solution governs here.

Zone III: $\alpha \leq 1$; $\gamma \leq \alpha$

Here, the $k_{asy_{m-cont}}$ solution governs and the results of Ref. 3 hold.

For ring stiffened cylinders which correspond to Zones IV, V and VI, the results of Ref. 3 apply directly.
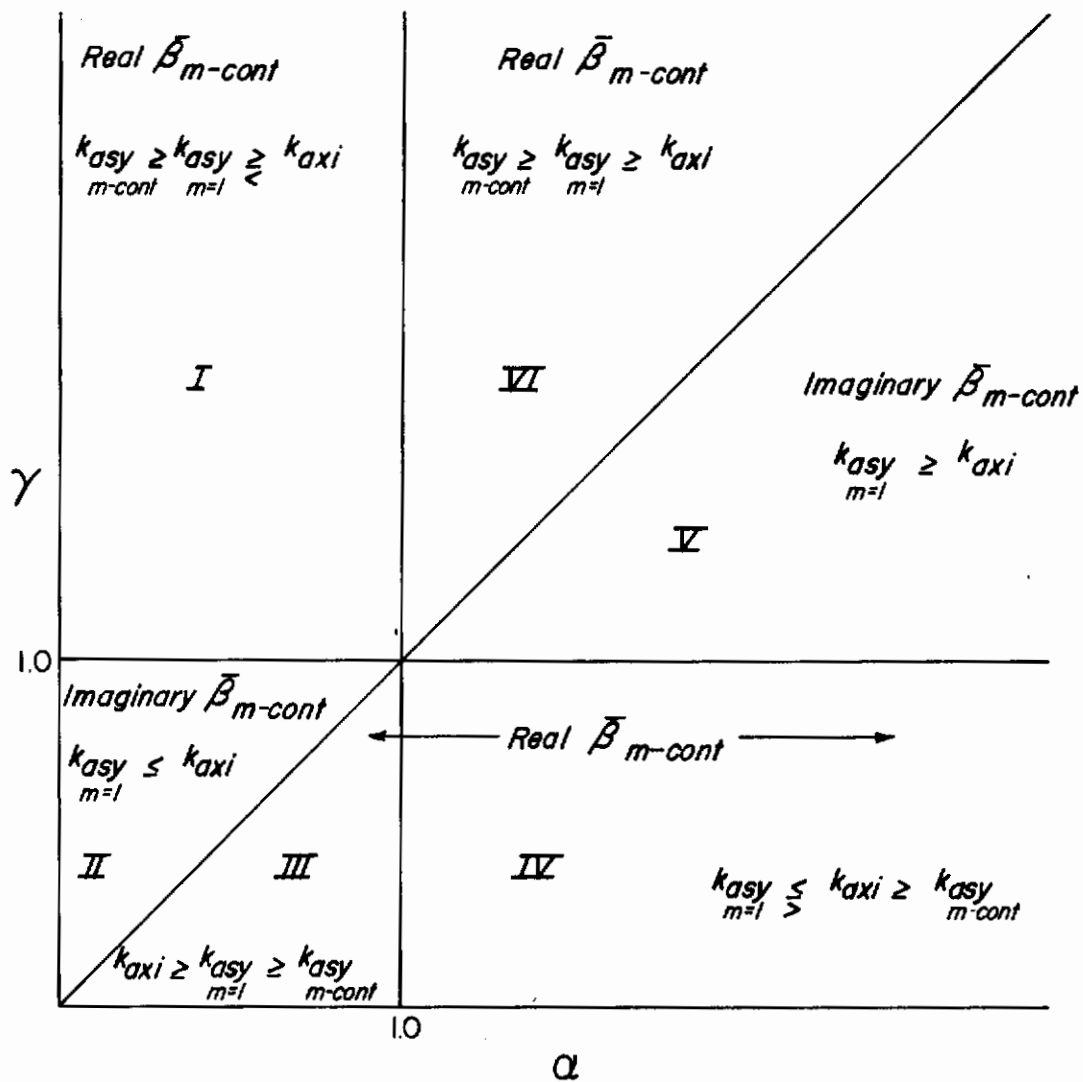
92

Fig. A. 1   Comparison of Axisymmetric and Asymmetric Solutions in the
γ - α Plane for General Instability of Orthotropic Cylinders
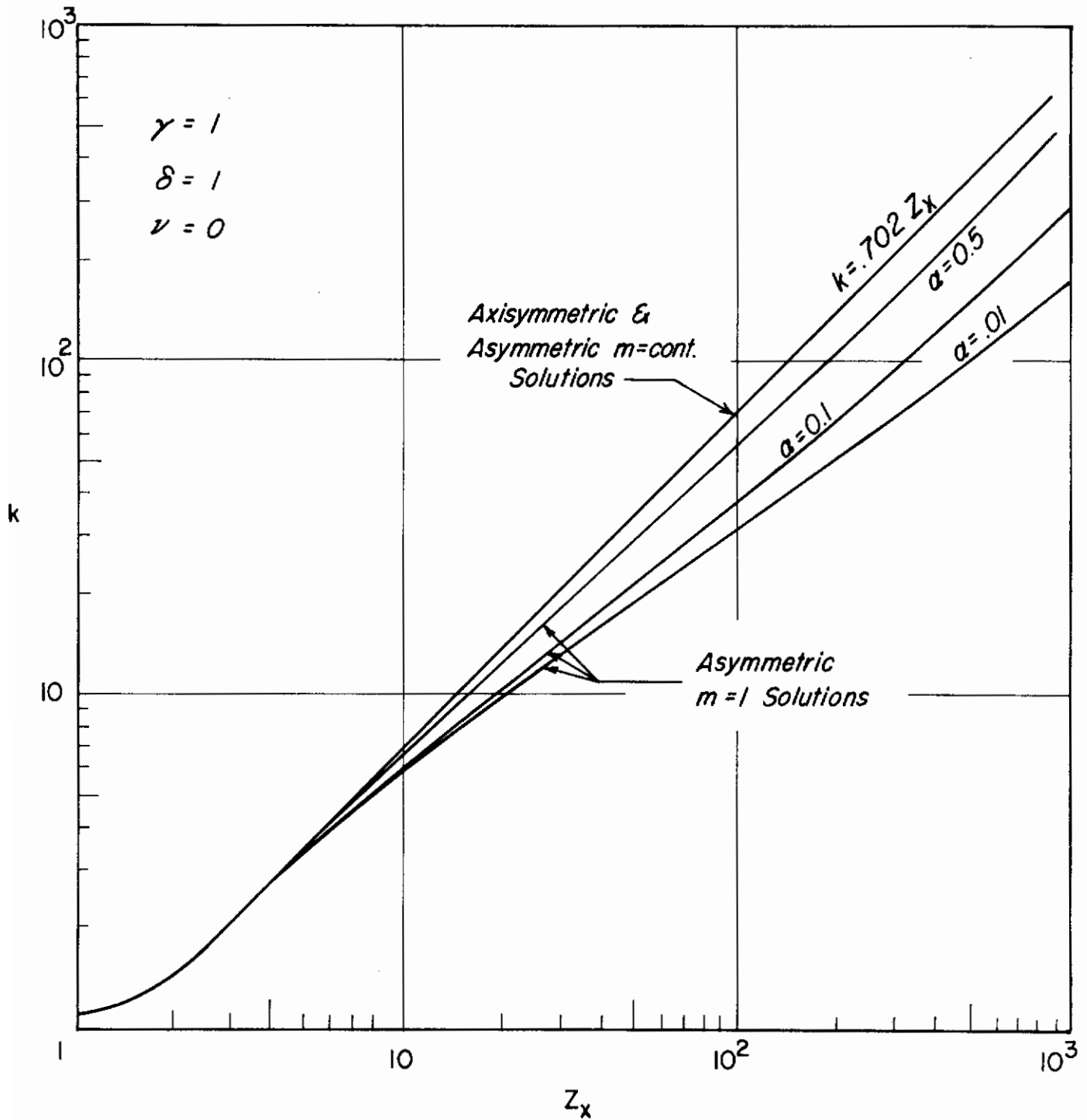
93

Fig. A.2 Various Solutions Obtained in Zone II for an Orthotropic
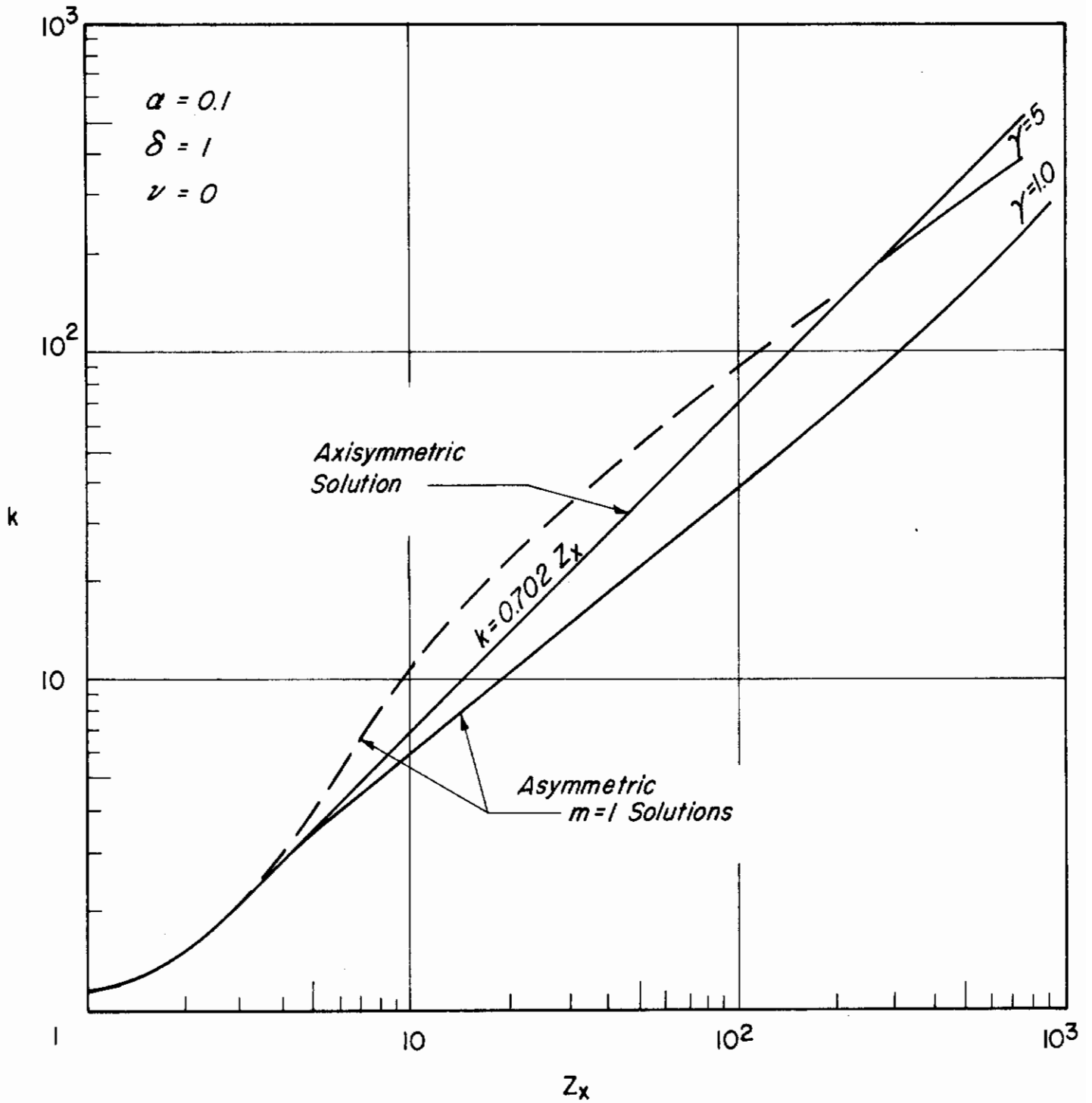Cylinder Under Compression

Fig. A. 3   Various Solutions Obtained in Zone III for an Orthotropic
Cylinder Under Compression

APPENDIX B

ELASTIC STABILITY OF CLAMPED ORTHOTROPIC
CYLINDERS UNDER HYDROSTATIC PRESSURE

Introduction

The inherent difficulty of obtaining a closed form exact solution for the Donnell equation in the case of clamped boundary conditions has led to approximate solutions using energy and other variational methods. Nash (Ref. 16) has obtained a solution for an isotropic cylinder using the energy method. The present report makes use of the Galerkin method as used by Batdorf (Ref. 17) for stability problems and extended by Lakshmikantham and Gerard (Ref. 18) for the ortho-tropic case.

Governing Equations

The basic stability equation for the orthotropic cylinder under hydrostatic pressure is written as follows:

$$L(w) \equiv \left[\partial^4/\partial x^4 + 2 \left\{ (D_3/D_1)(1-\nu) + \nu/2 \, (1 + D_2/D_2) \right\} \, \partial^4/\partial x^2 \partial y^2 + (D_2/D_1) \, \partial^4/\partial y^4 \right] w$$

$$+ (N_x/D_1)(\partial^2 w/\partial x^2) + (N_y/D_1)(1/R + \partial^2 w/\partial y^2) + \left[(B_2(1-\nu^2)/R^2 D_1) \right] \, \partial^2/\partial x^2$$

$$(\nabla_B^{-4} \, \partial^2 w/\partial x^2) = 0 \tag{B.1}$$

where ∇_B^{-4} is an inverse operator defined by:

$$\nabla_B^{-4} \, (\nabla_B^4 \, f) = f \tag{B.2}$$

where f is any scalar function; and ∇_B^4 is given by:

$$\nabla_B^4 = \partial^4/\partial x^4 + 2 \left\{ (B_2/B_3)(1 + \nu) - (\nu/2)(1 + B_2/B_1) \right\} \, \partial^4/\partial x^2 \partial y^2 + (B_2/B_1) \, \partial^4/\partial y^4 \tag{B.3}$$

Equation (B.1) is similar to that presented in Ref. 18, except for the presence of the circumferential stress resultant term N_y which arises on account of the external pressure. Furthermore, in the case of hydrostatic pressure

$$N_x = N_y/2 = pR/2 \tag{B.4}$$

where p is the uniform pressure.

96

In order to obtain a solution for Eq. (B.1) such that the clamped boundary condition is satisfied at $x = 0$ and $x = L$ we assume the following form for w

$$w = A [1 - \cos (2\pi x/L)] \cos (ny/R) \tag{B.5}$$

Then the Galerkin equation is obtained by setting

$$\int_0^L \int_0^{2\pi R} L(w) [1 - \cos (2\pi x/L)] \cos n (y/R) \, dx \, dy = 0 \tag{B.6}$$

As a result of carrying out the integration in Eq. (B.6) we obtain an expression for N_y as follows:

$$(N_y/D_1) L^2/\pi^2 = \frac{4}{(3\beta^2 + 1/2)} \left[(1 + 2r\beta^2 + 3D_2/D_1\beta^4) \right.$$

$$\left. + \frac{12Z^2}{16\pi^4} \frac{1}{\left\{ 1 + 2s\beta^2 + (B_2/B_1)\beta^4 \right\}} \right] \tag{B.7}$$

where

$$r = (D_3/D_1)(1-\nu) + \nu/2 (1 + D_2/D_1)$$

$$s = (B_2/B_3)(1+\nu) - \nu/2 (1 + B_2/B_1)$$

$$12Z^2 = (B_2 L^4/R^2 D_1) (1 - \nu^2)$$

$$\beta = (nL/2\pi R)$$

Since the buckling coefficient k_y is given by $k_y = (N_y/D_1)_{min} (L^2/\pi^2)$, the right hand side of Eq. (B.7) is minimized with respect to β^2. By setting $(\partial/\partial\beta^2)(\ ) = 0$ we obtain:

$$\frac{3Z^2}{\pi^4} = (1 + 2s\beta^2 + B_2/B_1\beta^4)^2 \frac{4[(r-3) + 3D_2/D_1 \beta^2 + 9D_2/D_1 \beta^4]}{(s+3) + (12s + B_2/B_1)\beta^2 + 9B_2/B_1 \beta^4} \tag{B.8}$$

Upon substituting Eq. (B.8) into (B.9) we obtain:

$$k_y = \frac{4}{(3\beta^2 + 1/2)} \left\{ (1 + 2r\beta^2 + 3D_2/D_1 \, \beta^4) \right.$$

$$\left. + \frac{(r-3) + 3D_2/D_1 \, \beta^2 + 9\, D_2/D_1 \, \beta^4}{(s+3) + (12s + B_2/B_1)\beta^2 + 9B_2/B_1 \, \beta^4} \, (1+2s\beta^2 + B_2/B_1 \, \beta^4) \right\} \quad (B.9)$$

While for given values of Z one can find k_y with the help of Eqs. (B. 8) and (B. 9), it is more convenient to assume values of β and obtain k_y, Z values so that a k_y - Z plot can be drawn for specific orthotropic cylinders.

Limiting Solutions

Eqs. (B. 8) and (B. 9) yield simple expressions for k_y in certain cases. For cylinders of moderate length, β^2 is usually very large compared to unity, and if the orthotropic parameters s, r, B_2/B_1, D_2/D_1 are of the order of unity, then Eqs. (B. 8) and (B. 9) reduce to:

$$\beta^8 = (3/4) \, (Z^2/\pi^4) \, (B_1/B_2) \, (D_1/D_2) \quad (B.10)$$

$$k_y = 4 \, (4/3) \, (D_2/D_1 \, \beta^2) \quad (B.11)$$

Hence from Eqs. (B. 10) and (B. 11), we find:

$$k_y = (4/\pi) \, (4/3)^{3/4} \, [(D_2/D_1)^{3/4} \, (B_1/B_2)^{1/4} \, Z^{1/2}]$$

or $\qquad k_y = 1.58 \, Z_y^{1/2}$ $\qquad\qquad\qquad\qquad\qquad$ (B. 12)

where

$$Z_y = (B_1/B_2)^{1/2} \, (D_2/D_1)^{3/2} \, Z$$

For isotropic flat plates, $r = s = 1 = D_2/D_1 = B_2/B_1$ and $Z = 0$. Hence from Eq. (B. 8) we find:

$$9\beta^4 + 3\,\beta^2 - 2 = 0 \quad \text{or} \quad \beta^2 = 1/3 \quad (B.13)$$

98

By substituting $\beta^2 = 1/3$ into Eq. (B.9) we have:

$$k_y = 16/3 = 5.33 \qquad (B.14)$$

This solution corresponds to a biaxially compressed long flat plate, clamped along the long edges under a loading one-half of that applied to the short edges.

99

REFERENCES

1. Becker, H. and Gerard, G. , "Elastic Stability of Orthotropic Shells," Journal Aerospace Sciences, V. 29, No. 5, May 1962, pp. 505-513.

2. Gerard, G. , "Plastic Stability Theory of Geometrically Orthotropic Plates and Cylindrical Shells," Journal Aerospace Sciences, V. 29, No. 8, August 1962, pp. 956-962.

3. Gerard, G. , "Compressive Stability of Orthotropic Cylinders," Journal Aerospace Sciences, V. 29, No. 10, October 1962, pp. 1171-1180.

4. Becker, H., Gerard, G. , and Winter, R. , "Experiments on Axial Compressive General Instability of Monolithic Ring-Stiffened Cylinders," AIAA Journal, V. 1, No. 7, July 1963, pp. 1614-1618.

5. Almroth, B. O. , "Postbuckling Behavior of Orthotropic Cylinders Under Axial Compression," AIAA Journal, V. 2, No. 10, October 1964, pp. 1795-1799.

6. Thielemann, W. F. , "New Developments in the Nonlinear Theories of the Buckling of Thin Cylindrical Shells," Aeronautics and Astronautics, Pergamon Press, London, 1960, pp. 76-119.

7. Dow, N. F. , Libove, C. and Hubka, R. E. , Formulas for the Elastic Constants of Plates with Integral Waffle-Like Stiffening, NACA TR 1195, 1954.

8. Crawford, R. F. and Libove, C. , Shearing Effectiveness of Integral Stiffening, NACA TN 3443, June 1955.

9. Hoppmann, W. H., "Bending of Orthogonally Stiffened Plates," J. App. Mech. , V. 22, No. 2, June 1955, pp. 267-271.

10. Hoppmann, W. H. , Huffington, N. J. and Magness, L. S. , "A Study of Orthgonally Stiffened Plates," J. App. Mech. , V. 23, No. 3, September 1956, pp. 343-350.

11. Becker, H. and Gerard, G. , Measurement of Torsional Rigidity of Stiffened Plates, NASA TN D-2007, July 1963.

12. Timoshenko, S. , Theory of Elasticity, McGraw-Hill Book Company, Inc. , New York.

13. Gerard, G. and Becker, H. , Handbook of Structural Stability Part III- Buckling of Curved Plates and Shells, NACA TN 3783, August 1957.

14. Niles, A. S. and Newell, J. S. , Airplane Structures - Volume I, Third Edition, J. Wiley and Sons, Inc. , New York, 1949.

15. Becker, H. , General Instability of Stiffened Cylinders, NACA TN 4237, July 1958.

References

16. Nash, W. A., "Buckling of Thin Cylindrical Shells Subject to Hydrostatic Pressure," Journal of Aeronautical Sciences, V. 21, No. 5, May 1964, pp. 354-355.

17. Batdorf, S. B., A Simplified Method of Elastic-Stability Analysis for Thin Cylindrical Shells, II, NACA TN 1342, June 1947.

18. Lakshmikantham, C., Gerard, G., and Milligan, R., General Instability of Orthotropically Stiffened Cylinders - Bending and Combined Compression and Bending - Part II, ARA Technical Report No. 258-2, Allied Research Associates, Concord, Mass., August 1965.

Unclassified
Security Classification

DOCUMENT CONTROL DATA · R&D
(Security classification of title, body of abstract and indexing annotation must be entered when the overall report is classified)

1. ORIGINATING ACTIVITY (Corporate author)	2a. REPORT SECURITY CLASSIFICATION
Allied Research Associates, Inc.	Unclassified
Virginia Road, Concord, Massachusetts	2b. GROUP

3. REPORT TITLE

GENERAL INSTABILITY OF ORTHOTROPICALLY STIFFENED CYLINDERS
PART I - AXIAL COMPRESSION, TORSION AND HYDROSTATIC PRESSURE
LOADINGS

4. DESCRIPTIVE NOTES (Type of report and inclusive dates)

Final Report

5. AUTHOR(S) (Last name, first name, initial)

Milligan, Roger - Gerard, George - Lakshmikantham, C.- Becker, Herbert

6. REPORT DATE	7a. TOTAL NO. OF PAGES	7b. NO. OF REFS
July 1965	101	18

8a. CONTRACT OR GRANT NO.	9a. ORIGINATOR'S REPORT NUMBER(S)
AF 33(615)-1228	
b. PROJECT NO. 1467	ARA Technical Report No. 258-2
c. Task No. 146703	9b. OTHER REPORT NO(S) (Any other numbers that may be assigned this report)
d. BPSN 4(6199-146703-62405334)	Technical Report AFFDL-TR-65-161, Part I

10. AVAILABILITY/LIMITATION NOTICES

The distribution of this report is unlimited.

11. SUPPLEMENTARY NOTES	12. SPONSORING MILITARY ACTIVITY
	Air Force Flight Dynamics Laboratory
	Research and Technology Division
	Air Force Systems Command - USAF
	Wright-Patterson AFB, Ohio 45433

13. ABSTRACT

The general applicability of orthotropic stability theory to aerospace shell structures was examined experimentally. For this purpose a series of careful experiments were performed on orthotropically stiffened cylinders designed to fail in the elastic general instability mode under three separate loading conditions: axial compression, torsion and hydrostatic pressure. Experimental results obtained during the program verified that for all loading conditions considered linear orthotropic theory results in accurate predictions of cylinder strength.

As a result of observed discrepancies between experiment and previously existing theory for longitudinally stiffened cylinders under axial compression, theoretical studies were initiated which resulted in the discovery of a new asymmetric failure mode for this cylinder configuration. Based on this new failure mode, good correlation between experiment and theory was obtained except when the longitudinal stiffened cylinder configurations approached that corresponding to an isotropic cylinder. Other theoretical investigations performed during the program established that cylinder boundary conditions have a pronounced effect on the buckling strength of orthotropic cylinders under hydrostatic pressure loading.

DD FORM 1473
1 JAN 64

Unclassified
Security Classification

14. KEY WORDS	LINK A		LINK B		LINK C	
	ROLE	WT	ROLE	WT	ROLE	WT
Stability of Cylindrical Orthotropic Shells						
Axial Compression Loading						
Torsion Loading						
Hydrostatic Pressure Loading						
Experimental Results						
Theoretical Results						

INSTRUCTIONS

1. ORIGINATING ACTIVITY: Enter the name and address of the contractor, subcontractor, grantee, Department of Defense activity or other organization (*corporate author*) issuing the report.

2a. REPORT SECURITY CLASSIFICATION: Enter the overall security classification of the report. Indicate whether "Restricted Data" is included. Marking is to be in accordance with appropriate security regulations.

2b. GROUP: Automatic downgrading is specified in DoD Directive 5200.10 and Armed Forces Industrial Manual. Enter the group number. Also, when applicable, show that optional markings have been used for Group 3 and Group 4 as authorized.

3. REPORT TITLE: Enter the complete report title in all capital letters. Titles in all cases should be unclassified. If a meaningful title cannot be selected without classification, show title classification in all capitals in parenthesis immediately following the title.

4. DESCRIPTIVE NOTES: If appropriate, enter the type of report, e.g., interim, progress, summary, annual, or final. Give the inclusive dates when a specific reporting period is covered.

5. AUTHOR(S): Enter the name(s) of author(s) as shown on or in the report. Enter last name, first name, middle initial. If military, show rank and branch of service. The name of the principal author is an absolute minimum requirement.

6. REPORT DATE: Enter the date of the report as day, month, year; or month, year. If more than one date appears on the report, use date of publication.

7a. TOTAL NUMBER OF PAGES: The total page count should follow normal pagination procedures, i.e., enter the number of pages containing information.

7b. NUMBER OF REFERENCES: Enter the total number of references cited in the report.

8a. CONTRACT OR GRANT NUMBER: If appropriate, enter the applicable number of the contract or grant under which the report was written.

8b, 8c, & 8d. PROJECT NUMBER: Enter the appropriate military department identification, such as project number, subproject number, system numbers, task number, etc.

9a. ORIGINATOR'S REPORT NUMBER(S): Enter the official report number by which the document will be identified and controlled by the originating activity. This number must be unique to this report.

9b. OTHER REPORT NUMBER(S): If the report has been assigned any other report numbers (*either by the originator or by the sponsor*), also enter this number(s).

10. AVAILABILITY/LIMITATION NOTICES: Enter any limitations on further dissemination of the report, other than those imposed by security classification, using standard statements such as:

(1) "Qualified requesters may obtain copies of this report from DDC."

(2) "Foreign announcement and dissemination of this report by DDC is not authorized."

(3) "U. S. Government agencies may obtain copies of this report directly from DDC. Other qualified DDC users shall request through
_____."

(4) "U. S. military agencies may obtain copies of this report directly from DDC. Other qualified users shall request through
_____."

(5) "All distribution of this report is controlled. Qualified DDC users shall request through
_____."

If the report has been furnished to the Office of Technical Services, Department of Commerce, for sale to the public, indicate this fact and enter the price, if known.

11. SUPPLEMENTARY NOTES: Use for additional explanatory notes.

12. SPONSORING MILITARY ACTIVITY: Enter the name of the departmental project office or laboratory sponsoring (*paying for*) the research and development. Include address.

13. ABSTRACT: Enter an abstract giving a brief and factual summary of the document indicative of the report, even though it may also appear elsewhere in the body of the technical report. If additional space is required, a continuation sheet shall be attached.

It is highly desirable that the abstract of classified reports be unclassified. Each paragraph of the abstract shall end with an indication of the military security classification of the information in the paragraph, represented as (*TS*), (*S*), (*C*), or (*U*).

There is no limitation on the length of the abstract. However, the suggested length is from 150 to 225 words.

14. KEY WORDS: Key words are technically meaningful terms or short phrases that characterize a report and may be used as index entries for cataloging the report. Key words must be selected so that no security classification is required. Identifiers, such as equipment model designation, trade name, military project code name, geographic location, may be used as key words but will be followed by an indication of technical context. The assignment of links, rules, and weights is optional.